Politecnico di Torino

Master's degree in Civil Engineering

Master's degree Thesis

Spatial analysis of road crashes involving vulnerable road users in support of road safety management strategies

Supervisor

Prof. Marco Bassani

Author

Sinem Sisman

March, 2022

ABSTRACT

Road traffic crashes result in the deaths of approximately 1.3 million people around the world each year and leave between 20 and 50 million people with non-fatal injuries. Due to insufficient physical protection in the event of a collision, more than half of all road traffic deaths are among vulnerable road users (VRU), i.e., pedestrians, cyclists, and motorcyclists.

The urban road environment poses a high risk to VRU. However, traffic crashes can be reduced by using appropriate safety countermeasures on “hazardous road locations” (HRL) where higher collision frequency are observed with respect to the average expected level. It is important to highlight that evaluating each sub-category of VRU separately plays a key role to find the most effective countermeasures for each specific VRU.

This study presents the analyses and results about the spatial distribution of traffic collisions to identify HRL in Turin from 2006 to 2019 by considering all VRU and related sub-categories (pedestrians, cyclists, moped and motorcycle users respectively).

The Italian National Institute of Statistics (ISTAT) provided the official database of traffic collisions . Firstly, the crash data relating to regional (Piedmont), provincial (Turin), and municipal (Turin) levels was evaluated by using descriptive statistics. The crash data of Turin was then prepared and organized to carry out a detailed analysis. Due to the absence of a complete geographic coordinates in the crash database, data was geo-localized firstly and then analysed with the help of Geographic Information System (GIS) technologies.

The distance-based and density-based methods were used for the spatial distribution analyses of the traffic collisions. While distance-based methods (Nearest Neighbor Analysis, G and F Functions) evaluate distances between events to define areas where traffic crashes are clustered, density-based methods (the Kernel Density Estimation) were used to examine the crash density to identify HRL.

The crash database was extracted as six time intervals by dividing it into 2–3-year periods to highlight the presence of false-positive and false-negative HRL. All critical road segments and intersections which presented 3 out of 6 positive time intervals in the road network were identified as HRL. These analyses were carried out for all VRU and the related VRU sub-categories.

The results indicate collisions were concentrated in the main intersections of the city, which deal with heavy traffic flows and conflicts between users during the day. It is a clear fact that wide cross-sections in the urban road environment cause some difficulties to VRU due to significant speed differences with respect to motorized users, the absence of signalized junctions and protected pedestrian crossings in some points. It seems that most of hazardous road locations (HRL) are for specific sub-categories rather than others. So, safety countermeasures should be differentiated based on the specific VRU sub-category to be protected.

TABLE OF CONTENTS

1. INTRODUCTION

A road traffic crash is a collision or incident that lead to injury, fatality, and/or property damage only occurring on a public road and involving at least one moving vehicle (Peden *et al.*, 2004). Road collisions are one of the leading causes of death in many countries and anyone using the roads is at risk of injury or death in the event of a road accident.

According to World Health Organization (WHO, 2021), road traffic crashes result in the deaths of approximately 1.3 million people around the world each year and leave between 20 and 50 million people with non-fatal injuries. Young people are particularly vulnerable on the world's roads; in fact, road traffic injuries are the leading cause of death for children and young adults aged 5-29. Young males under 25 years are more likely to be involved in road traffic crashes than females, with 73% of all road traffic deaths occurring among young males in that age. In 2016, low- and middle-income countries had higher road fatality rates per 100 000 population (27.5 and 19.2, respectively) compared to high-income countries (8.3). The African region had the highest road traffic fatality rate, at 26.6, while the European region had the lowest rate, at 9.3.

As stated by World Health Organization (WHO, 2021), more than half of all road traffic deaths are among vulnerable road users: pedestrians, cyclists, and motorcyclists due to insufficient physical protection in the event of a collision with cars, trucks or buses. Globally, pedestrians and cyclists represent 26% of all deaths, with those using motorized two- and three-wheelers comprising another 28%. Car occupants make up 29% of all deaths and the remaining 17% are unidentified road users. According to EC (European Comission, 2018), between 2001 and 2010, the number of road fatalities in the EU decreased by 43 percent, and between 2010 and 2017 by another 20 percent. Nonetheless, 25,300 people still lost their lives on EU roads in 2017, equivalent to some 70 lives lost per day, and about 135,000 people were seriously injured, including a large percentage of pedestrians, cyclists and motorcyclists.

More than half of the world's population now live in urban areas — increasingly in highly-dense cities (Ritchie and Roser, 2018). In urban areas, nowadays more and more people prefer walking or cycling to reach their destination instead of taking public transportation or using a car due to traffic problems. This situation makes more people vulnerable due to a high

risk of injury in any traffic collision. Specific solutions for the protection of vulnerable road users not only ensure greater safety in urban traffic but also increase efficiency of the transportation system.

With the developments in technology in recent years, different types of two-wheeled vehicles have changed to mobility. Fuel-powered two-wheelers (motorcycles and mopeds) are a means of transportation that people are accustomed to seeing in urban mobility today, the other is electric-powered two-wheelers (electric motorcycles, pedelec, scooters, and hoverboards) which play a crucial role in urban vehicle ecosystem nowadays. Electric two-wheelers are an environmentally more sustainable alternative to conventional powered two-wheelers. However, the users of both types of vehicles are particularly vulnerable based on accident statistics.

According to EC (European Commission, 2021), as a result of Covid-19 pandemic, cycling has experienced a significant rise in popularity for the last two years, and many cities around the world (temporarily) reallocated road space to cyclists and pedestrians. This encouraging development can have a significant positive impact on air and climate quality but at the same time creates new road safety challenges. EU-wide, around 70% of road fatalities in urban areas involve vulnerable road users. Therefore, tackling road safety in cities is a crucial area of focus for urban mobility planning.

As stated in Horizon Europe - Work Programme (European Commission Decision, 2021), European Commission has allocated a fund for research and innovation actions within the aim of a safer urban environment for vulnerable road users. Project results are expected to contribute to the following expected outcomes:

- 50% reduction in serious injuries and fatalities in road crashes by 2030, with a focus on measures addressing unprotected vulnerable road users,
- better prediction of all road users behaviour and the use of new transport modes,
- new concepts and guidelines for safe inclusion of new types of vulnerable road users, i.e.those using new means of transport into the traffic system,
- new solutions that facilitate inclusion of all vulnerable users in the transport system, including people with disabilities, the elderly, and children by providing a safe environment for walking and cycling,

- a modal shift to active and clean modes of transport, improving the health of road users and the quality of urban environments.

Road traffic crashes are not “accidents” since preventable. The likelihood of traffic collisions can be reduced by using appropriate countermeasures such as traffic monitoring and control devices, managing exposure to risk through transport policies, modifying the road layout, or increasing protection of vehicle occupants. The basis of the most appropriate countermeasure is the safety analysis which concerns the identification of hazardous road locations (HRL), or hot spots, by using evidence-based measures based on crash data. HRL are specific points on the road with higher crash frequency than expected at some threshold level of significance.

Identifying accident hotspots and appending value-added data to understand the processes occurring in these hotspots is important for the appropriate allocation of resources for safety improvements (Anderson, 2009). Safety analyses are carried out by using statistical and spatial analysis tools in Geographic Information System (GIS). GIS-based techniques are relatively simple to use and can convert raw statistical and geographical data into meaningful information for spatial analysis, mapping, and identifying any factors contributing to accidents (Choudhary *et al.*, 2015).

This work presents the application of the spatial analysis methods in GIS Software to identify hazardous road locations (HRL) in Turin using ISTAT data as a case study. Among all accident, the interest is on those where vulnerable road users were involved in. For this purpose, accident data in the period 2006-2019 collected from police records by ISTAT was used. According to the literature, there are two approaches for the spatial analysis of traffic collisions: the link-attribute and the event-based approaches. In the first, spatial events such as traffic crashes are not analyzed directly but assigned to geographic features, such as areas or segments of the road network. In event-based analyzes, traffic collisions are just points in space. In this study, event-based approach is used and this approach consists of distance-based and density-based methods. While distance-based methods (Nearest Neighbor Analysis, G and F functions) evaluate distances between events to define areas where traffic crashes are clustered, density-based methods (Kernel Density Estimation) examine the density of the point patterns to identify hazardous road locations (HRL).

2. SPATIAL ANALYSIS OF ROAD COLLISIONS

This chapter aims to analyze the historical developments in road safety strategies and spatial analysis for road traffic collisions which represent the starting point for any methodological study relating to Road Safety.

2.1. Road Safety in urban areas

According to the UN, in 2018, an estimated 55.3 percent of the world's population lived in urban settlements. By 2030, urban areas are projected to house 60 percent of people globally and one in every three people will live in cities with at least half a million inhabitants (United Nations, The World's Cities, 2018). The rapid increase in population and motorization will cause a close interaction between vulnerable and motorized road users. As a result, the safety of vulnerable road users will be a more prominent issue in the coming years.

In order to understand the development of road safety research, it is important to know how the scientific view has changed during the short history of systematic road safety research. It consists of four phases of scientific paradigms (Loo and Anderson, 2015):

Paradigm I (1900-1925/35) : Control of the automobiles was seen as the problem. There was limited research but more of a description of what was happening. This phase coincided with the rise of the automobiles from the beginning of the twentieth century to 1935.

Paradigm II (1925/35-1965/70) : Control of traffic situations was seen to be the problem. The countermeasures and the research were centered on the classical three "Es" approach of engineering, education, and enforcement. This is when systematic road safety research was born and when a number of new disciplines came into road safety research.

Paradigm III (1965/70-1980/85) : Management of the traffic system was seen to be a problem. In this systems approach, mathematical models for the description and prediction of traffic collisions were developed.

Paradigm IV (1980/85-present) : Management of the transport system as a whole was seen as the problem. The scope is widened from just focusing on the road itself. This is the current trend of road safety thinking.

In industrialised countries, road infrastructure and its environment have been gradually developed to meet the needs of growing traffic and mobility. Their present state reflects the conflicts and compromises between the different transport modes -- particularly between the vulnerable road users and motorised traffic -- the traffic regulations, and the beliefs and doctrines of the engineers responsible for road design and traffic management, particularly with regard to road users' duties and behaviour (OECD, 1998). Anyone using the roads is at risk of injury or death in the event of a road accident. Some people are more at risk than others and are commonly referred to as Vulnerable Road Users (VRU). The term has been defined in different ways:

- World Health Organisation in 2013 considered VRUs to be "pedestrians, cyclists, and motorcyclists"
- US DOT's National Strategy on Highway Safety has a more complex definition: "road users who are most at risk for serious injury or fatality when they are involved in a motor-vehicle-related collision. These include pedestrians of all ages, types and abilities, particularly older pedestrians and people with disabilities. VRU's also include bicyclists and motorcyclists. Older drivers may also be considered to fit into this same user group"
- European Union's ITS Directive refers to "non-motorised road users, such as pedestrians and cyclists as well as motor-cyclists and persons with disabilities or reduced mobility and orientation"

According to Organisation for Economic Co-operation and Development (OECD, 1998), there have been developments regarding VRU in the 1960s and 1970s. Some new residential areas were built by architects and planners on the principle of complete segregation of pedestrians and motorised vehicles, first in Sweden (Scaft guidelines), then in some British new towns.

In the 1980s, the idea of comprehensive networks for pedestrians and cyclists started to make way in some countries, thus acknowledging walking and cycling as full-fledged means of transport. Cycle tracks or cycle lanes were introduced, with various degrees of success or failure from a safety viewpoint. In a number of cities, pedestrian footpaths were organised to provide continuing routes and were often widened and resurfaced. Pedestrianised streets in

city centres became better integrated into overall schemes aimed at providing better mobility for all with less private car traffic.

The concepts of mixed traffic and traffic calming spread and extended from the previous schemes in residential areas to the treatment of urban thoroughfares with heavy traffic. The idea that fast motorised traffic may have to yield priority to local traffic and vulnerable road users through some parts of urban areas generating a lot of activity onto the street finally became acceptable. Such form of transport planning usually implies operating modal transfers from motorised road transport to rail and non-motorised means. VRU should thus get better attention.

Today the growing view is that road safety is a system-wide and shared multi-sectoral responsibility which is becoming increasingly ambitious in terms of its results focus. Sustaining the level of ambition now evident in high-income countries requires a road safety management system based on effective institutional management functions that can deliver evidence-based interventions to achieve desired results.

The road safety management system as depicted in Figure 2.1 can be viewed as three inter-related elements: institutional management functions, interventions, and results. Managing for road safety results requires an integrated and accountable response to these system elements (Bliss and Breen ,2009).

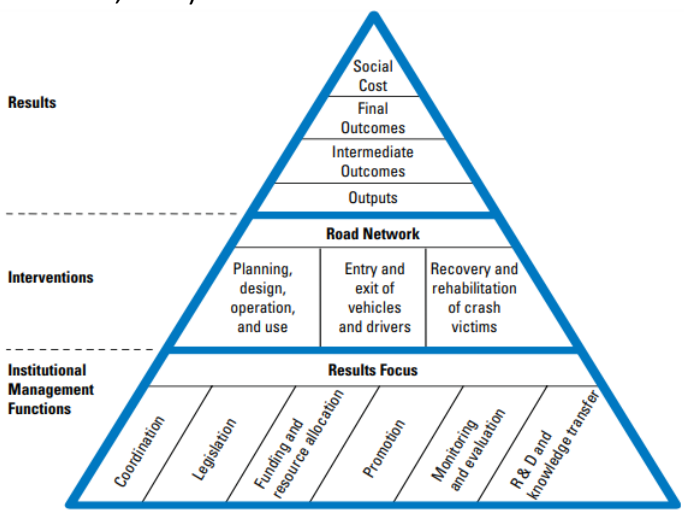

Figure 2.1 : Road Safety Management System *(Bliss and Breen, 2000; Wegman, 2001; Koornstra et al, 2002; Bliss, 2004)*

2.2. Spatial Autocorrelation Analysis

Spatial analysis of traffic crashes is a fundamental study in road safety because it helps to understand how crashes are affected by locations, how the parameters vary spatially, and which areas need priority for countermeasures. It is the most preferred technique for road safety analysis in recent years since it provides a depth analysis instead of a simple visual evaluation.

Collision events are records in a 2D space, which can be expressed in geographic terms (longitude, latitude), in cartographic (East, North) coordinates, or in the local plane (X, Y), (Bassani *et al.*, 2020). GIS stores information as thematic layers, all linked by their geographic coordinates. Unlike standard databases, GIS allows users to compare and manipulate data based on the spatial relationships. In this way, it is possible to manage the large amount of crash data which can be visualized with high resolution on the maps thanks to GIS software. GIS tools provide to identify the locations where accidents are clustered, or where the consequences of such events reach the critical threshold, while also evaluating the attributes of the data associated with each element.

Traffic accidents are random events that vary in time and space. The number of accidents varies from month to month and year to year in the road network. Although there may be a spatial dependence between the accidents, the distribution of traffic collisions is not uniform in space. To evaluate this spatial dependence between events, the so-called distance-based methods are used, which define the presence of spatial aggregations of accidents in the road network.

Moreover, it is also possible to evaluate accidents in restricted areas as cluster events, to understand which points on the network have a higher incidental density. These points can be defined as *hazardous road locations (HRL)* due to the higher expected number of accidents than other locations. Therefore, in addition to the distance-based methods, the density-based approach is used to assess high densities in certain areas for identifying hazardous road locations. In this way, it is possible to evaluate whether high densities in certain areas are the consequence of specific characteristic of the road environment. Generally, when increasing the level of granularity of the analysis, the correlation between output areas will become weaker. This introduces another issue in road safety analysis, that is the spatial

autocorrelation (Loo and Anderson, 2015). Spatial autocorrelation refers to the extent to which the value of a variable at a given location influences values of that variable at contiguous locations (Cliff & Ord, 1973; Goodchild, 1986; Griffith, 1987; Odland, 1988). If positive spatial autocorrelation is present, it results in a spatial clustering of similar variable values (Black, 1991). It means that two traffic collisions occurring close to each other may be caused by the same reason. By identifying the reason, it is possible to take precaution to prevent accidents (reduction of the frequency of occurrence) or reduce its consequences (reduction of incidental severity).

Approaches to identify positive spatial autocorrelation can be divided into two major groups (Loo and Yao, 2013):

- link-attribute approach,
- event-based approach.

In the first approach, spatial events such as traffic crashes are not analyzed directly but are instead assigned to geographic features, such as areas or a road network. Traffic crashes are assigned to line and point features, namely roads (links) and junctions (nodes). Links are, in turn, divided into shorter segments called basic spatial units (BSUs) for detailed spatial analysis. Traffic crash numbers or rates are treated as attribute values of these geographic features (Loo and Yao, 2013). Both geometric (such as road width and gradient) and nongeometric features (such as traffic volume and presence of road markings) of the BSUs can be stored in the relational database of the road network. The link-attribute approach provides to analyze traffic collisions by considering them as attributes of the road features. Traffic collisions are treated as attributes of these base spatial units; information from different databases is integrated: collision, hospital, traffic, land use.

The link-attribute methodologies allow deriving some spatial statistics that provide information on the degree of aggregation of points, showing the areas where concentrations are higher than the threshold. The main spatial statistics relating to this approach are the Moran's I and the Getis-Ord General G. Generally, Moran's I is the most common spatial statistics since it is at the global level (Loo and Anderson, 2015).

On the other hand, in event-based analyzes, collisions are just points in space. The link-attribute approaches, as mentioned, involve segmentation of the road network as base

space units (BSUs). By counting the crashes within them, collisions become attributes of these segments. However, these operations involve a significant computational effort, and entail different difficulties: (i) the correct choice of the BSU length, (ii) the impossibility of dividing different parts of a road network into segments of equal sized length, (iii) the difficulty with the interpretation of data from sections with different length, and (iv) the consequent loss of information (Bassani *et al.*, 2020).

Event-based approaches consist of distance-based and density-based methods. Road collisions being dealt with as two-dimensional (2D) point patterns, where the data are only locations of a set of point objects. This represents the simplest possible spatial data (Loo and Anderson, 2015). While distance-based methods that examine distances between events, density-based methods that examine the crude density or overall intensity of a point pattern (O'Sullivan and Unwin,2003).

The most common methodology of the density-based methods is the *"Kernel density estimation"*. This methodology is a spatial interpolation technique that estimates the density of points in the 2D plane with coordinated (ϕ , λ), (E, N) or (X, Y) for each collision event. By cumulating the values, the final density estimation in the related area is obtained. A detailed description of the methods is introduced in Section 3.3.

2.3. Software tools

The different methodologies described in the previous paragraphs are applied with the help of the QGIS, ArcGIS and R software. QGIS is an open geographic information system (GIS) source, released under the GNU General Public License (GPL); it is used for the management of the huge amount of data, providing adequate tools for data processing.

Another well-known software for GIS services is ArcGIS developed and maintained by Esri. ArcGIS is a command line-based GIS system for manipulating data. ArcGIS provides great insights using contextual tools to visualize and analyze your data. ArcGIS Desktop consists of several integrated applications, including ArcMap, ArcCatalog, ArcToolbox, ArcScene, ArcGlobe, and ArcGIS Pro. ArcMap is the application used to view, edit and query geospatial data, and create maps. It helps to collaborate and share via maps, apps, dashboards, and reports.

R software is a programming language for statistical analysis that can be used by integrating it into QGIS and ArcGIS. Series of algorithms extend its functionality. In this way, it can be used for the analysis of geographic data. Thanks to the “Processing R Provider” extension, it is possible to use R in QGIS. R uses external libraries (called "packages") that expand its functionality. In the present study, it was necessary to install some packages (abind, tensor, goftest, proxy, DBI, Rcpp, classInt, rgdal, sp, spatstat) for the point pattern analysis.

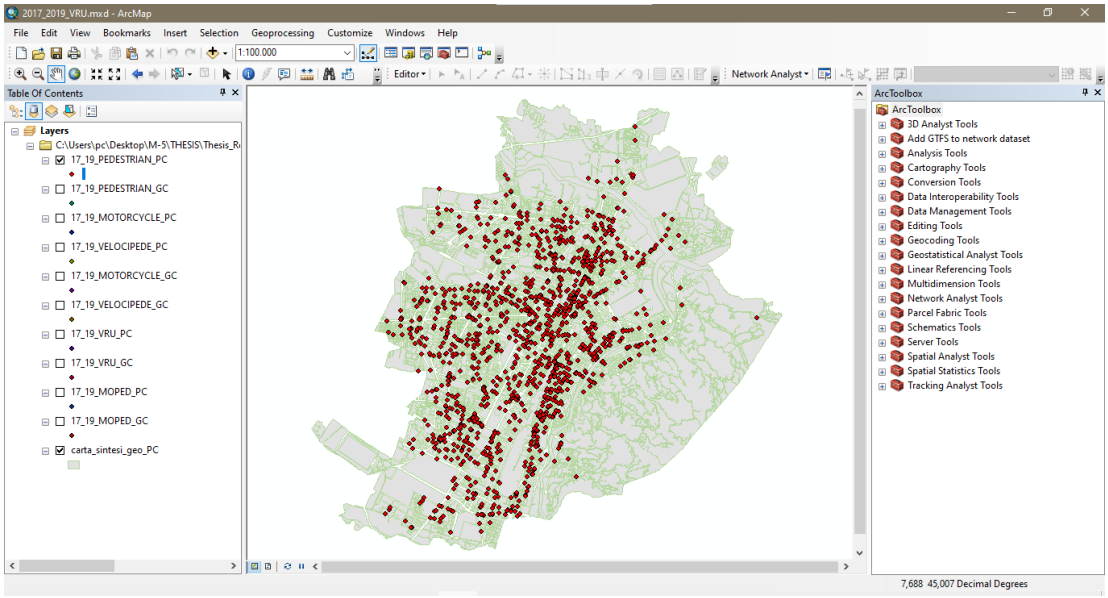

(a)

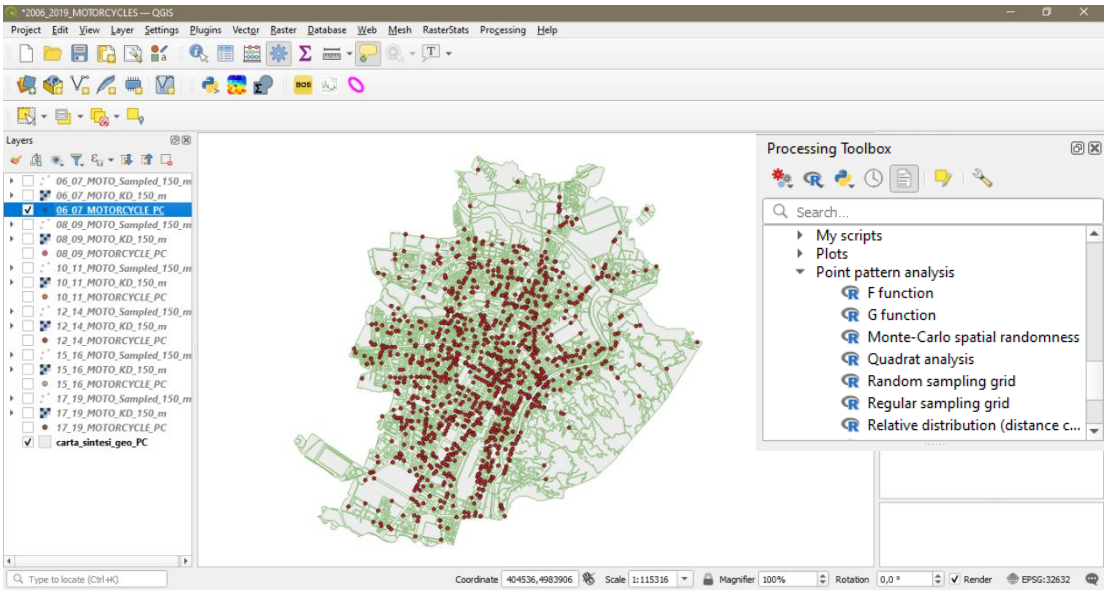

(b)

Figure 2.2 : Interfaces of the software’s : (a) ArcGIS, (b) QGIS & “Processing R Provider” extension

3. MATERIALS AND METHODS

This chapter concerns the definition of the case study, procedures for the acquisition and processing of incidental data, and the methods for spatial analysis of traffic crashes that are developed in the case study. While the first part of this chapter is related to the description of the case study, the second part provides method for the acquisition and processing of crash data relating to the period 2006-2019 for the city of Turin.

The third part of this chapter illustrates the methods for analyzing the spatial distribution of traffic crashes including VRU to identify the HRL in Turin. As explained in Chapter 2.2., there are two methodologies: the first is the Link-Attribute approach that considers accidents as attributes of linear elements such as road segments; the second one is the Event-Based approach, in which accidents are considered as a set of points in space. In this case study, methods of the Event-Based approach which are given below are used:

- distance-based methods,
- density-based methods.

The results of these analyses for the Turin case study are presented in Chapter 4.

3.1. The Case Study

3.1.1. Area of Study

One of the largest metropolitan cities in Italy, Torino has been chosen as a study area. Turin is an Italian municipality of 842,612 inhabitants (ISTAT, August 2021), the fourth Italian municipality by population and capital of the Piedmont Region. The infrastructural network of the central area of the city has as a plan like a chessboard. The roads develop in a straight line crossing orthogonally, with an orientation similar to the Roman castrum: a cardo maximus (north-south direction) and a decumanus maximus (east-west direction) are crossing at the center of the castrum, and parallel to which develop all the other streets inside the castrum. The exception is the eastern side, where the structure of the road network is conditioned by the presence of the Turin hills. The chessboard layout considerably facilitates orientation. Thanks to the large tree-lined avenues (which naturally follow the directions of the other streets), it also makes mechanized circulation, both public and private transport, smoother.

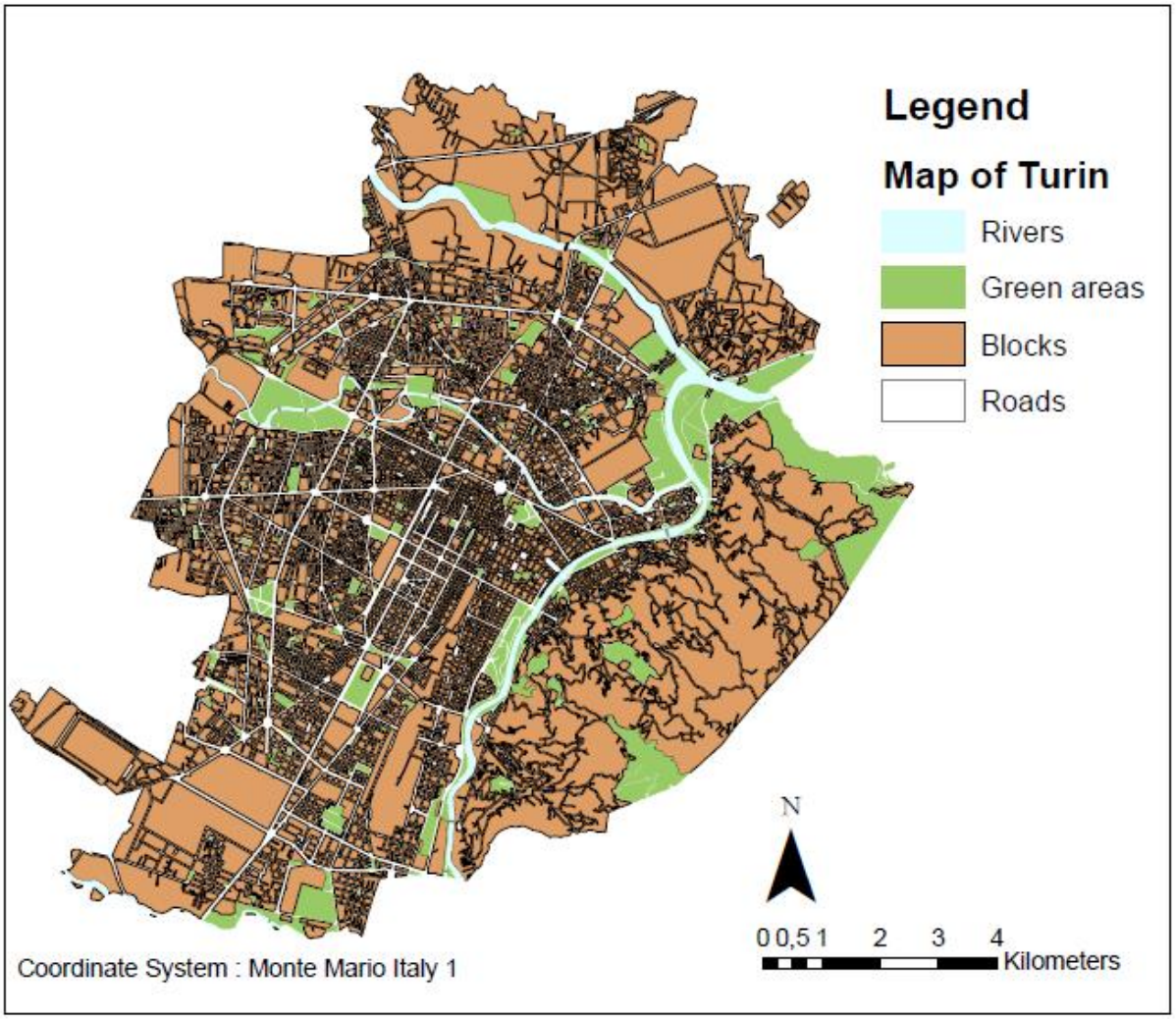

Fig 3.1 : Map of the city of Turin *(Shapefile "Carta di sintesi" from Geportale Regione Piemonte)*

3.1.2. Description of the Case Study

This study deals with the spatial analysis of traffic crashes from 2006 to 2019 that involves only VRU (pedestrians, cyclists, and motorcyclists, etc.) in Turin. The main aim of this case study is the identification of HRL where the number of accidents is abnormally high in Turin, by using Geographic Information Systems (GIS) with the help of QGIS, ArcGIS, and R Software. The database which is related to the traffic accidents in Turin was obtained from ISTAT. Acquisition and Processing of Incidental Data are introduced in the next section. Specifically, distance-based methods are applied to verify the clustering of the spatial pattern of points (point pattern); subsequently, we proceeded with the application of the Kernel density estimation that allows the identification of the critical points of the road network.

3.2. Acquisition and Processing of Incidental Data

The final database from the regional collision database provided by ISTAT (Italian National Institute of Statistics), which involves only VRU in the period from 2006 to 2019 for the city of Turin, was obtained through the following activities:

1. extraction of traffic collisions only involving VRU,
2. geolocation of accidents in a GIS system,
3. database formation for the analysis of the spatial distribution of accidents.

The results of descriptive analyses are shown in Chapter 4.1.

3.2.1. Traffic collisions involving Vulnerable Road Users (VRU)

The incidental database of Italy has been obtained thanks to ISTAT for the years from 2006 to 2019. According to the definition of a traffic accident adopted from the ISTAT, the database contains only accidents that involve at least one injured person. In Italy, traffic accidents that only result in material damage (i.e., the property damage only crashes) are not considered statistically as an accident.

In the database, the rows (records) are related to individual incidents while the columns (fields) present a series of information like accident location, nature of the accident, vehicles involved, users involved, consequences, etc. The following paragraphs describe the various operations carried out to obtain the final database, containing only the incidental events of interest for the case study.

In the first place, it was necessary to filter only incidents relating to the Piedmont Region, Turin's Province, and the Municipality of Turin. The Crash database of the Piedmont Region was created by filtering province numbers of Piedmont region (001 : Turin, 002: Vercelli, 003: Novara, 004: Cuneo, 005: Asti, 006: Alessandria, 096: Biella,103: Verbano-Cusio-Ossola) while Province and Municipality of Turin database are extracted by filtering the number of 001 for the Province of Turin and the number of 272 for the Municipality of Turin.

Fig 3.2 : ISTAT identification codes; Province -blue box , Municipality- red box *(retrieved from ISTAT Database)*

Once the incidents relating to the Municipality of Turin have been selected, it was proceeded with the identification of accidents involving only VRU. The different definitions of VRU are explained in Section 2.1. In this current study, pedestrians, velocipede [1] , moped and motorcycle users are evaluated as VRU. The information relating to those users was filtered in the excel file obtained from ISTAT. This process was carried out by using the code numbers of those users:

• "natura_i" is related to the nature of the accident: selected records are a value of 5 in this field (5 = Pedestrians involved);

• "type_vA", "type_vB" and "type_vC" are related to the type of vehicle involved: all the records in which at least a "vulnerable" user in these three fields, a value between 14 and 17 (14 = Velocipede, 15 = Moped, 16 = Motorcycle alone, 17 = Motorcycle with passenger);

• "pm1_sex", "pm1_eta", "pf1_sex", "pf1_eta", "pm2_sex", "pm2_eta", "Pf2_sex", "pf2_eta", "pm3_sex", "pm3_eta", "pf3_sex", "pf3_eta", "Pm4_sex", "pm4_eta", "pf4_sex" and "pf4_eta", referring to any pedestrians involved in the accidents: all the records have selected to find the presence of at least one injured / dead pedestrian.

In the ISTAT database, there is an inconsistency between the nature of the accident (5=Pedestrians involved) and pedestrian fields. The number of accidents coming from the nature of the accidents does not coincide with the number of accidents relating to the pedestrians' fields. This apparent inconsistency comes from the ISTAT database. So,

[1] Velocipede is a human-powered land vehicle with one or more wheels, the most common type today is the bicycle.

pedestrian fields are used directly to obtain the number of accidents in which pedestrians are involved.

3.2.2. Geolocation of accidents

The database from 2006 to 2016 was taken from the previous study carried out by Bassani, M., Rossetti, L., and Catani, L. in 2018. In the current study, the database for the period 2017-2019 was obtained by ISTAT includes only the address information of the accidents. Therefore, GPS Visualizer's Address Locator was used to convert addresses of accidents into geographic coordinates; this was done through a JavaScript-On-Demand (JSON) code executed by the web browser, capable of take advantage of the APIs (Application Programming Interfaces) provided by various mapping (Google Maps, Bing Maps, etc.).

A total of 3916 street addresses for the period 2017-2019 were converted to geographic coordinates (Latitude, Longitude). The coordinate information of addresses was obtained by entering all address information on website as in Figure 3.4. An excel file containing all information was prepared to this scope.

Figure 3.3 : Interface of GPS Visualizer's Address Locator (*http://www.gpsvisualizer.com/geocoder/*)

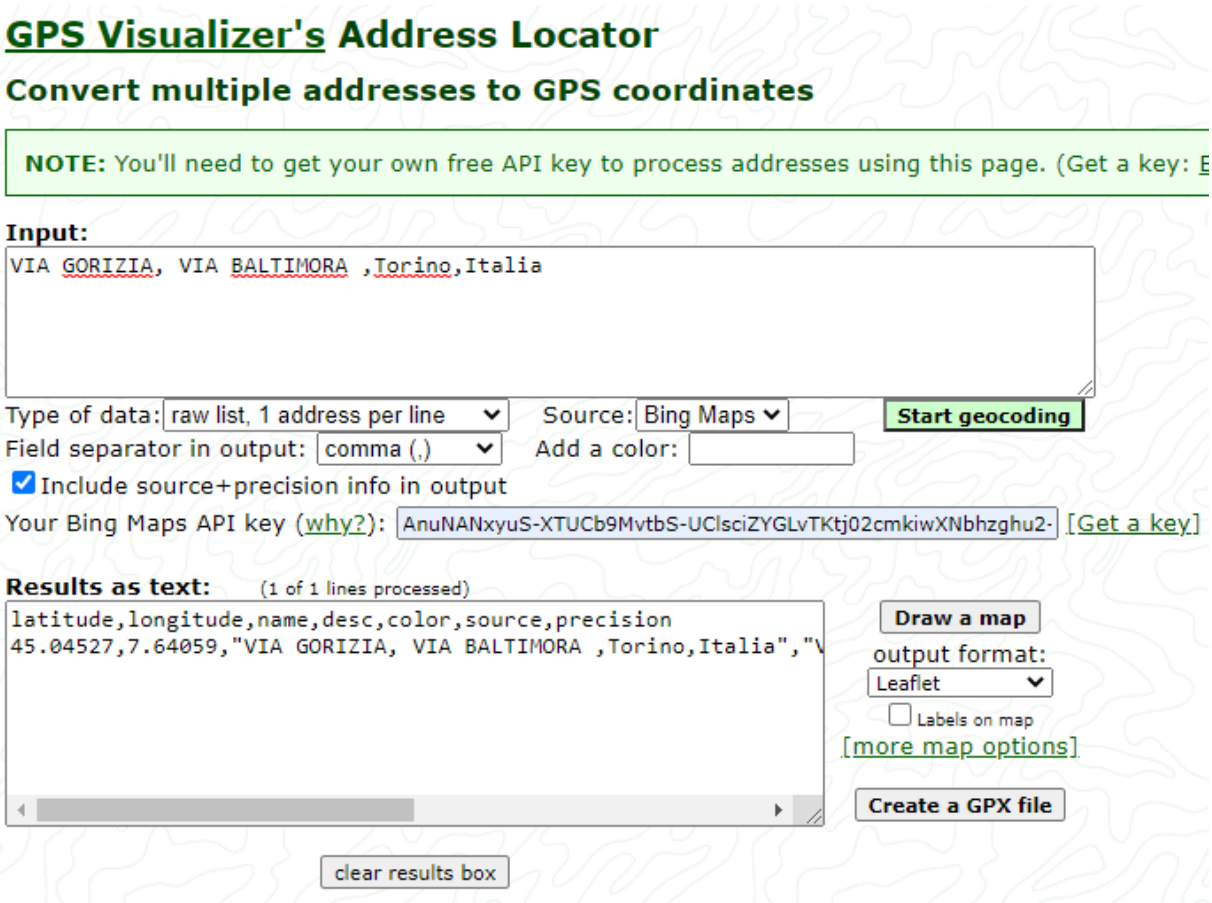

Figure 3.4 : The example for the usage of GPS Visualizer's Address Locator

For intersection points, generally, the coordinate information of addresses are directly correct but some addresses include building number information to refer to the location of the accidents (e.g., Via Pietro Cossa, 68, Torino, Italia). To fix these kinds of addresses and eliminate wrong address and coordinate information in the database, each coordinate information was checked by Google Maps as indicated in Figure 3.5(a). If there is an apartment number in the address, the point in the street where the building is 90 degrees perpendicular to the street was chosen (Figure3.5 (b)). At the end of this operation, 181 out of 3,916 accidents (approximately 5%) were eliminated from the crash database of VRU for the period 2017-2019.

The information relating to the final database is given in Section 4.1.1.

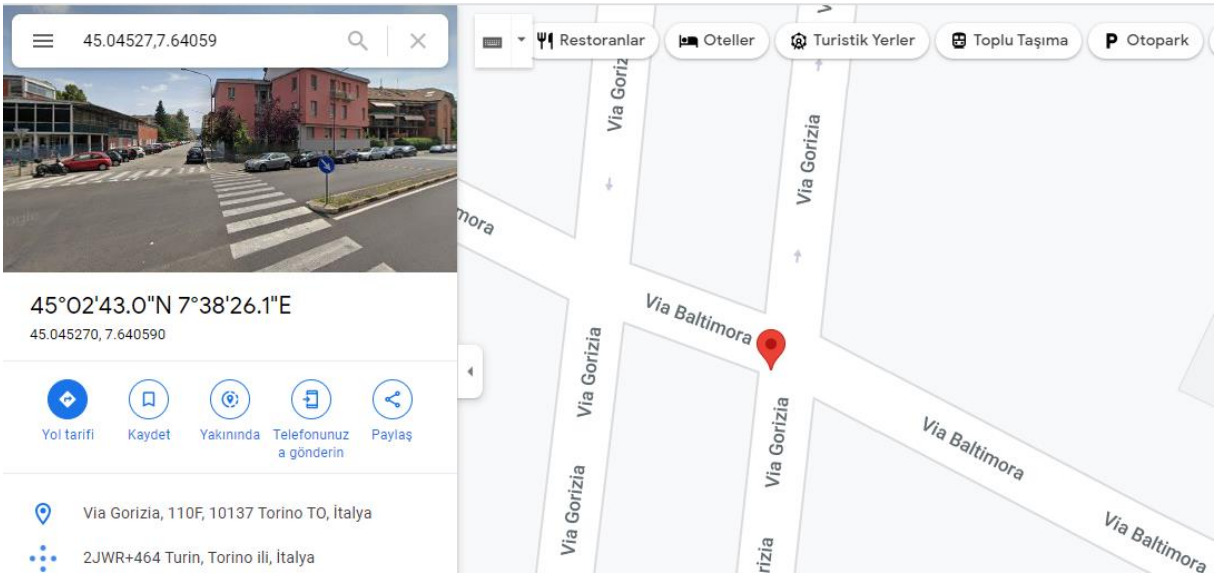

(a)

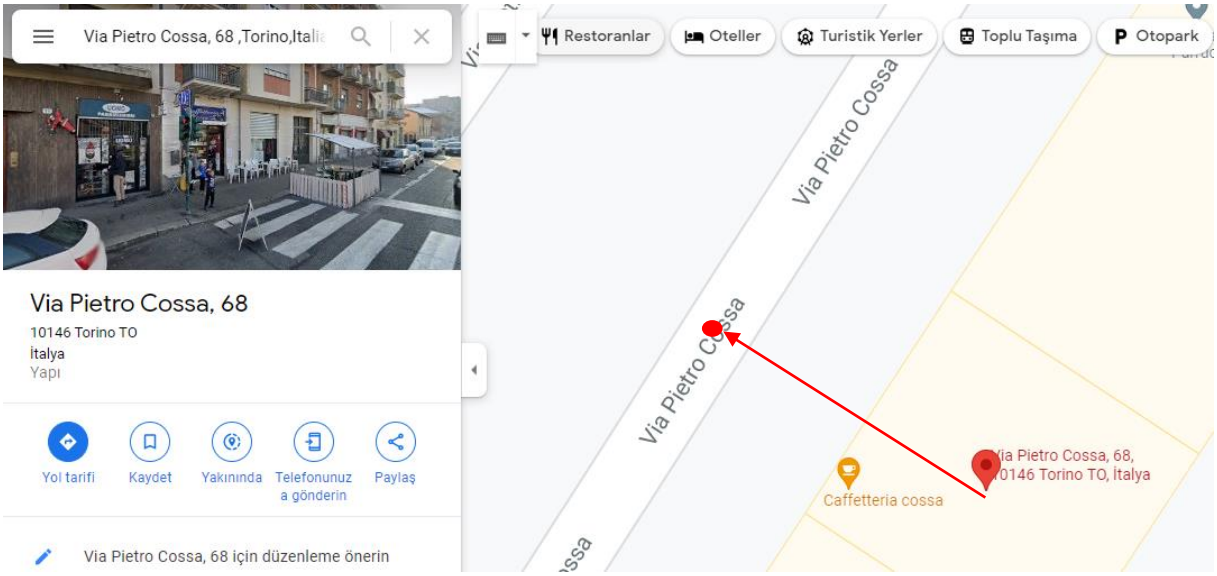

(b)

Figure 3.5: The example for the usage of Google Maps

3.3. Methods of Spatial Distribution Analysis

This chapter introduces the event-based methods which were used in the case study to identify HRL. The event-based approach considers the physical locations of individual crashes (events) directly (Yamada and Thill, 2007). When the event-based approach is used to identify local clusters, this goal is accomplished by directly measuring the (physical or network) distance or the degree of concentration among the traffic crashes (Loo and Yao, 2013).

Event-Based methods are divided into two groups:

- Distance-based,
- Density-based.

3.3.1. Distance-based Methods

Among the different distance-based methods, the Nearest Neighbor Analysis, G Function and F function are applied in the present study. In this way, it is possible to identify spatial aggregations of a set of points that are clustered or uniformly spaced.

3.3.1.1 Nearest Neighbor Analysis

Nearest Neighbor analysis is commonly used to analyze point pattern datasets based on distance. This analysis leads to the determination of the Nearest Neighbor (NN) index. This index provides an indication for the degree of aggregation of the points.

According to the Nearest Neighbor (NN) method (Clark and Evans, 1954), in a random distribution of a set of points on a given area, it is assumed that any point has the same chance of occurring on any sub-area as any other point, that any sub-area of specified size has the same chance of receiving a point as any other sub-area of that size, and that the placement of each point has not been influenced by that of any other point. Thus, randomness as here employed is a spatial concept, intimately dependent upon the boundaries of the space chosen by the investigator.

A nearest neighbor analysis compares the characteristics of an observed set of distances between pairs of closest points with distances that would be expected if points were randomly placed. During the analysis, the distance from each point to its nearest neighbor is calculated. This value gets added to a running total of all minimum distances, and once every point has been examined, the sum is divided by the number of points. This produces what we call a “mean minimum distance” or “nearest neighbor distance” (Loo and Anderson, 2015).

The equation is given in the below :

$$\bar{d}_{obs} = \frac{\sum_i^n d_{ij}}{n} \tag{3.1}$$

where

- $\bar{d}$= observed mean distance from the nearest point;
- d_{ij} = distance between the point i and its nearest j;
- n = number of points in the dataset.

The expected mean distance under the hypothesis of random arrangement of the points for the considered area (Complete Spatial Randomness - CSR) can be also calculated through the following equation:

$$\bar{d}_{exp} = \frac{0{,}5}{\sqrt{n/a}} \tag{3.2}$$

- $\bar{d}$= expected mean distance from the nearest point;
- n = number of points under study;
- a = the size of the area under study.

The ratio of the observed mean distance to the expected mean distance serves as the measure of departure from randomness (Clark and Evans, 1954). This ratio is called Nearest Neighbor Index. It is the measure of the degree to which the observed distribution departs from random expectation with respect to the distance to nearest neighbor.

It can be evaluated as :

$$\text{difference : } d = \bar{d}_{obs} - \bar{d}_{exp} \tag{3.3}$$

$$\text{ratio: } r = \bar{d}_{obs}/\bar{d}_{exp} \tag{3.4}$$

Depending on the value of this index, three different "structures" of points (Point Patterns) can be obtained, as shown in Tab. 3.1 and in Fig. 3.6:

1. *Clustered*: many points are concentrated close together, and large areas that contain very few, if any, points (attraction);
2. *Random:* any point is equally likely to occur at any location and the position of any point is not affected by the position of any other point;
3. *Uniform (regular/dispersed):* every point is as far from all of its neighbors as possible(repulsion).

Table 3.1: Possible values of the NN index and difference

Pattern	d	r
Clustered	<0	<1
Random	=0	=1
Uniform	>0	>1

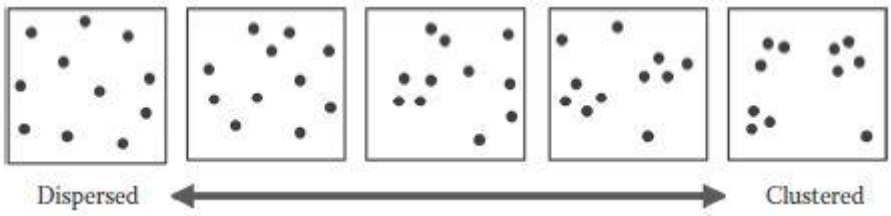

Fig 3.6 : Diagram showing patterns of dispersion to being clustered *(Loo and Anderson, 2015)*

This process leads to the identification of a structure of point patterns. However, the usefulness of any measure of spacing will be increased if its reliability can be ascertained (Clark and Evans, 1954). Therefore, it is better to conduct a statistical test that gives information about the level of statistical significance for significant patterns in the data.

The statistical test begins by identifying the problem in terms of a hypothesis about the parameter under study. The hypothesis to be tested is called the null hypothesis (H_0). In the present study, the null hypothesis predicts that the events exhibit complete spatial randomness (CSR) either of the features themselves or of the values associated with those features . The z-scores and p-values gives an information about whether you can reject that null hypothesis or not. Both z-scores and p-values are associated with the standard normal distribution.

Z-scores are standard deviations, which provide a numerical measure among the observed value and the expected value related to the null hypothesis; specifically, the extent of the observed value differs from the expected one. The value of the Z-score can be determined with the formula given below:

$$Z = \frac{\bar{d}_{obs} - \bar{d}_{exp}}{SE} \tag{3.5}$$

where $\bar{d}_{obs}$ is the mean “observed” distance from the nearest point, $\bar{d}_{exp}$ is the mean "expected" distance from the nearest point and, SE is the standard error of the mean distance

to the nearest neighbor in a randomly distributed population of the same density as that of the observed population. The value of SE can be calculated from the formula given below:

$$SE = \frac{0{,}26136}{\sqrt{\frac{n^2}{a}}} \tag{3.6}$$

where n is the number of observations and a is the surface of the study area.

The p-value is a probability. For the pattern analysis tools, it is the probability that the observed spatial pattern was created by some random process. When the p-value is very small, it means it is very unlikely (small probability) that the observed spatial pattern is the result of random processes, so the null hypothesis can be rejected. The range of the z-score and p value depend on the confidence level. Typical confidence levels are 90, 95, or 99 percent.

Table 3.2: The criteria of z-score, p-value, and confidence level *(Shi et al., 2019)*

z-score	p-value	Confidence Level
<-1.65 or >1.65	< 0.10	90%
<-1.96 or >1.96	< 0.05	95%
<-2.58 or >2.58	< 0.01	99%

For a level of 95% confidence, the limits of the interval are ± 1.96; by values falling outside of this range we have:

- z-score > 1.96: dispersed pattern,
- z- score <-1.96: clustered pattern.

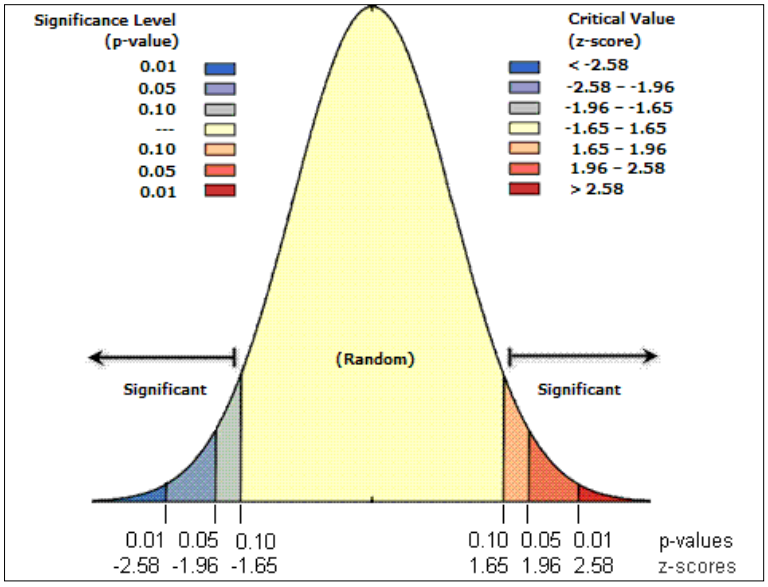

Fig 3.7 : Average nearest neighbor analysis indicates a clustering pattern based on the z-score and p-value(*https://pro.arcgis.com/en/pro-app/2.8/tool-reference/spatial-statistics/what-is-a-z-score-what-is-a-p-value.htm)*

Fig. 3.7 shows the trend of the parameter r that is computed by the ratio between the observed and expected NN distance under the hypothesis of random spatial distribution (CSR). The yellow band is relative to the confidence interval that declares the randomness in the distribution of the point patterns. Thanks to the contribution of the NN index and the statistical test, it is possible to identify point patterns that are clustered, random, or uniformly spaced as seen in Fig. 3.8.

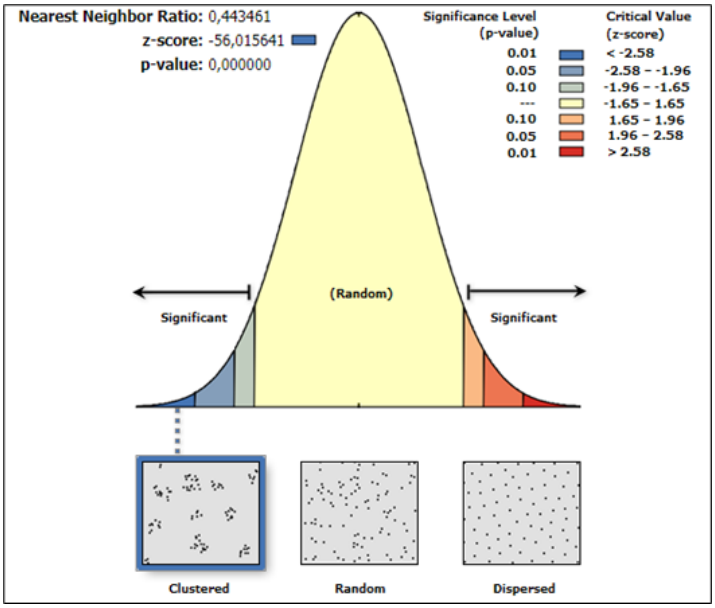

Fig 3.8 : The output of Nearest Neighbor Analysis from ArcGIS Software for the 2015-2016 crash data

3.3.1.2 G and F functions

G and F functions are an extension of the Nearest Neighbor approach. The G function, sometimes called the refined nearest neighbor, is the simplest. G function uses the same information contained in NN analysis, but instead of summarizing it using the mean, we examine *the cumulative frequency distribution* of *the nearest-neighbor distances* (O'sullivan and Unwin, 2010). Formally, this is defined as

$$G_d = \frac{\#(d_{min}(s_i) < d)}{n} \tag{3.7}$$

where the value of G for any particular distance, d, tells us what fraction of all the nearest-neighbor distances in the pattern is less than d. An explanatory example of this method is shown in Fig. 3.9.

The information related to Fig 3.9 in above:

(a) the nearest neighbor for a small point pattern. The nearest neighbor to each event lies in the direction of the arrow pointing away from it.

(b) calculations for the NN distances for the point pattern shown in (a).

(c) the G function for the point pattern of (a) and (b).

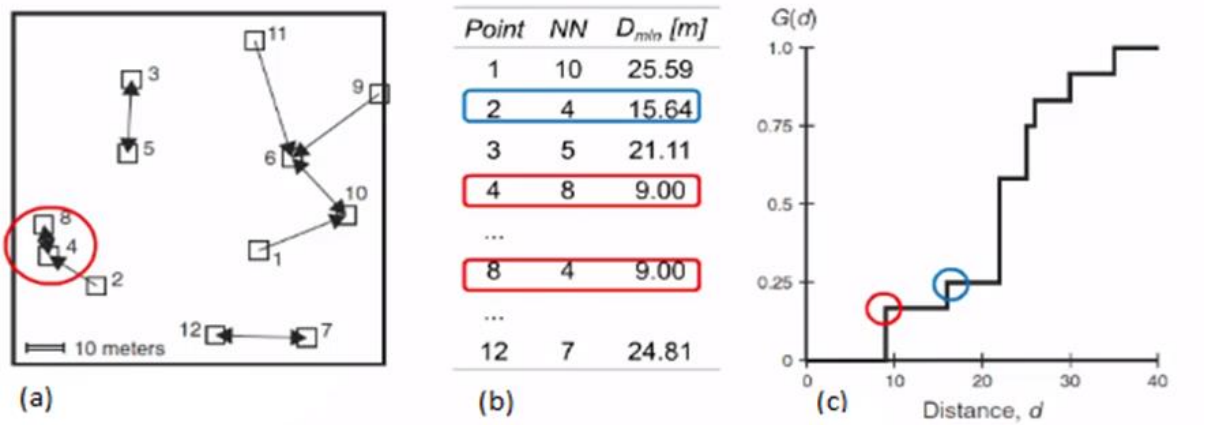

Fig 3.9 : Application of NN analysis and G function *(O'sullivan and Unwin, 2003)*

The shortest nearest-neighbor distance is 9.00 between events 4 and 8. Thus, 9.00 is the nearest-neighbor distance for two events in the pattern. Since 2 out of 12 is a proportion of 2/12=0.167, G(d) at distance d=9.00 has the value 0.167. The next nearest-neighbor distance is 15.64, for event 2, and three events have nearest neighbors at this distance or less. Since 3 out of 12 is a proportion of 0.25, the next point plotted in G(d) is 0.25 at d=15.64. As d increases, the fraction of all nearest-neighbor distances that are less than d increases. This process continues until we have accounted for all 12 events and their nearest-neighbor distances.

The shape of this function tells us a lot about how events are spaced in a point pattern:

- if events are closely clustered together, G increases rapidly at short distances;
- if events tend to be evenly spaced, G increases slowly up to the range of distances at which most events are spaced, and only then increases rapidly.

The F function is closely related to G but may reveal other aspects of the pattern. Instead of accumulating the fraction of nearest-neighbor distances between events in the pattern, point locations anywhere in the study region are selected at random, and the minimum distance from these locations to any event in the pattern is determined. The F function is the cumulative frequency distribution of shortest distances from random points to nearest events. If {p1. . .pi. . .pm} is a set of *m* randomly selected locations used to determine the F function, then formally

$$\mathrm{F_d} = \frac{\#[d_{min}(\mathrm{p_i}, \mathrm{S}) < \mathrm{d}]}{\mathrm{m}} \tag{3.8}$$

where $d_{min}(p_i; S)$ is the minimum distance from location p_i in the randomly selected set to any event in the point pattern S (O'sullivan and Unwin, 2010).

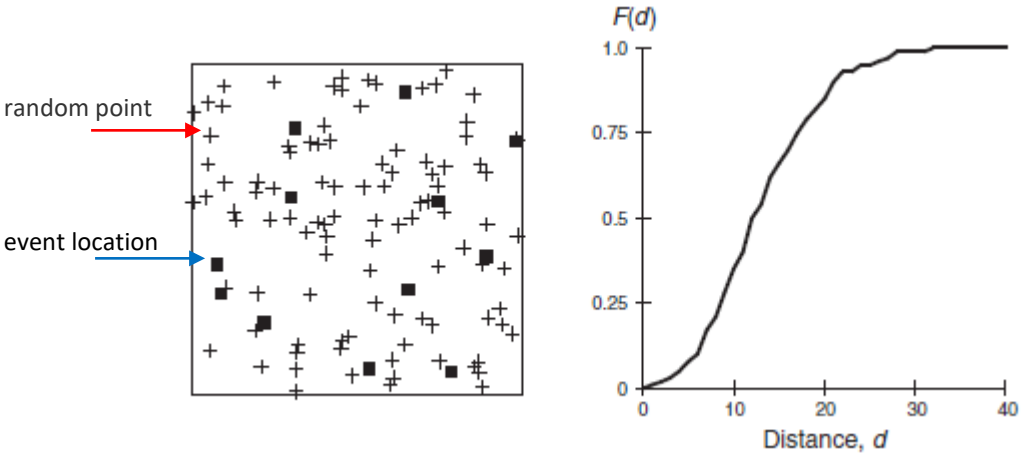

Fig 3.10 : Random points (shown as crosses) for the same point pattern as before and the resulting F function *(O'sullivan and Unwin, 2003)*

One advantage of the F-function over the G function is that we can increase the sample size of random points to get a smoother cumulative frequency curve. The shape of the F function also indicates the type of spatial arrangements of events:

- if events are closely clustered together, F-function increases slowly at short distances but more rapidly at longer distances. This is due to a good portion of the study area being empty. Therefore, many random point locations are long distances from the nearest event in the pattern.
- if events tend to be evenly spaced, F-function rises quickly at short distances as many random points are placed in proximity of the observed events. In this case, most random point locations are relatively close to an event.

The difference between the F and G functions is that they behave differently for clustered and evenly spread patterns. While G shows how close together events in the pattern are, F relates to how far events are from arbitrary locations in the study area. So, if events are clustered in a corner of the study region, G rises sharply at short distances because many events have a very close nearest neighbor. The F function, on the other hand, is likely to rise slowly at first, but more rapidly at longer distances, because a good proportion of the study area is empty, so that many locations are at quite long distances from the nearest event in the pattern. Fig 3.11 is an example to show the relationship between G and F functions.

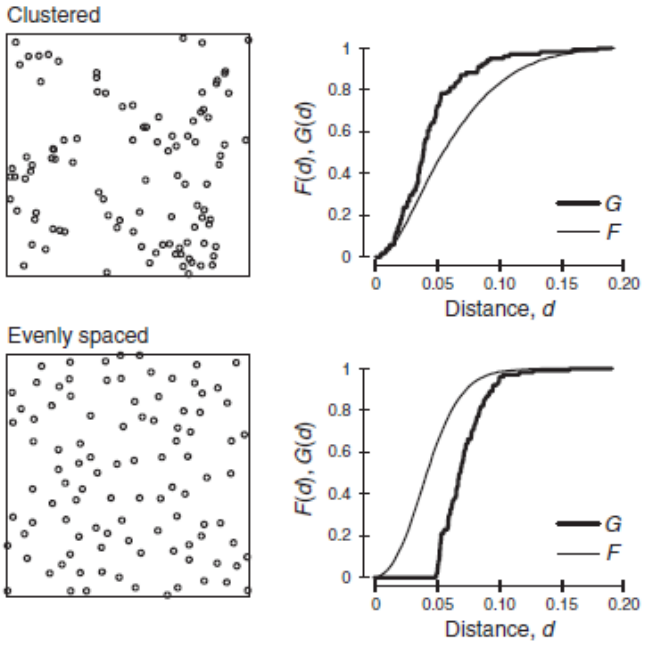

Fig 3.11 : Comparing F and G functions for clustered and evenly distributed data *(O'sullivan and Unwin, 2003)*

In Figure 3.11, the upper example is clearly clustered. As a result, most events (around 80% of them) have close near neighbors, so that the G function rises rapidly at short distances up to about 0.05. In contrast, the F function rises steadily across a range of distances. The lower example is evenly spaced, so that G does not rise at all until the critical spacing of about 0.05, after which it rises quickly, reaching almost 100% by a distance of 0.1. The F function again rises smoothly in this case. Note that the horizontal scale has been kept the same in these graphs. The important difference between the two cases is the relationship between the functions, which is reversed (O'sullivan and Unwin, 2003).

3.3.2. Density-based Methods

Density-based methods allow assessing high densities in certain areas for identifying HRL. Cluster location identification is useful to take action based upon the location of one or more closers. In this way, it is possible to explain collisions as being a consequence of shared common characteristics in the surrounding area. In the present study, Kernel Density Estimation (KDE) is used.

3.3.2.1. Kernel Density Estimation(KDE)

Kernel Density Estimation is an exploratory method to identify the location of clusters as areas of high local event densities. The concept is that the event pattern has a density at any location in the study region and not just at locations where there is an event. This principle results in continuous surfaces of density estimates. Kernel density estimation methods have a variety of applications including exploratory point data analysis, point data smoothing and, the creation of continuous surfaces from point data.

KDE estimates the event density by counting the number of events in a region, called *"kernel"*, and it is centered at the location where the estimate is to be made. KDE allows to identify the location of point clusters (areas with a high density of events). In road safety research, kernel density estimation is an interpolation technique, which is a method for generalizing collision locations (points) to an entire area (Silverman 1986; Bailey & Gatrell, 1995). In this way, the collision point data interprets in the form of a density surface.

Kernel density estimation involves placing a symmetrical surface over each point and then evaluating the distance from the point to a reference location based on a mathematical function and then summing the value for all the surfaces for that reference location. This procedure is repeated for successive points (Loo and Anderson, 2015).

This method therefore allows to place a kernel over each observation, and summing these individual kernels gives us the density estimate for the distribution of collision points (Fotheringham *et al.,* 2000).

The KDE equation is (Fotheringham *et al.,* 2000):

$$\hat{f}(u,v) = \frac{1}{nh^2}\sum_{i=1}^{n} K(\frac{d_i}{h}) \quad (3.9)$$

- (u, v) is the density estimate at the location (u, v) ,
- n is the number of observations,
- h is the bandwidth or kernel size,
- K is the kernel function,
- d_i is the distance between the location (u, v) and the location of the *i*-th observation.

The Crashes within the kernels are weighted based on their Euclidean distance from the kernel center, and the resulting density value is assigned to that center (Mohaymany *et al.*, 2013). The distance is weighted according to a kernel function which was displayed by K in Equation (3.9). KDE functions are used to weigh nearby events more heavily than distant ones in estimating the local density. Many different kernel density functions exist. Their symmetric functions are centered at zero with an area underneath that equals one. The units along the horizontal axis of kernel density functions are multiples of bandwidth.

The kernel function K (e.g., uniform, triangle, quartic, etc.) as shown in Fig 3.12. defines the shape of the humps to be placed over individual observations, and the bandwidth controls their widths. In this way, the resulting density is smooth and is a probability density. The continuous surface will be created and, it is possible to obtain the density anywhere in the study area, not only at the locations where the observed data have been sampled. Typically, we compute f(x,y) at the mesh points of a rectangular grid. The choice of the K function does not significantly affect the result (Loo and Anderson, 2015). Quartic (biweight) K Function is used in the case study.

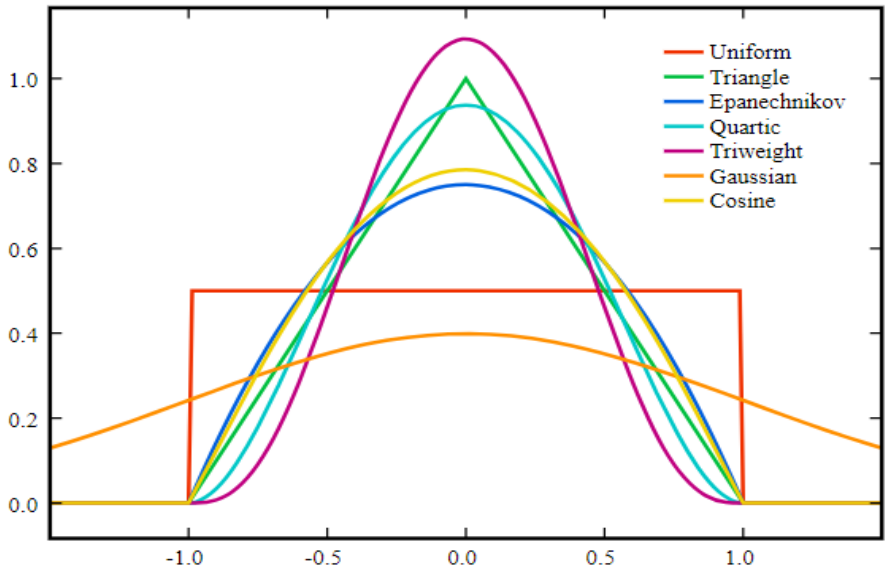

Fig 3.12 : Different Kernel functions with the same reference system*(https://upload.wikimedia.org/wikipedia/commons/4/47/Kernels.svg)*

Another important parameter that should be defined is the bandwidth. Most of the kernel density functions are bounded which means that they count only events within a given threshold distance from the location where the density estimate is made. This threshold distance is called *the bandwidth*. In other words, the bandwidth is the search radius within which intensity values for each point are calculated. Points are weighted, where collisions closer to the kernel center contribute a higher value to the cell's intensity value of the cell (Ratcliffe, 1999).

The kernel method divides the entire study area into predetermined number of cells and draws a circular neighborhood around each feature point (the collision) and then a mathematical equation is applied that goes from 1 at the position of the feature point to 0 at the neighborhood boundary. If the radius is increased, all other things being equal, the kernel becomes flatter. This kernel function is applied to each collision point, and individual cell density value is the sum of the overlapping kernel values over that cell divided by the area of the search radius (Loo and Anderson, 2015).

Large values of *h* result in an overlap of surfaces and mask the structure of the data; small values produce a surface characterized by the presence of numerous peaks and hard to interpret (Gutierrez-Osuna, 2004). Figure 3.13 reports the example of the one-dimensional case, which helps to understand the strong dependence of the result on the value of the parameter h.

The choice of kernel is relatively unimportant it is a continuous function in which the weights decrease as distance increases; the selection of an appropriate bandwidth is much more important (Brunsdon *et al.*, 1996; Fotheringham et al., 1997b; 1999). Okabe *et al.,* (2009), as well as Porta *et al*., (2009), suggest a range of values for h between 100 and 300 m with respect to urban areas, based on the average length of arcs in the road network. Therefore, h strongly depends on the case study.

While the K function is chosen as Quartic (biweight), the bandwidth (h) is defined as 150 m in the case study. 100 meters of bandwidth is enough to assess the locations on the scale of the individual intersections. However, this value does not provide a correct solution in the presence of widespread problems in larger areas, where characterized by a high number of accidents such as main squares. Therefore, 150 meters of bandwidth is chosen. By selecting this value, not only intersections but also squares are identified.

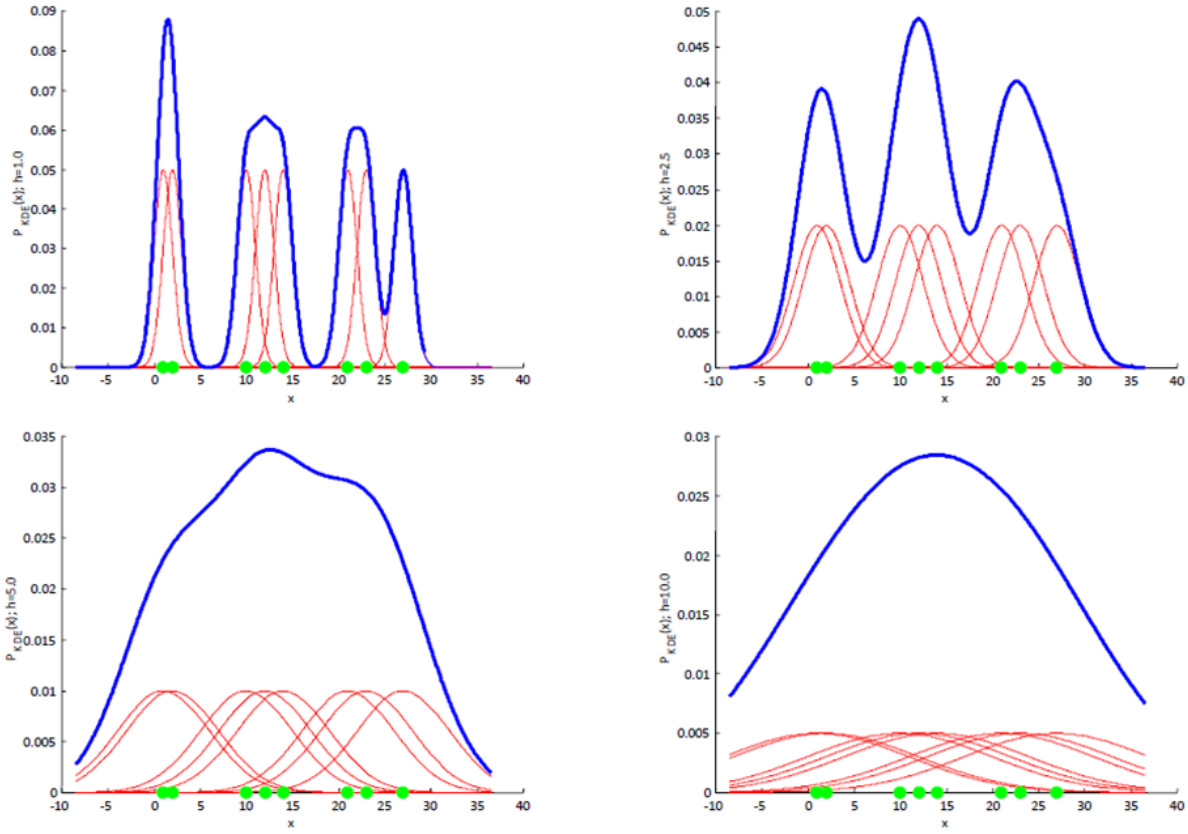

Fig 3.13 : Kernel density function (blue); the density functions of every single point(red) are cumulated with each other to obtain the estimate of the final density. The amplitude of the density functions of every single point (bandwidth) can be narrow (two upper images) or wide (two lower images) and greatly affects the density estimate of the final density (Gutierrez-Osuna, 2004).

Fig 3.14. shows some outputs from QGIS software relating to the motorcycle users for the period 2017-2019 as an example. Fig 3.14 (a) illustrates the map including traffic collisions for motorcycle users in the years from 2017 to 2019. The output of the KDE method is given in Fig 3.14 (b) as a heat map. After this step, the subdivision of the density band was determined based on the information given below by using the map statistics :

- values lower than the average value (M);
- M + 2 *standard deviations (SD);
- M + 4*SD;
- M + 6*SD;
- values greater than M + 6*SD.

The location of traffic collisions where the density values are higher than M + 6*SD is identified as hazardous road locations(HRL) as shown in Fig 3.14 (c).

(a)

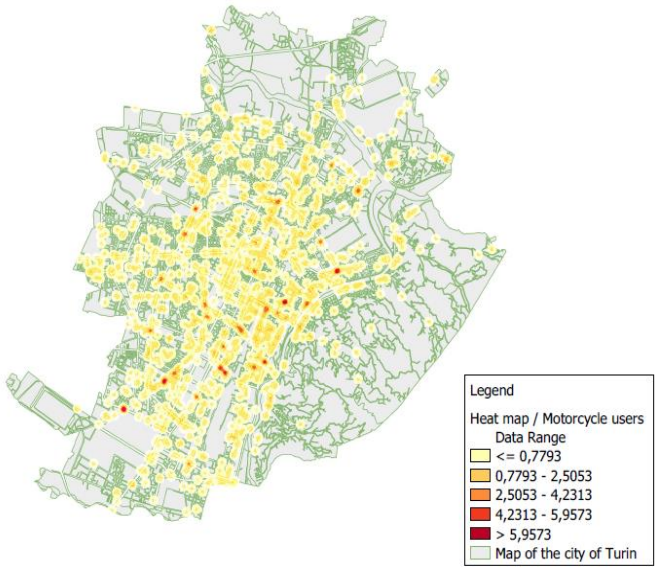

(b)

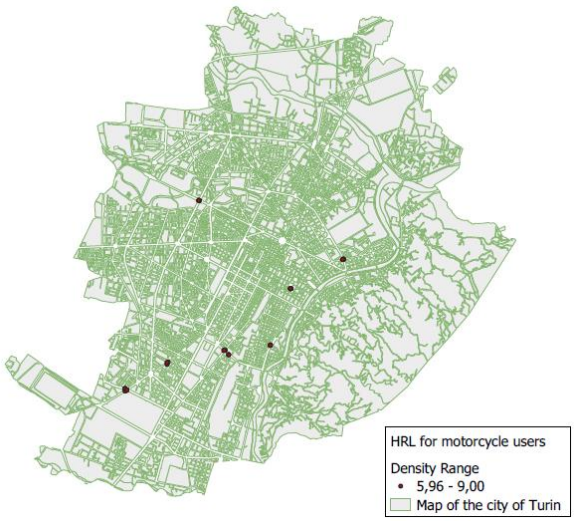

(c)

Fig 3.14 : (a) Traffic collisions for motorcycle users in the period 2017-2019, (b) The output of the KDE method for motorcycle users in the period 2017-2019, (c) Hazardous road locations (HRL) for motorcycle users in the period 2017-2019

4. RESULTS

Chapter 4 shows the results of the descriptive statistics and all analyses. Chapter 4.1 gives the descriptive statistics results of the crash database for the years from 2006 to 2019. Section 4.2 shows the results of clustering analysis by using Nearest Neighbor Analysis, G Function, and F Function while Section 4.3 indicates the identification of the hazardous road locations(HRL) by using the Kernel methodology for all VRU and related sub-categories (pedestrians, cyclists, moped and motorcycle users respectively).

The spatial distribution analysis of the accidents was carried out by using the distance-based and density-based methods as explained in Chapter 3.3. All analyzes are applied for VRU of given periods below and additionally VRU sub-categories (pedestrians, velocipedes, mopeds, and motorcycles).

In the previous study, analyzes were carried out for 2-3 years periods. The last three years are included in the study as 3 years period: 2006 – 2007, 2008 – 2009, 2010 – 2011, 2012 – 2014, 2015 – 2016, 2017 – 2019.

4.1. Results of Descriptive Statistics of crash database

The Italian National Institute of Statistics (ISTAT) provided the official database of traffic collisions. Firstly, the crash data relating to regional (Piedmont), provincial (Turin), and municipal (Turin) levels was evaluated by using descriptive statistics. The crash data of Turin was then prepared and organized to carry out a detailed analysis.

As it can be seen in Figure 4.1, although there are fluctuations in some years, it is a clear that there is a decreasing trend in the number of accidents from 2006 to 2019 for all levels. 51.86% of the traffic accidents in the Piedmont region belong to the Province of Turin while it is 28.42% at the municipality level for the period 2006 to 2019. The incidental data relating to the three different scales have shown in Fig. 4.1.

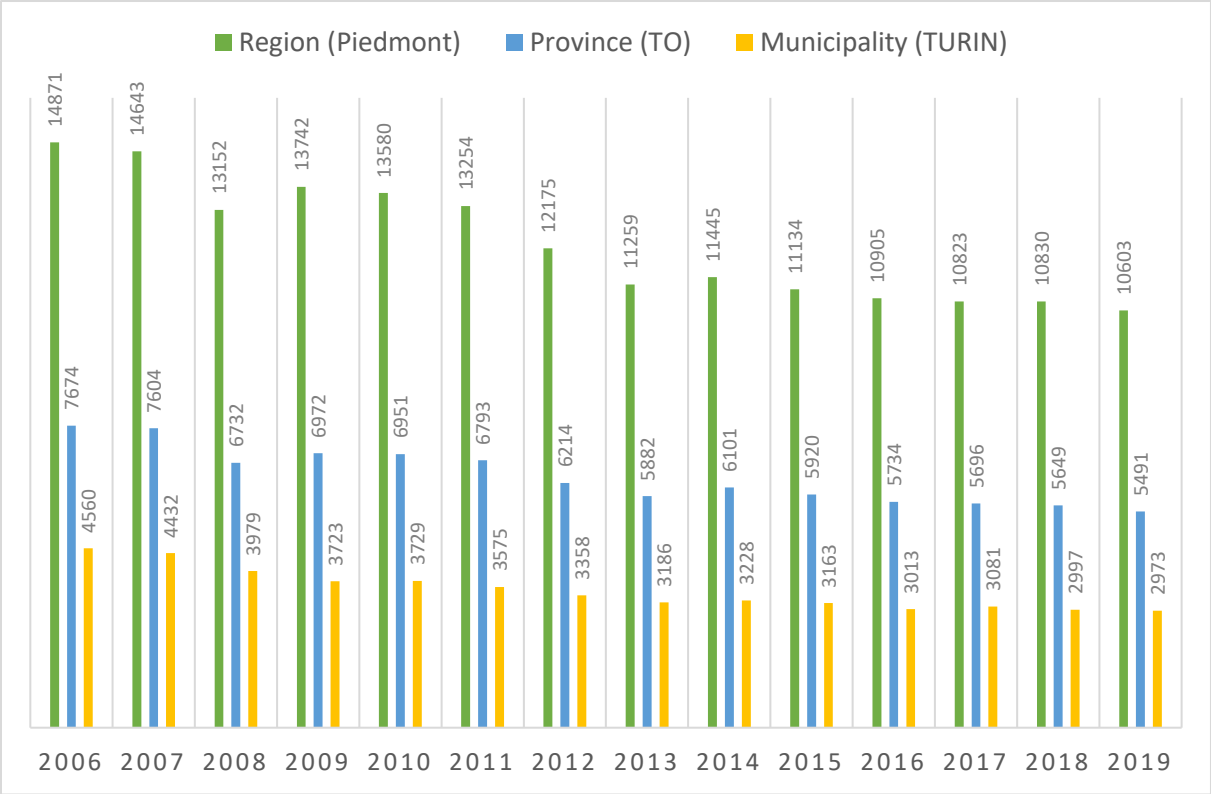

Figure 4.1 : The number of accidents based on Region, Province, and Municipality, from 2006 to 2019

The trend shown in the graph in Fig. 4.2 is consistent with the trend of a reduction in accidents observed at national level in recent years.

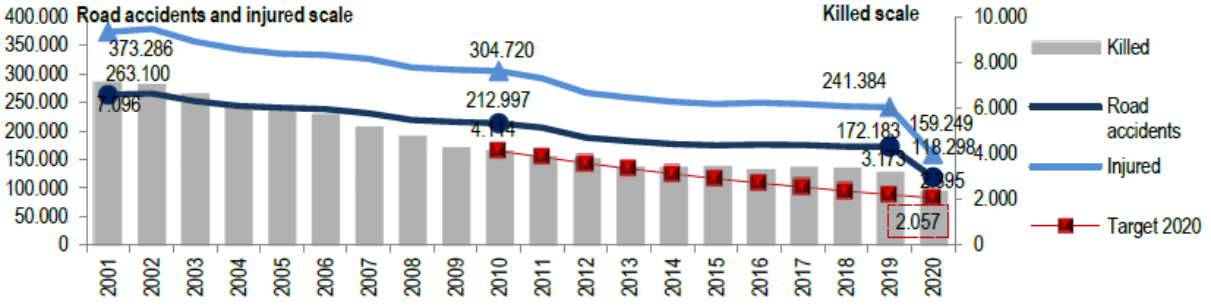

Figure 4.2 : Road accidents resulting in death or injury, killed and injured, from 2001 to 2020, absolute values *(ACI-ISTAT, 2020)*

A descriptive statistic was carried out to analyze the road accidents in the municipality of Turin as hourly, daily, and annual distributions. The annual distribution is summarized in Fig. 4.3. As reported in previous paragraph, a decreasing trend is observed over the years, with a reduction in accidents from 2006 to 2019 of approximately 34.80% (from 4560 to 2973 accidents). The daily distribution of the number of accidents in the municipality of Turin is given in Table 4.1. According to the percentage distribution, it is determined that the highest accident rate from 2006 to 2019 is on Thursday, Friday, or Saturday that are indicated with red color as in the table below:

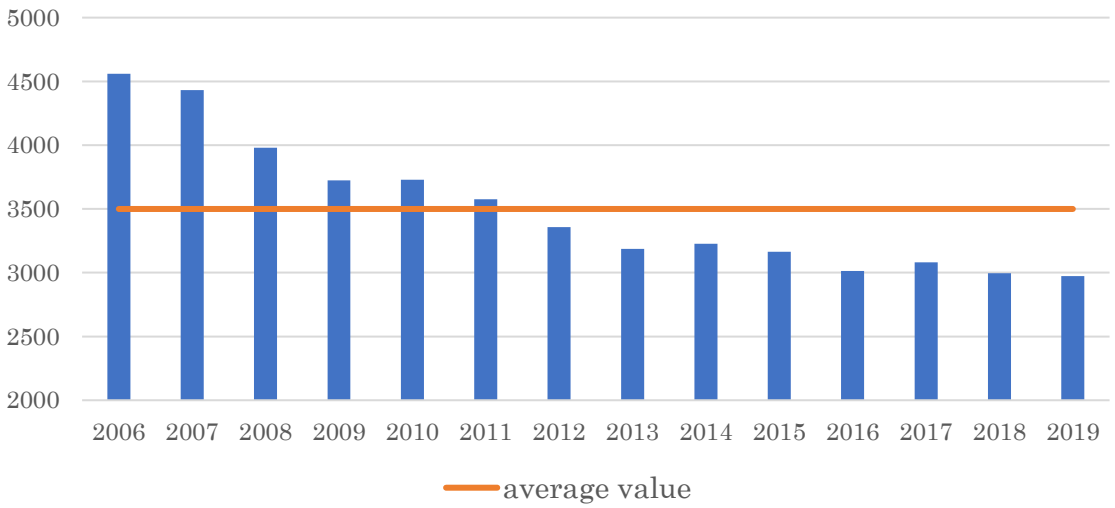

Figure 4.3 : Annual distribution of accidents in Turin, from 2006 to 2019

Table 4.1 : The daily distribution of the number of accidents as a percentage(%), from 2006 to 2019 / Municipality (TURIN)

Day	MONDAY %	TUESDAY %	WEDNESDAY %	THURSDAY %	FRIDAY %	SATURDAY %	SUNDAY %	TOTAL %
2006	14.45	13.42	14.14	14.93	15.15	15.37	12.52	100
2007	14.08	14.19	13.61	16.06	16.20	13.85	12.00	100
2008	14.35	15.26	13.65	13.95	16.54	15.15	11.11	100
2009	14.61	13.35	15.34	15.01	15.50	13.89	12.30	100
2010	14.85	14.32	14.64	14.32	16.33	14.45	11.25	100
2011	13.34	14.99	14.41	14.97	16.45	14.80	11.05	100
2012	15.69	14.50	15.40	14.62	15.54	13.88	10.36	100
2013	14.22	14.16	14.69	15.07	15.60	14.56	11.71	100
2014	13.88	14.93	15.52	15.83	15.27	13.72	10.84	100
2015	13.88	13.59	15.52	15.78	14.86	14.57	11.79	100
2016	14.77	15.57	15.10	14.90	15.40	13.71	10.55	100
2017	13.47	15.06	14.02	16.75	15.71	13.99	11.00	100
2018	13.61	14.98	14.25	16.42	15.85	12.91	11.98	100
2019	15.20	15.71	14.19	15.07	15.30	13.19	11.34	100
TOTAL	14.32	14.52	14.56	15.23	**15.72**	14.20	11.46	100

Fig. 4.4 shows the daily distribution from 2006 to 2019. The day characterized by the highest number of accidents is Friday (7,700) while the least critical is on Sundays (5,614). Regarding the hourly distribution, shown in Fig. 4.5, there is a peak in correspondence of the time slot 18-19, with 3,490 accidents. There are high values, smaller but still significant, in the time slot 8-9 and 9-10. These values are consistent with critical time slots for mobility regarding entry and exit from work and opening/closing activities.

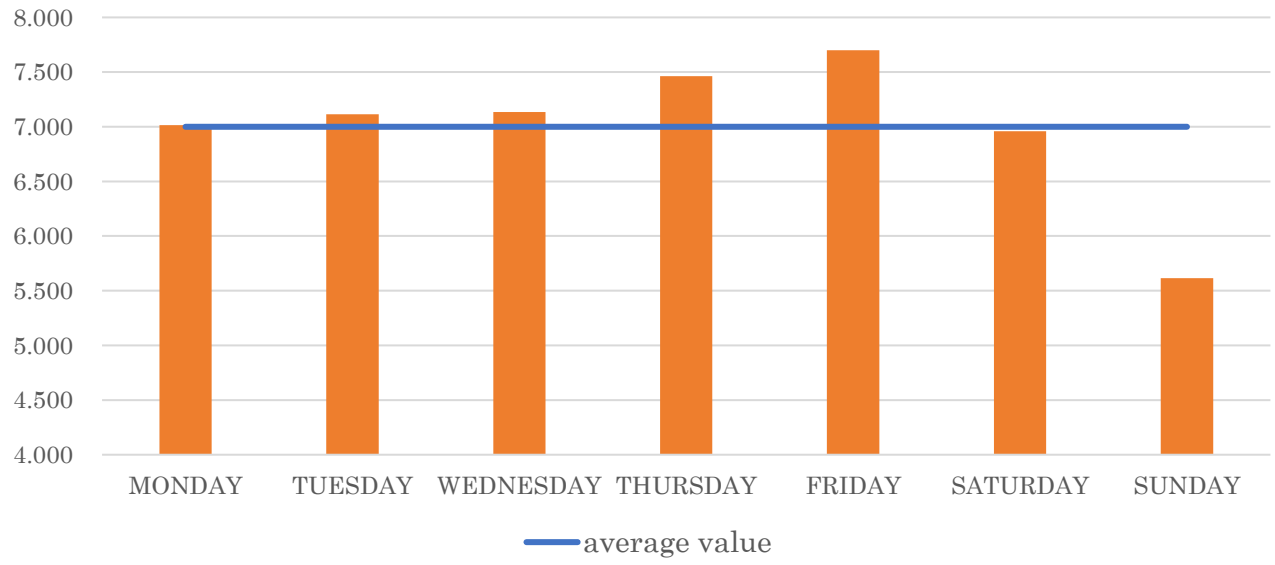

Figure 4.4 : Daily distribution of the number of accidents in Turin from 2006 to 2019

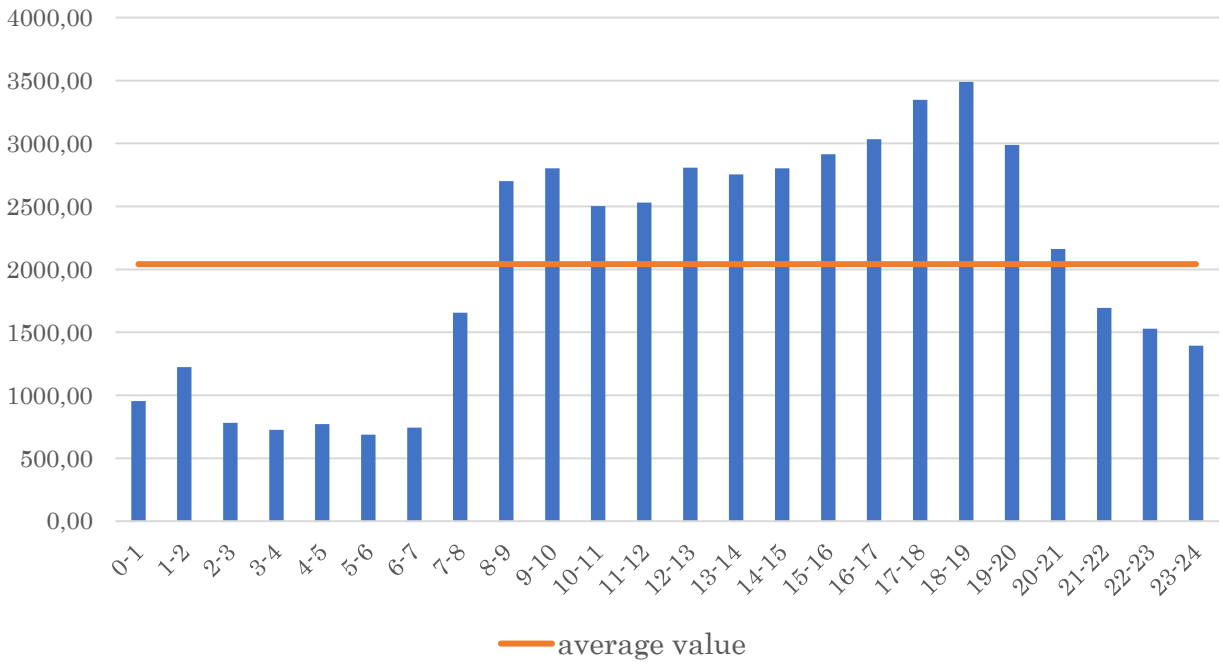

Figure 4.5 : Hourly distribution of the number of accidents in Turin, from 2006 to 2019

From Figure 4.6, it was determined that the highest number of accidents for all years was reached at 17-18 or 18-19 time slots.

Records including at least one of the field codes listed above were identified in the database as “VRU”. By filtering this information, a database is obtained by 20,770 records (42.40% of total accidents in the municipality of Turin). The breakdown of the number of accidents over fourteen years is shown in Tab. 4.2. while their trend is shown in Fig. 4.7.

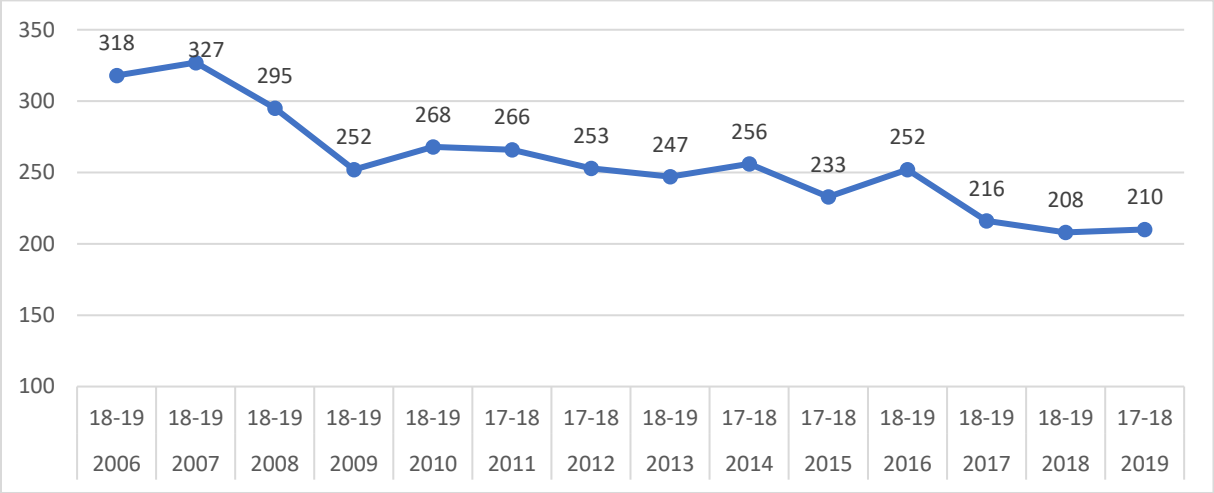

Figure 4.6 : The maximum number of accidents based on time slot &years in Turin

Table 4.2 : Total number of accidents and, the number of accidents involving at least one vulnerable user for the Municipality of Turin, from 2006 to 2019

Year	Accidents_Total	Accidents_VRU	% VRU
2006	4,560	1,835	40.24
2007	4,432	1,817	41.00
2008	3,979	1,624	40.81
2009	3,723	1,575	42.30
2010	3,729	1,539	41.27
2011	3,575	1,473	41.20
2012	3,358	1,421	42.32
2013	3,186	1,358	42.62
2014	3,228	1,439	44.58
2015	3,163	1,429	45.18
2016	3,013	1,344	44.61
2017	3,081	1,354	43.95
2018	2,997	1,227	40.94
2019	2,973	1,335	44.90
Total	**48,997**	**20,770**	**42.40**

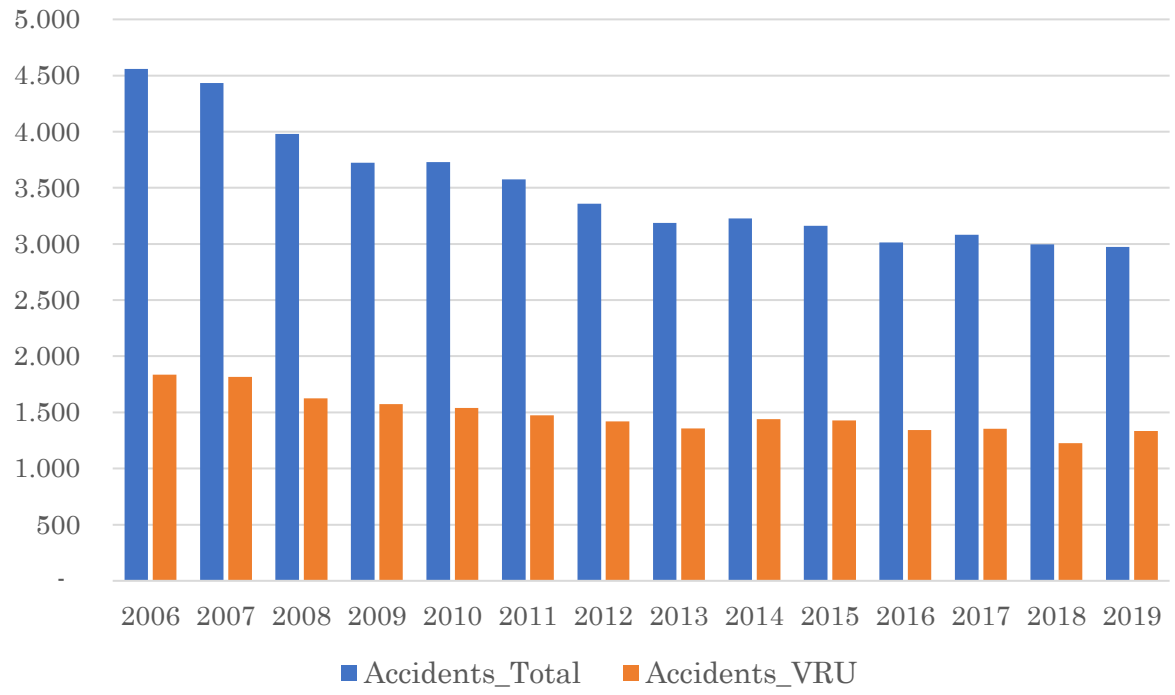

Figure 4.7: Total number of accidents and, the number of accidents involving at least one vulnerable user for the municipality of Turin, from 2006 to 2019

The decrease in the total number of accidents does not correspond with the increasing trend in VRU. The data shows a slight increase in the percentage of the total number of accidents that involve at least one vulnerable user compared to the total accidents, from 40.24% in 2006 to around 44.90% in 2019. Fig. 4.8 and Fig. 4.9 show the number of injured and dead VRU over fourteen years. There are some fluctuations in the number of injured and dead VRU but it is clear that there is a decrease from 2006 to 2019.

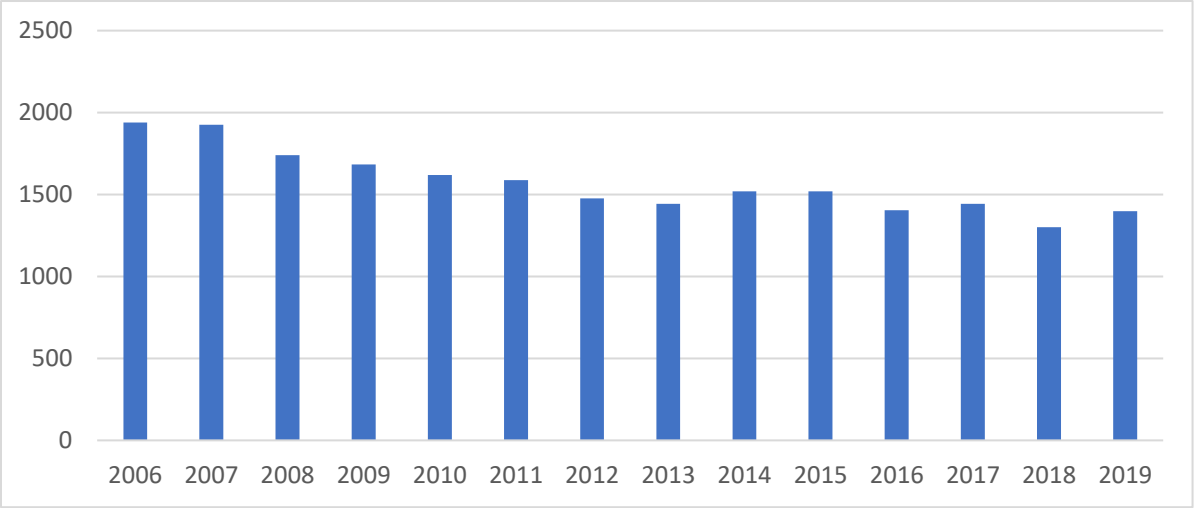

Figure 4.8 : The total number of injured VRU from 2006 to 2019

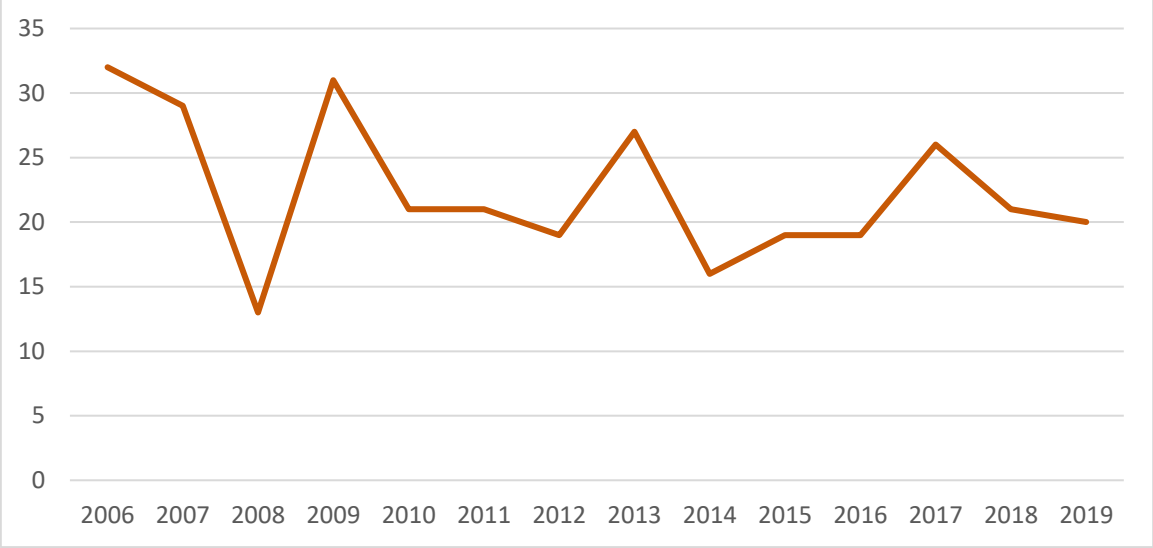

Figure 4.9 : The total number of dead VRU from 2006 to 2019

The number of accidents based on the road user categories is given in the Table 4.3 below in more detail from 2006 to 2019. The database shows that some accidents involve more than one VRU. Therefore, there is one additional row in the table to indicate the number of accidents between VRU. The total number of accidents involving VRU is computed by subtracting the total number of accidents between VRU's from the total number of accidents involving pedestrians, velocipedes, mopeds, and motorcycles. It is seen from the table that the number of accidents involving velocipedes increases approximately 50% from 2006 to 2019 while there is a decreasing trend for other VRU over fourteen years.

Table 4.3 : The number of accidents based on road user categories in Turin from 2006 to 2019

Road User Category	2006	2007	2008	2009	2010	2011	2012	2013	2014	2015	2016	2017	2018	2019	Total
Pedestrians	666	683	607	606	632	538	527	555	620	566	587	551	535	543	**8216**
Velocipedes	171	210	168	142	188	203	255	245	268	265	234	257	206	256	**3068**
Mopeds	269	239	212	187	131	133	96	71	59	71	47	51	44	56	**1666**
Motorcycles	800	766	698	699	632	648	597	544	549	588	520	538	486	525	**8590**
Between VRU's	71	81	61	59	44	49	54	57	57	61	44	43	44	45	**770**
Total VRU	1835	1817	1624	1575	1539	1473	1421	1358	1439	1429	1344	1354	1227	1335	**20770**
Other road users	2725	2615	2355	2148	2190	2102	1937	1828	1789	1734	1669	1727	1770	1638	**28227**
Total- All road users	**4560**	**4432**	**3979**	**3723**	**3729**	**3575**	**3358**	**3186**	**3228**	**3163**	**3013**	**3081**	**2997**	**2973**	

Tab. 4.4 shows the distribution of the number of accidents between vulnerable road users in Turin from 2006 to 2019. This table indicates the individual distribution of sub-categories of vulnerable road users. The total number of accidents is evaluated based on sub-categories, but it is noted in the table that there are 770 accidents between vulnerable road users.
Table 4.4 shows that 78.02% of the accidents involving VRU includes motorcycles and pedestrians while velocipedes and mopeds are at 21.98%. Motorcycle users and pedestrians have the highest risk of injury on the roads. Fig. 4.10 indicates the the number of injured people relating to VRU categories over the fourteen years.

The data relating to the number of accidents involving VRU is consistent with the the data about injured people based on VRU categories. Fig 4.10 highlights that the number of injured velocipede users rises to approximately 46.4% from 2006 to 2019 while it decreases for other VRU categories. Moreover, the data shows how the road enviroment causes health risk for pedestrians and motorcycle users.

Table 4.4 : The distribution of the number of accidents between vulnerable road users in Turin

Vulnerable User Category	Number of accidents	% VRU
Pedestrians	8216	38.14
Velocipedes	3068	14.24
Mopeds	1666	7.74
Motorcycles	8590	39.88
Total	**21,540**	
The number of accidents between VRU's is 770.		

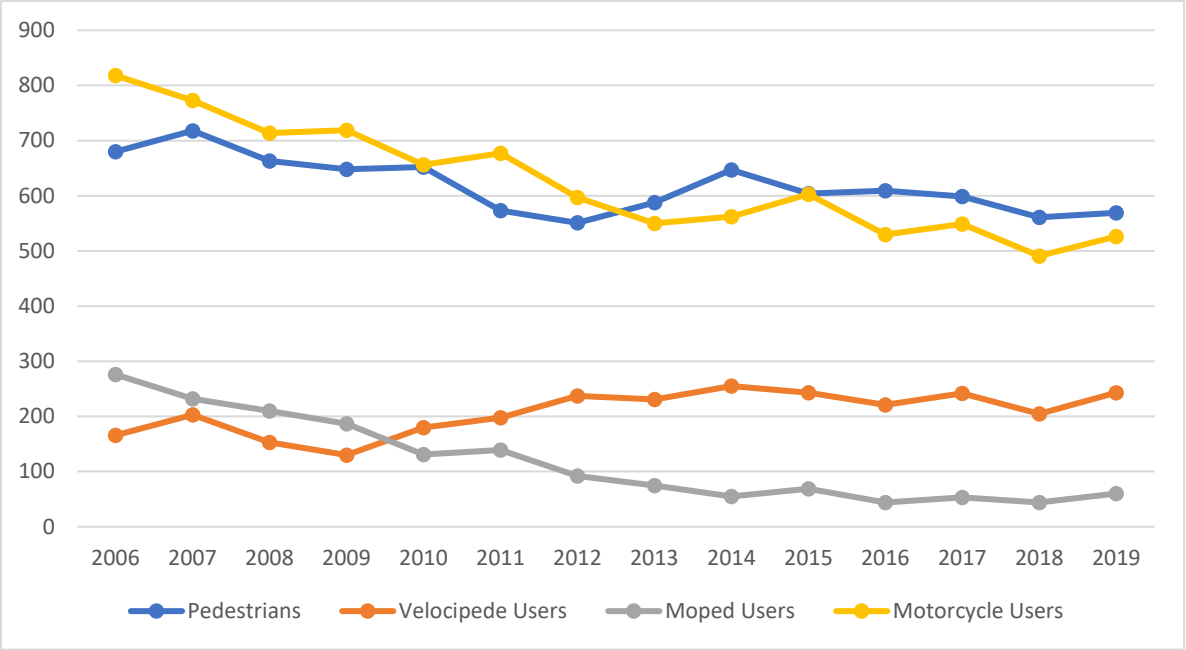

Figure 4.10: The distribution of the number of injured people based on VRU categories in Turin over fourteen years

Fig. 4.11 shows the data about vulnerable road users who lost their lives due to traffic crashes in Turin from 2006 to 2019. Here again, we can see that traffic accidents cause the death of pedestrians and motorcycle users the most among VRU.

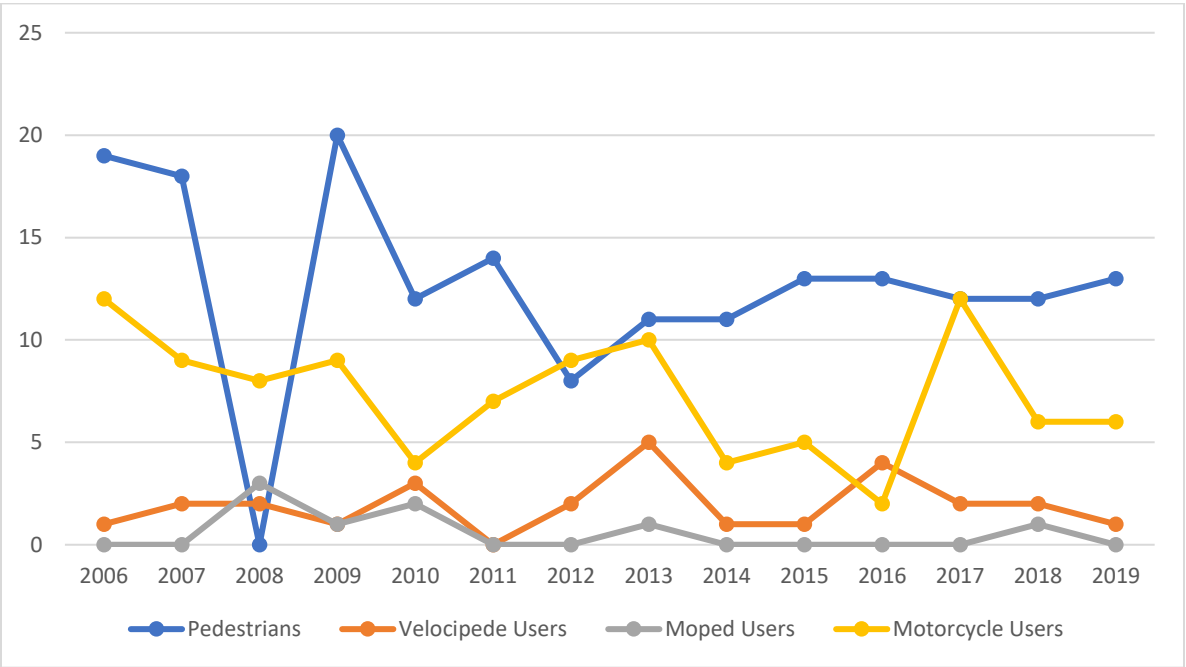

Figure 4.11 : The distribution of the number of dead people based on VRU categories in Turin over fourteen years

4.1.1. Final Database

All the operations described in the previous paragraphs led to the creation of the crash database of VRU containing 16,079 records relating to 11 years 2006-2016 and 3,735 records relating to 3 years 2017-2019 for the Municipality of Turin with at least one vulnerable user involved; all these accidents have geographic coordinates (latitude, longitude) WGS84.

The prepared databases have been called "*DB 2006_2016_VRU (TO)_revised"* and "*DB 2017_2019_VRU (TO)_revised".*

The following paragraph describes in detail all the operations that led to the processing of the final crash database, starting with the regional database provided by ISTAT for the period 2006-2019.

This procedure can be summarized as follows:

1. Regional database - Piedmont, consisting of 172,416 records,
2. Filtering of only provincial incidents- Turin (To), equal to 89,413 records,
3. Filtering of only municipal incidents, equal to 48,997 records,
4. Identification of only the accidents in which the presence is found of at least one vulnerable user, equal to 20,770 records*,
5. selection of only the Geo localizable records, obtaining a database final consisting of 19,814 records.

Note: *775 of 16,854 accidents for the period 2006-2016 and 181 of 3,916 accidents for the period 2017-2019 are removed from the crash database of VRU.

4.2. Clustering Analysis

Clustering analyses are performed through distance-based methods which are Nearest Neighbor Analysis, G Function, and F Function. Analyses are carried out to verify the clustering of the spatial pattern of points for six study periods relating to all VRU categories.

4.2.1. Nearest Neighbor Analysis

The NN index and z-score can be determined using the "Nearest Neighbor Analysis" tool of ArcGIS, which allows to determine the Nearest Neighbor statistics of the set of points selected,

allowing us to evaluate the level of aggregation of the points (Chapter 3.3.1.1 Nearest Neighbor Analysis).

Fig 4.12 shows the interface of Nearest Neighbor analysis in ArcGIS. Once point layers are created by using an excel file relating to the location of accidents, they can be used as input features and processing extent can be defined by Turin map.

NN index can be evaluated as a difference or ratio. In this case, NN index is a ratio (r<1: clustered, r=1: random, r>1:uniform). For a level of 95% confidence, the limits of the interval are ± 1.9. By values falling outside of this range; z-score > 1.96 refers to dispersed pattern and z- score <-1.96 refers to clustered pattern. Such result is corroborated by the high negative value of the Z-score. Table 4.5 shows the results of Nearest Neighbor Analysis for all vulnerable road users(VRU).

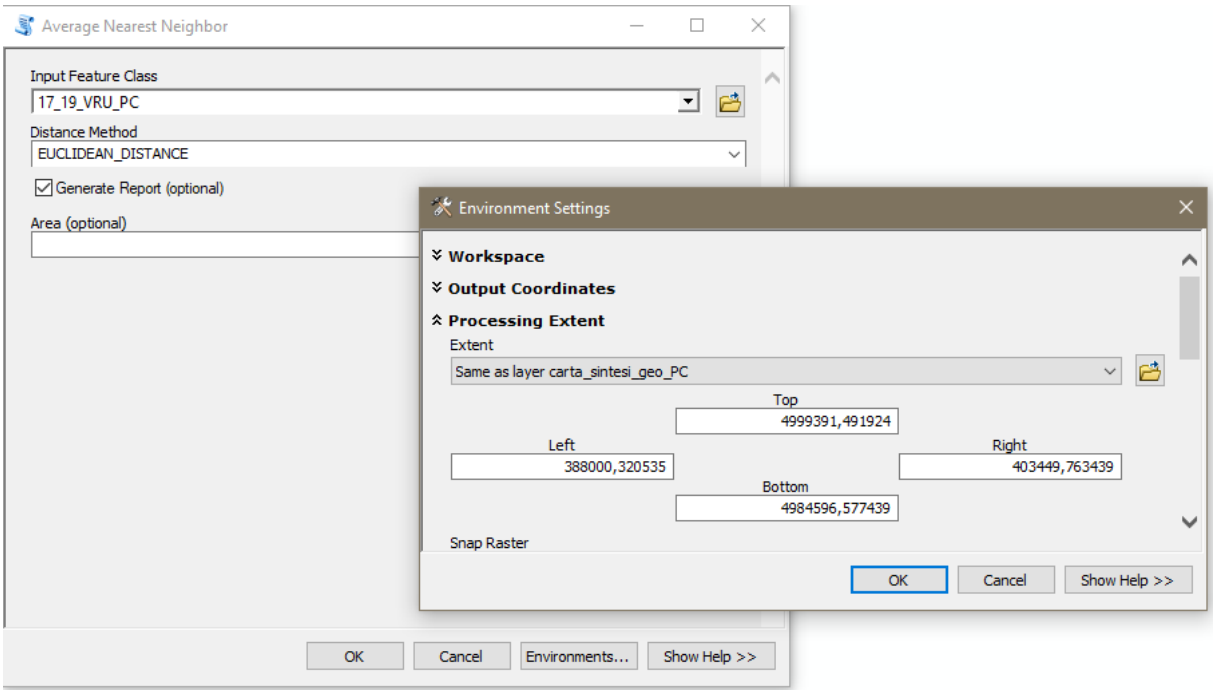

Fig 4.12 : Interface of Nearest Neighbor Analysis in ArcGIS

Tab 4.5 : The results of Nearest Neighbor Analysis for all VRU

All VRU		
Study Periods	**NN Index**	**Z-score**
2006-2007	0.387	-67.99
2008-2009	0.419	-60.50
2010-2011	0.435	-57.32
2012-2014	0.398	-74.49
2015-2016	0.437	-56.70
2017-2019	0.380	-72.54

As can be seen, the NN indexes of the six study periods show very high values less than 1 and the respective Z-scores underline the high statistical significance of such results. Therefore, we confirm what was previously expected that accidents are concentrated mainly at specific points. The reports of Nearest Neighbor analyses are shown in Annex I.

Table 4.6 shows the results of Nearest Neighbor Analysis for each sub-category of vulnerable road users(VRU). It can be seen from the results that all point patters of sub- categories of VRU are clustered for the six study periods.

Tab 4.6: The results of Nearest Neighbor Analysis for sub-categories of VRU

PEDESTRIANS				VELOCIPEDES		
Study Periods	**NN Index**	**Z-score**		**Study Periods**	**NN Index**	**Z-score**
2006-2007	0.532	-31.77		**2006-2007**	0.657	-12.23
2008-2009	0.503	-32.28		**2008-2009**	0.748	-8.13
2010-2011	0.549	-28.79		**2010-2011**	0.653	-12.55
2012-2014	0.533	-36.78		**2012-2014**	0.600	-21.06
2015-2016	0.579	-27.36		**2015-2016**	0.680	-13.67
2017-2019	0.479	-39.62		**2017-2019**	0.627	-18.77
MOPEDS				**MOTORCYCLES**		
Study Periods	**NN Index**	**Z-score**		**Study Periods**	**NN Index**	**Z-score**
2006-2007	0.650	-14.56		**2006-2007**	0.510	-35.42
2008-2009	0.670	-11.76		**2008-2009**	0.472	-35.99
2010-2011	0.701	-8.93		**2010-2011**	0.509	-32.29
2012-2014	0.762	-6.83		**2012-2014**	0.484	-40.32
2015-2016	0.799	-4.18		**2015-2016**	0.539	-29.27
2017-2019	0.944	-1.28		**2017-2019**	0.471	-38.51

4.2.2. G Function

The "G function" algorithm in the “R scripts” section of the QGIS was used to determine the G function. Figure 4.13 shows the outputs of the G function relating to the six study periods considered for all VRU. The x-axis shows the nearest-neighbor distances while the y-axis illustrates the cumulative frequency distribution of the nearest-neighbor distances (G-function). While the black line represents the “observed” G function, the red dotted line indicates the theoretical G function.

The value of G for any particular distance, d, tells us what fraction of all the nearest-neighbor distances in the pattern is less than d. The default algorithm sets the maximum NN distance equal to 140 m; in correspondence with this value, we have that 100% of the NN distances are less than it. Then, the different distances are normalized based on this maximum value.

It is worth noting that the curve relating the actual structure of the points ("observed" G-function) seems above the theoretical curve in all six periods analyzed for all VRU. As it can be seen from the figures below the G function rapidly increases over short distances. It means that collision events are closely clustered together in specific locations.

It is interesting to highlight that there is a "jump" in the trend of the observed G function relating to the years from 2006 to 2011 and 2017 to 2019. This situation is due to the geolocation procedure based on the GPS Visualizer's Address Locator adopted for the years before 2011 and from 2017 to 2019. In this case, some incidental events relating to these years were assigned to the same coordinates, although they may have occurred at different points on the road network. It causes a substantial number of NN distances that are equal to zero. This situation precisely causes a sudden increase in the G function near the origin of the axes. Traffic collisions with the geographic coordinates provided directly by the ISTAT database give more precise results.

The maximum NN distance for the period 2012-2014 and 2017-2019 is 100 m which is less than the maximum NN distance among all periods highlighted as 140 m above. This is basically due to three-year periods. These periods have more traffic collisions than others and, therefore, the distance between collision events decreases and, at the same time, NN distances also decrease.

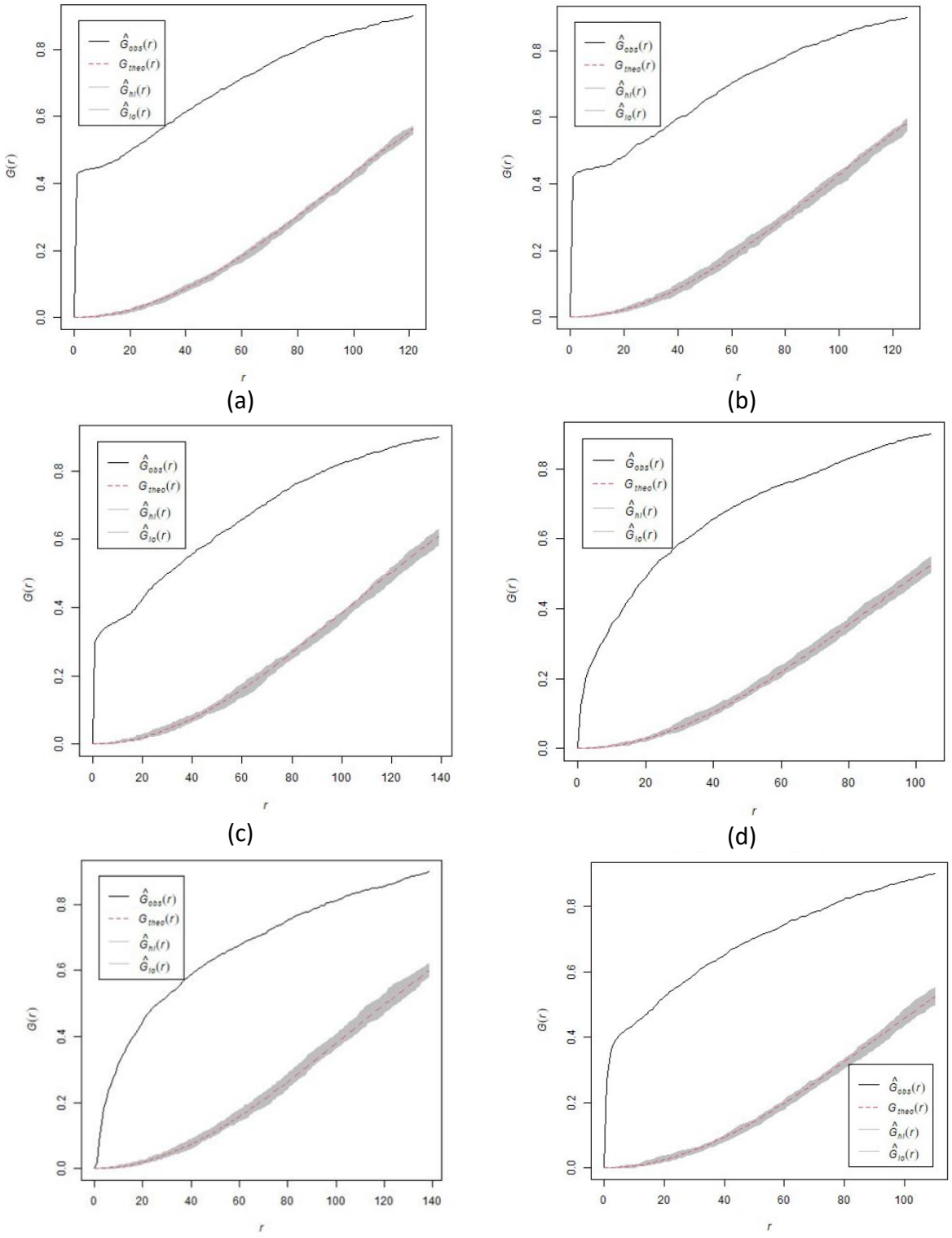

Fig 4.13 : The results of G function for all VRU (a) 2006-2007,(b) 2008-2009, (c) 2010-2011, (d) 2012-2014, (e)2015-2016, (f) 2017-2019

The following figures show the output graphs of the six study periods considered for pedestrians. The default algorithm sets the maximum NN distance equal to 200 m; in correspondence with this value, we have that 100% of the NN distances are less than it. As it can be seen from the figure that the curve of “observed” G function is above the curve relating to the “theoretical” G function. It indicates that collision events are closely clustered together in specific locations.

As in the previous analysis, there is a "jump" in the observed G function relating to the years from 2006 to 2011 and 2017 to 2019 due to the geolocation process. It is also obtained that when the study period extends, the distance between accidents decreases since the number of accidents relating to these periods rises. At the same time, NN distances decrease as shown in (d) and (f) in the Figure 4.14.

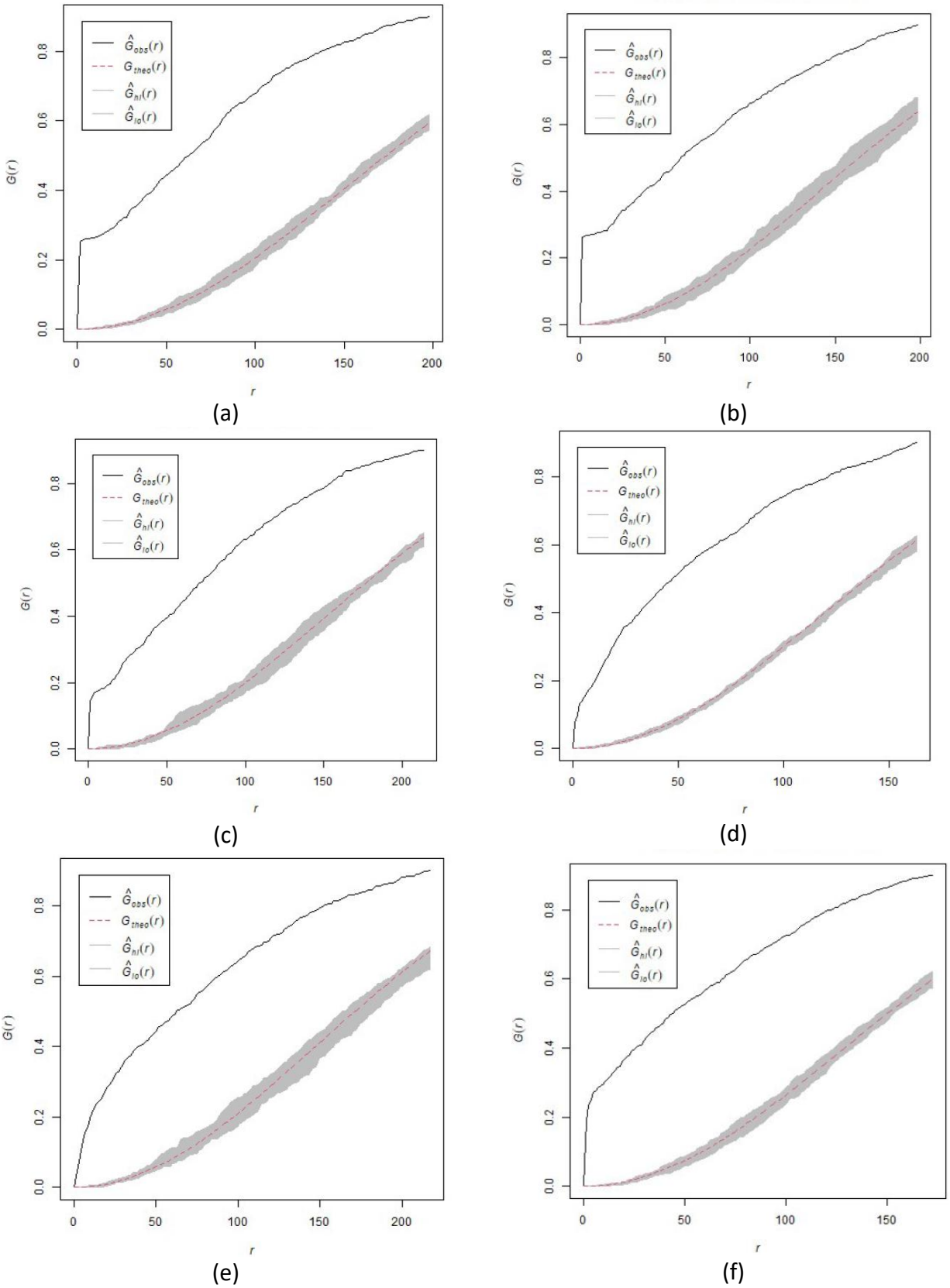

(a) (b)

(c) (d)

(e) (f)

Fig 4.14 : The results of G function for Pedestrians (a) 2006-2007,(b) 2008-2009, (c) 2010-2011, (d) 2012-2014, (e)2015-2016, (f) 2017-2019

Figure 4.15 shows the output graphs of the six study periods considered for velocipede users. As it can be seen from the figure that the curve of the “observed” G function is above the curve relating to the “theoretical” G function. It indicates that collision events are closely clustered together in specific locations. The maximum NN distance is equal to 500 m; in correspondence with this value, we have that 100% of the NN distances are less than it. The maximum NN distance is seriously high since the number of accidents is low for this road user type. This leads to an increase in the distance between collision events. There are some fluctuations in the outputs shown in Fig. 4.15. It is due to the low number of accidents concerning velocipede users. So, there is a long-distance among traffic collisions and, it causes a fluctuation in the results.

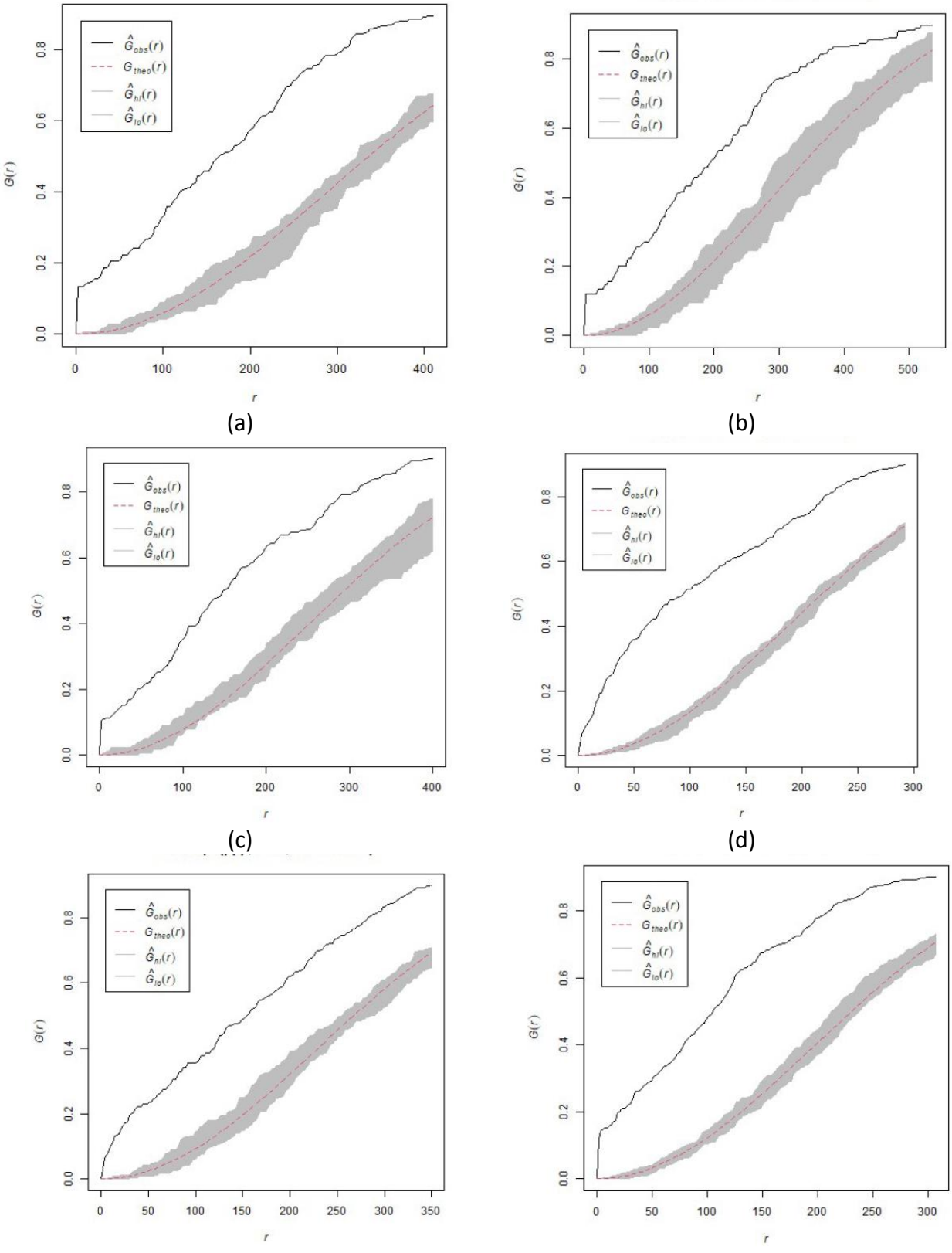

Fig 4.15 : The results of G function for Velocipedes (a) 2006-2007,(b) 2008-2009, (c) 2010-2011, (d) 2012-2014, (e)2015-2016, (f) 2017-2019

The following figures show the output graphs of the six study periods considered for moped users. The results indicate that collision events are closely clustered together in specific locations since the figure that the curve of the “observed” G function is above the curve relating to the “theoretical” G function.

It indicates that the maximum NN distance is equal to 700 m; in correspondence with this value, we have that 100% of the NN distances are less than it. The maximum NN distance is seriously high since the number of accidents is low for this road user type. There are some fluctuations in the outputs shown in Fig. 4.16., especially for the period 2017-2019. The maximum NN distance is also obtained for this period. It means that the distance between crashes is relatively high in this study period.

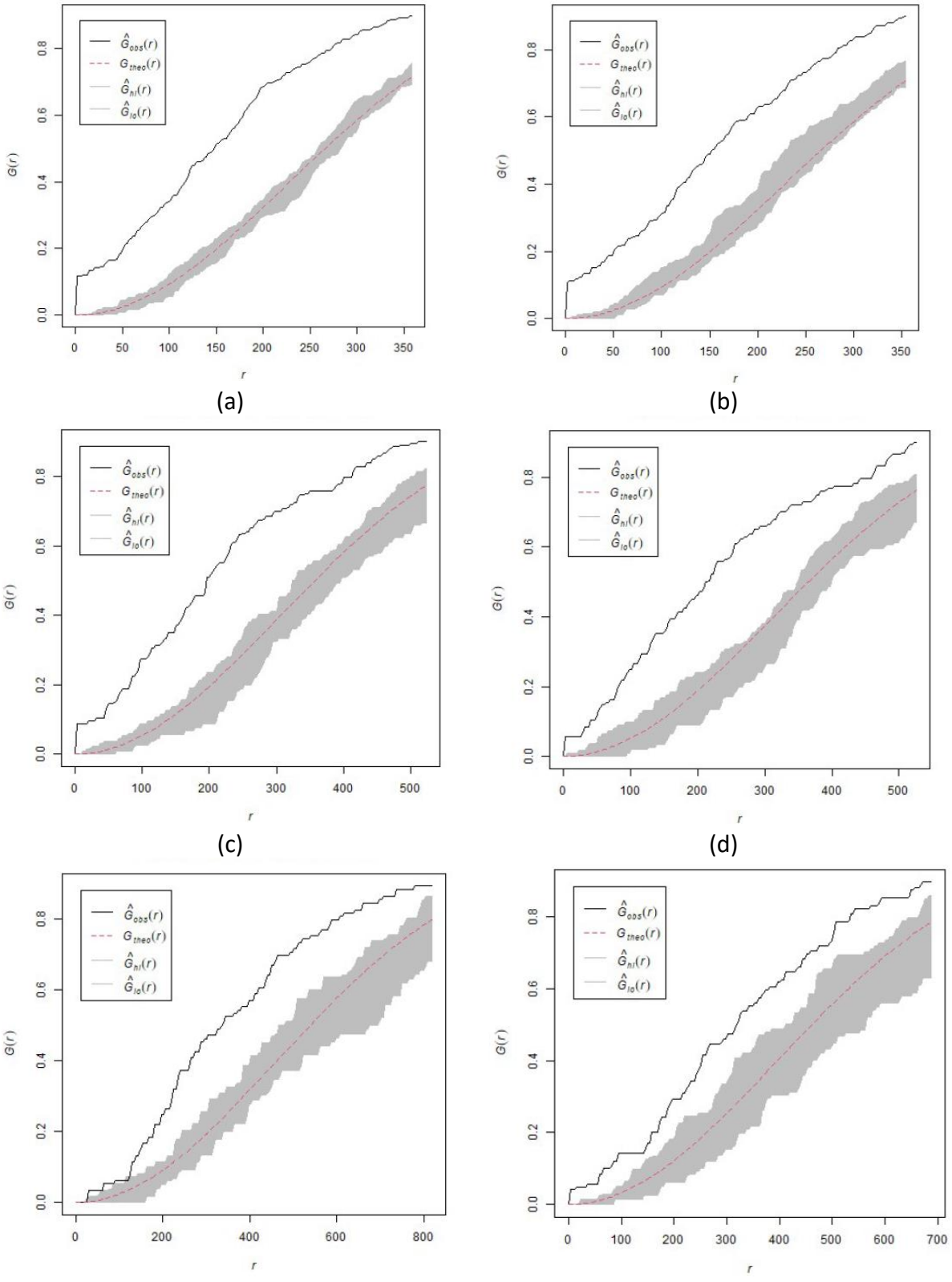

Fig 4.16 : The results of G function for Mopeds (a) 2006-2007,(b) 2008-2009, (c) 2010-2011, (d) 2012-2014, (e)2015-2016, (f) 2017-2019

The following figures show the output graphs of the six study periods considered for motorcycle users. The default algorithm sets the maximum NN distance equal to 200 m; in correspondence with this value, we have that 100% of the NN distances are less than it. As it can be seen from the figure that the curve of “observed” G function is above the curve relating to the “theoretical” G function. It indicates that collision events are closely clustered together in specific locations.

As in the previous analysis, there is a "jump" in the observed G function relating to the years from 2006 to 2011 and 2017 to 2019 due to the geolocation process. It is also obtained that when the study period extends, the distance between accidents decreases since the number of accidents relating to these periods rises. At the same time, NN distances decrease as shown in (d) and (f) in the Figure 4.14.

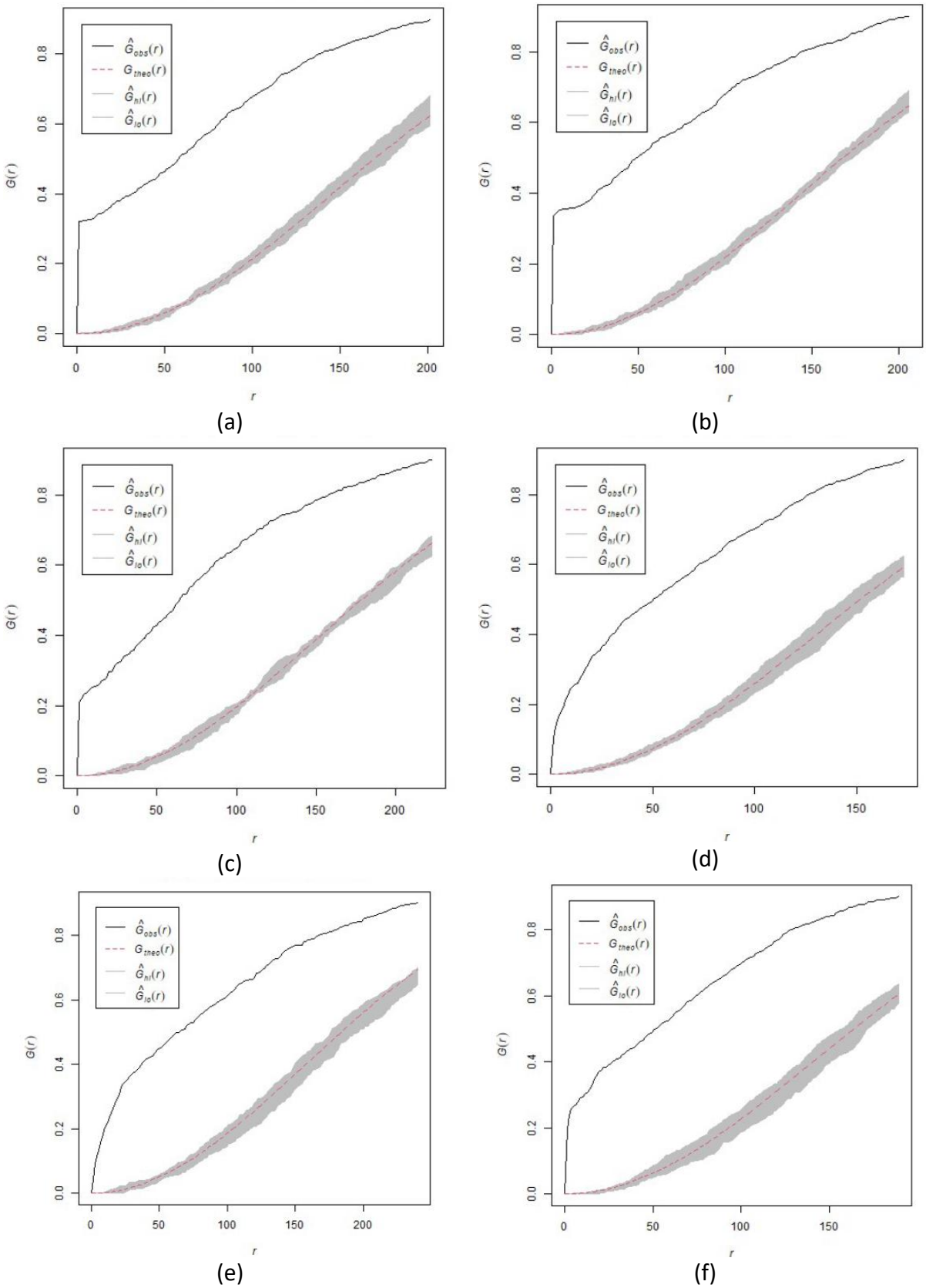

(a) (b)

(c) (d)

(e) (f)

Fig 4.17 : The results of G function for Motorcycles (a) 2006-2007,(b) 2008-2009, (c) 2010-2011, (d) 2012-2014, (e)2015-2016, (f) 2017-2019

Overall, the outputs of the G function for all VRU and related sub-categories are listed above regarding six study periods.

It is obtained from the results that the curve relating the actual structure of the points ("observed" G-function) is above the theoretical curve in all six periods analyzed. It means that collision events are closely clustered together in specific locations of the road network for all VRU and related sub-categories of VRU.

Moreover, the G function is an extension of the Nearest Neighbor approach. The results of the NN analysis should be consistent with the output of the G functions. In this case study, the results of the G function and Nearest neighbor were compatible with each other. All results highlight that collision events are closely clustered together.

4.2.3. F Function

The "F function" algorithm in the “R scripts” section of the QGIS was used to determine the F function. Figure 4.18 shows the output graphs of the six study periods considered for all VRU.

The x-axis shows the nearest-neighbor distances while the y-axis illustrates the cumulative frequency distribution of shortest distances from random points to nearest events (F-function). While the black line represents the “observed” F function, the red dotted line indicates the theoretical F function. F-function increases slowly at short distances but more rapidly at longer distances. It is noted that the "observed" F-function is below the theoretical curve in all six periods analyzed. This result indicates that the collision events are distributed in space as a "clustered" structure which is characterized by the presence of different aggregations in specific locations.

The maximum NN distance is 500 m and, there are no significant differences between the results of two and three-year periods since point locations anywhere in the study area are selected randomly.

It is also important to highlight that the F function is less sensitive to the geolocation process. In this case, there were no significant differences in the results shown in figure 4.18 below, as happened in the previous methodology.

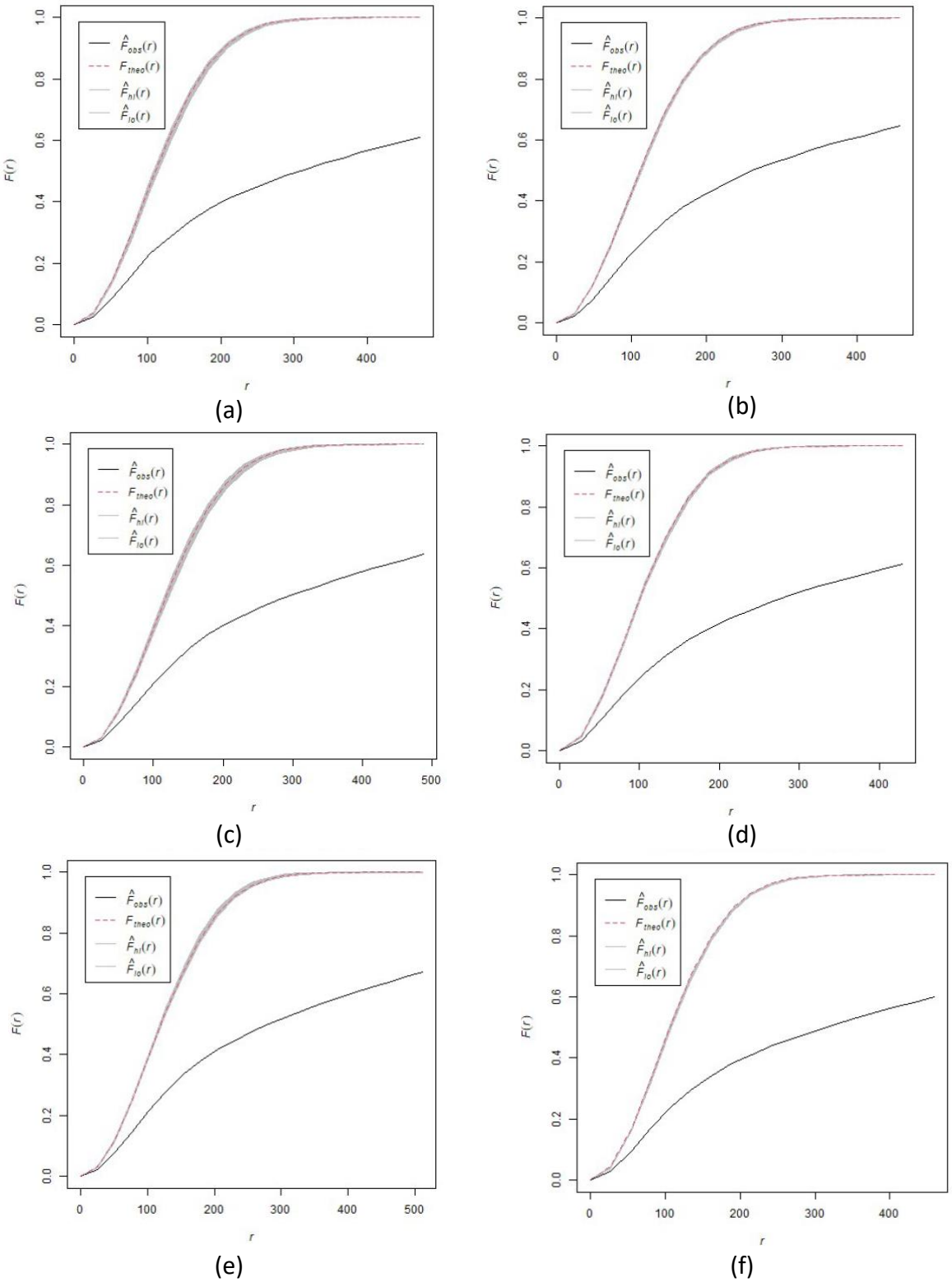

Fig 4.18 : The results of F function for all VRU (a) 2006-2007,(b) 2008-2009, (c) 2010-2011, (d) 2012-2014, (e)2015-2016, (f) 2017-2019

The following figures show the output graphs of the six study periods considered for pedestrians. The "observed" F-function is below the theoretical curve in all six periods analyzed. It means that traffic collisions are clustered in specific locations of the road network.

The maximum NN distance is 700 m and, there were no significant differences in the results shown in figure 4.19 below, as happened in the G function methodology.

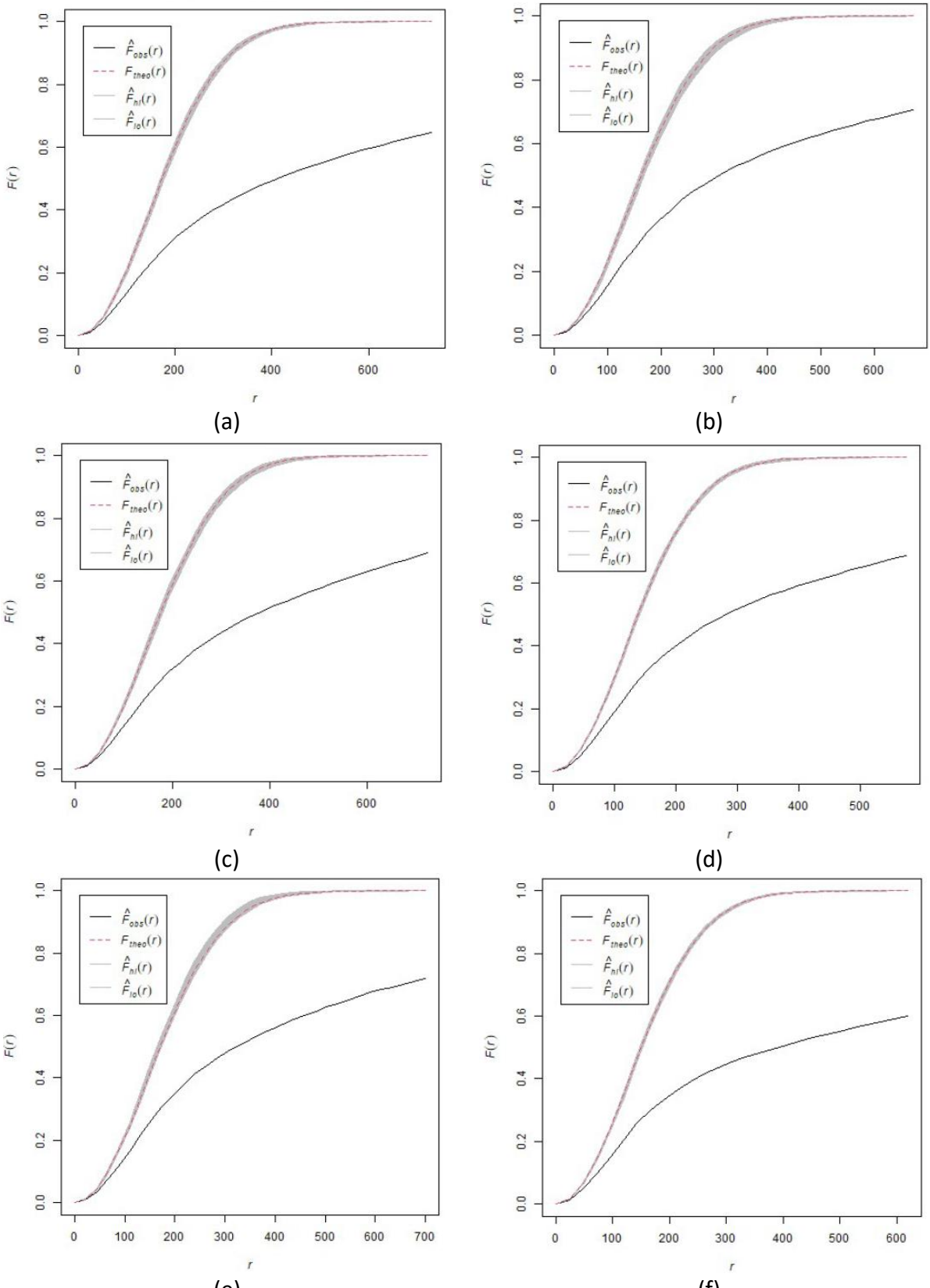

Fig 4.19 : The results of F function for Pedestrians (a) 2006-2007,(b) 2008-2009, (c) 2010-2011, (d) 2012-2014, (e)2015-2016, (f) 2017-2019

The following figures show the output graphs of the six study periods considered for velocipede users. The "observed" F-function is below the theoretical curve in all six periods analyzed. It means that traffic collisions are clustered in specific locations of the road network. The maximum NN distance is 1400 m and, it can be realized that when the number of accidents decreases, the observed distance between collision events rises conversely. Whereas there were no differences in the results shown in figure 4.20 below.

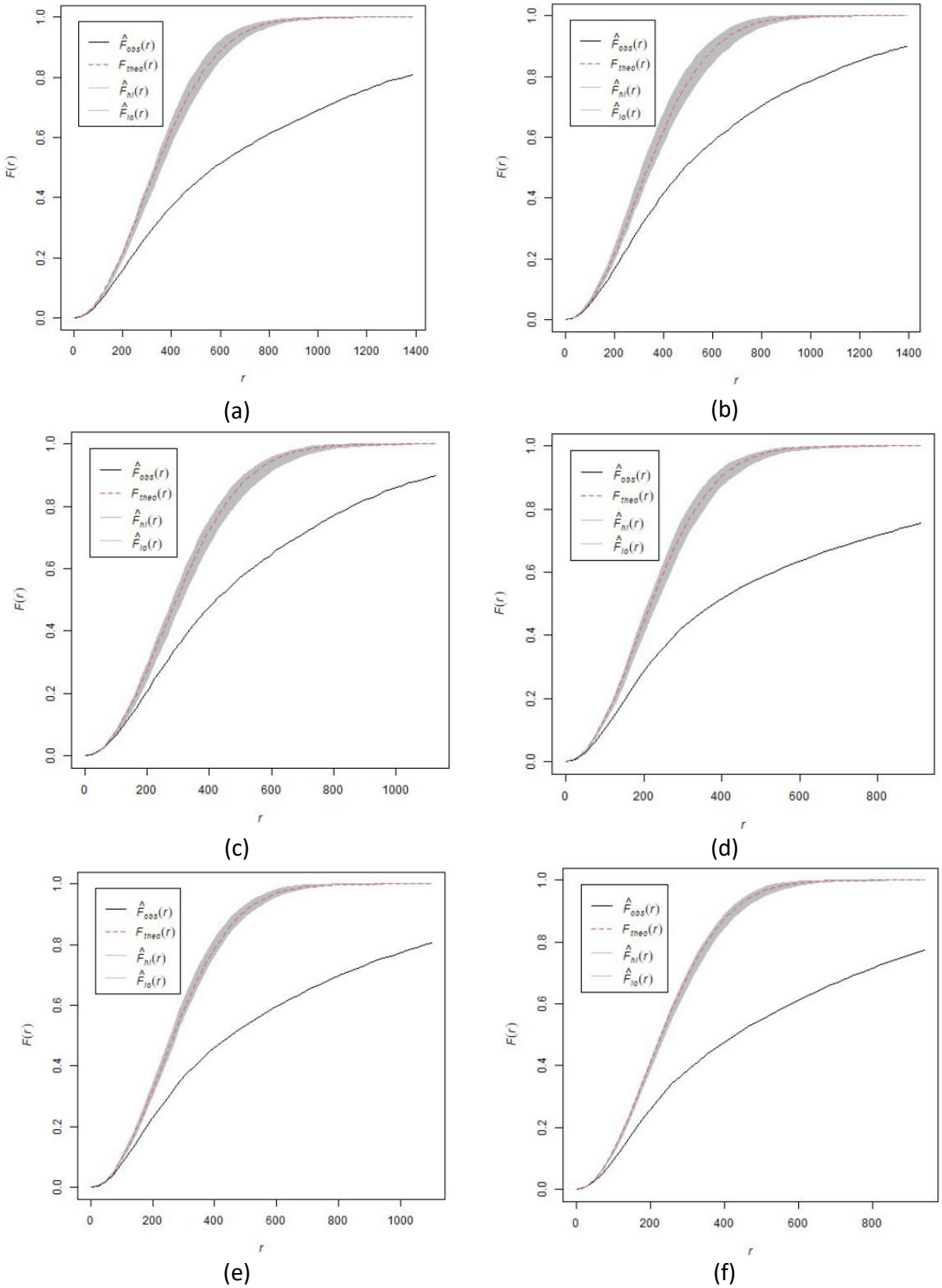

Fig 4.20 : The results of F function for Velocipedes (a) 2006-2007,(b) 2008-2009, (c) 2010-2011, (d) 2012-2014, (e)2015-2016, (f) 2017-2019

Figure 4.21 shows the output graphs of the six study periods considered for moped users. The "observed" F-function is below the theoretical curve in all six periods analyzed. It means that traffic collisions are clustered in specific locations of the road network. The maximum NN distance is 1500 m and, it can be realized that when the number of accidents decreases, the observed distance between collision events rises conversely. Whereas there were no differences in the results. The extension in the theoretical curve for the period 2015-2016 and 2017-2019 is due to the low number of traffic collisions related to moped users.

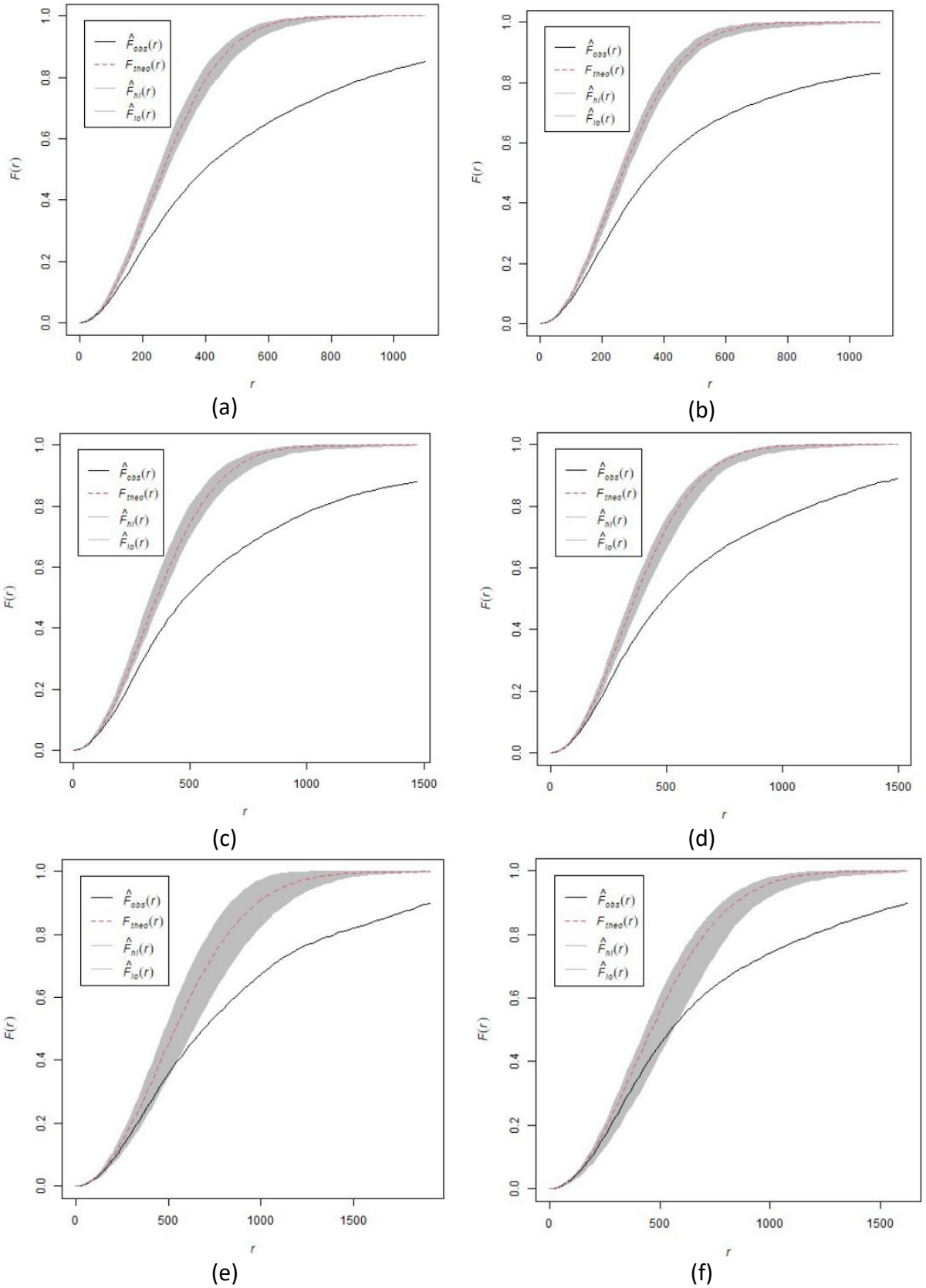

Fig 4.21 : The results of F function for Mopeds (a) 2006-2007,(b) 2008-2009, (c) 2010-2011, (d) 2012-2014, (e)2015-2016, (f) 2017-2019

The following figures show the output graphs of the six study periods considered for motorcycle users. The "observed" F-function is below the theoretical curve in all six periods analyzed. It means that traffic collisions are clustered in specific locations of the road network. The maximum NN distance is 700 m and, there were no significant differences in the results shown in figure 4.22 below, as happened in the G function methodology.

The following figures show the output graphs of the six study periods considered for motorcycle u.

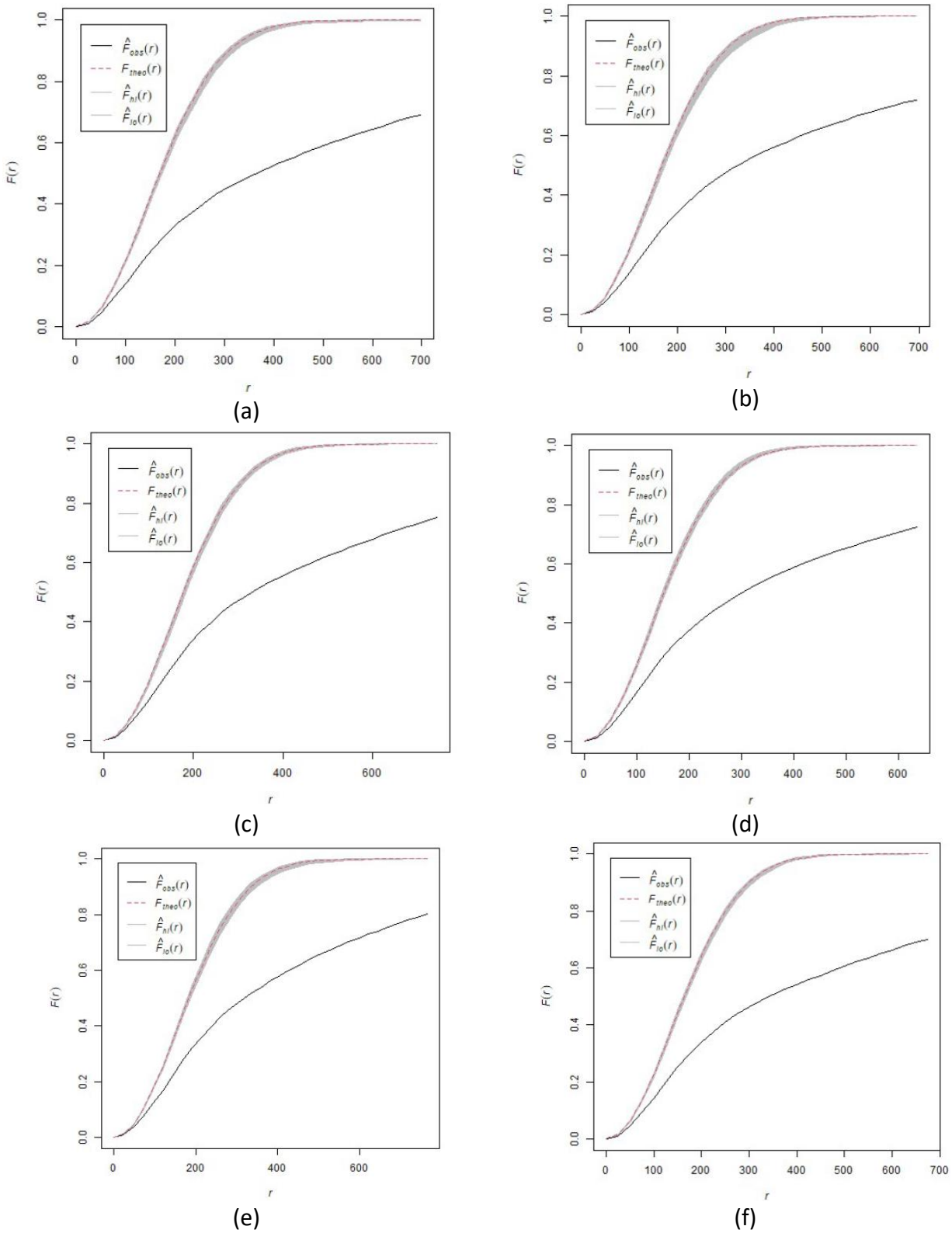

Fig 4.22 : The results of F function for Motorcycles (a) 2006-2007,(b) 2008-2009, (c) 2010-2011, (d) 2012-2014, (e)2015-2016, (f) 2017-2019

Overall, the outputs of the F function for all VRU and related sub-categories are listed above regarding six study periods. This third distance-based analysis methodology highlights how the point structures of the different study periods are characterized by numerous aggregations, a result witnessed by the presence of the F functions always observed below the theoretical curves. It means that collision events are closely clustered together in specific locations of the road network for all VRU and related sub-categories of VRU.

The F function is likely to rise slowly at first, but more rapidly at longer distances, because a good proportion of the study area is empty, so that many locations are at quite long distances from the nearest event in the pattern.

Unlike the G function, the F function is less sensitive to the accuracy of geolocation; in fact, no significant differences were found for short distances as happened in the previous methodology.

Moreover, the outputs of the F functions are consistent with the results of the NN method. All results highlight that collision events are closely clustered together for all VRU and related sub-categories in six time periods.

4.3. Identification of Hazardous Road locations (HRL)

This chapter introduces the results of the KDE method and the identification of hazardous road locations (HRL). The following steps are carried out until this chapter:

- The final database was prepared and, the excel files that include the crash records and geographic coordinates based on six study periods were created for all VRU and related sub-categories (pedestrians, motorcycle users, velocipede users, and moped users) for the analyses in GIS software.
- Then the Nearest Neighbor method was applied to identify spatial aggregations of the point patterns that are clustered or uniformly spaced in ArcGIS software. It was obtained that the collision events were closely clustered together for all VRU and related sub-categories regarding study periods.
- After the second step, G and F functions which are an extension of the Nearest Neighbor approach, are carried out in QGIS software. These functions were used to verify the NN method. The outputs of the G and F functions also highlight that the point patterns of the collision events were clustered closely.

So, after the steps mentioned above, the KDE method was applied to identify hazardous road locations (HRL). By applying this method, the heatmaps with the continuous surface of density were created. In this way, we were able to detect the high local event densities in such locations. The following steps are carried out in this chapter:

- By selecting 150 meters of the bandwidth(h) and quartic (biweight) Kernel function, the KDE method was applied. As a result of this analysis, the heatmaps with density bands were created.
- Each density band was subdivided based on the rule given below with the help of each heat map statistics;

    - values lower than the average value (M);

    - M + 2 *standard deviations (SD);

    - M + 4*SD;

    - M + 6*SD;

    - values greater than M + 6*SD.

- After the step above, the location of traffic collisions where the density values are higher than M + 6*SD is identified as the critical point in the road network.
- The critical points in the road network which presented 3 out of 6 positive study periods were identified as hazardous road locations(HRL).

The following sections show the results of the KDE analysis and hazardous road locations (HRL) for six study periods regarding all VRU and related sub-categories.

4.3.1. VRU Overall Analysis

Firstly KDE method was applied for all VRU regarding six study periods. Fig 4.23 shows the traffic collisions of all VRU based on the six study periods. Red dots represent each traffic collision in the city of Turin. It is clear to see that traffic collisions are more concentrated in urban areas than the rural areas.

Fig 4.23 : Spatial distributions of VRU collisions : (a) 2006-2007, (b) 2008-2009, (c) 2010-2011, (d) 2012-2014, (e) 2015-2016, (f) 2017-2019

By using the maps including all VRU for six study periods, the KDE method was applied for six study periods. As a result of the KDE method, heat maps were created. Heat maps of six study periods are shown in Annex 6. Then, the density band of each map was rearranged based on the rule given above with the help of each heatmap statistic. After this step, the location of traffic collisions where the density values are higher than M + 6*SD is identified as the critical point in the road network.

Critical points for all VRU from 2006 to 2019 are extracted as given below (Fig. 4.24).

The critical points for all VRU were analyzed related to each study period and, the number of accidents was determined for each identified point. Firstly, the results were obtained for the period related to years from 2006 to 2007 as shown in Fig 4.25. “Piazza Vittorio Veneto” (accident no:5) was the most critical location for all VRU in the 2006-2007 period. There has been a total of 26 collision events in this location. Another point should be mentioned is “Corso Vittorio Emanuele II” that is close and parallel to “Piazza Vittorio Veneto”.

Fig 4.24 : All critical points for all VRU, from 2006 to 2019 (red dots represents the traffic collisions)

It can be concluded that this area was much more critical than others for all VRU in this period. There was a total of 20 traffic collisions for an accident no 3 (intersection in corso Regina Margherita and corso Potenza) and 4 (intersection in corso Peschiera and corso Trapani) that are located in the same corridor.

2006 - 2007		
No	Location of the accident	The number of accidents
1	Strada Settimo, Lungo Stura Lazio	9
2	Via Francesco Cigna, Corso Vigevano	7
3	Corso Margherita / Corso Lecce(8) - Corso Potenza (2)	10
4	Corso Peschiera, Corso Trapani	10
5	Piazza Vittorio Veneto	26
6	Corso Vittorio Emanuele II / Corso Cairoli(7) - Viale Virgilio(4)	11
7	Corso Fiume / Corso Moncalieri(6), Ponte Umberto I(2)	8
8	Corso Bramante / Corso Unione Sovietica (6), Corso Turati(3)	9
9	Corso Turati, Corso Lepanto	3
10	Corso Orbassano, Via Filadelfia	8
11	Corso Piero Maroncelli, Via Nizza	5

Fig 4.25 : Critical points for VRU, for the period 2006-2007 (red dots represents the traffic collisions)

The following figure shows the critical points for all VRU in the period 2008-2009. “Piazza Rivoli” (accident no:4) was the most critical location for all VRU in the 2008-2009. There has been a total of 15 collision events in this location. It can be also highlighted that accident no 2 (intersection in corso Regina Margherita and corso Potenza) and 6 (intersection in corso Peschiera and corso Trapani) are in the same corridor with Piazza Rivoli.

2008-2009		
No	Location of the accident	The number of accidents
1	Corso Giulio Cesare, Corso Novara	11
2	Corso Regina Margherita / Corso Potenza(11), Corso Lecce(1)	12
3	Corso Regina Margherita / Piazza Maria Ausiliatrice(2), Corso Principe Eugenio(5)	7
4	Piazza Rivoli	15
5	Via Cernaia / Corso Giuseppe Siccardi(3), 14 (3)	6
6	Corso Peschiera, Corso Trapani	11
7	Piazza Sabotino	12
8	Corso Vittorio Emanuele II, Corso Re Umberto	9
9	Corso Moncalieri, Corso Fiume	6

Fig 4.26 : Critical points for VRU, for the period 2008-2009(red dots represents the traffic collisions)

Fig 4.27 shows the critical points for all VRU in the period 2010-2011. It is realized that critical points were close to each other in this study period. As in the previous period, “Piazza Rivoli” (accident no:7) was the most critical location for all VRU in 2010-2011. There has been a total of 14 collision events in this location. Moreover, accident no 1 (intersection in corso Regina Margherita and corso Potenza) and 2 (intersection in corso Lecce and corso Claudio Appio) supported this location with a total of 20 traffic collisions. It can be also seen that the accidents in “Piazza Rivoli” were in the same corridor as the accidents in corso Vittorio Emanuele II (accidents no 9, 10, and 11).

2010-2011 / VRU
Critical Points

2010-2011		
No	Location of the accident	The number of accidents
1	Corso Regina Margherita / Corso Potenza(8), Corso Lecce(4)	12
2	Corso Lecce, Corso Claudio Appio	8
3	Via Cibrario Liuigi / Corso Alessandro Tassoni(6), Via Netro(2)	8
4	Corso Umbria, Via Caserta	4
5	Corso Regina Margherita, Corso Principe Eugenio	7
6	Piazza Statuto	12
7	Piazza Rivoli	14
8	Corso Peschiera, Corso Racconigi	9
9	Corso Vittorio Emanuele II, Corso Duca Degli Abruzzi(6), Corso Vinzaglio(2)	8
10	Corso Vittorio Emanuele II, Piazza Carlo Felice(3), Via Paolo Sacchi(4)	7
11	Corso Vittorio Emanuele II, Via Albertina Accademia(4), Via Madama Cristina(4)	8
12	Corso Siracusa, Corso Sebastopoli	10

Fig 4.27 : Critical points for VRU, for the period 2010-2011 (red dots represents the traffic collisions)

The following figure shows the critical points for all VRU in the period 2012-2014. Generally, the critical points were detected in the squares of the city for this period. “Piazza Rivoli”, “Piazza Lorenzo Bernini” and “Piazza Statuto” are in the same corridor and, a total of 52 accidents occurred in these squares for the given study period. “Piazza Vittorio Veneto” (a total of 24 collision events for all VRU) was the most critical point based on the number of accidents in this study period. The number of accidents is relatively high since this period includes three years of crash records.

2012-2014 / VRU
Critical Points

2012-2014		
No	Location of the accident	The number of accidents
1	Piazza Derna / Corso Giulio Cesare, Via Sandro Botticelli	14
2	Corso Novara, Corso Palermo	12
3	Corso Lecce, Via Michele Lessona	9
4	Piazza Della Repubblica	22
5	Piazza Rivoli	20
6	Piazza Lorenzo Bernini / Corso Francia, Corso Alessandro Tassoni, Corso Francesco Ferrucci	18
7	Piazza Statuto	14
8	Corso Vittorio Emanuele II / Corso Castelfidardo(8), Corso Inghilterra(3)	11
9	Piazza Vittorio Veneto	24
10	Corso Vittorio Emanuele II, Via Nizza	7
11	Via Nizza / 2,3,4,5,7	8
12	Piazza Omero / Corso Orbassano	5
13	Via Guido Reni, Via Paolo Gaidano	5

Fig 4.28 : Critical points for VRU, for the period 2012-2014 (red dots represents the traffic collisions)

Figure 4.29 shows the critical points for all VRU in the period 2015-2016. “Piazza Rivoli” was the most critical point with a total of 18 collision events in this period. It can be seen from the figure that “Piazza Rivoli” is in the same corridor with accidents no 6, 7, and 10 while also crossing with “Piazza Lorenzo Bernini” in another direction.

2015-2016		
No	Location of the accident	The number of accidents
1	Corso Mortara / Via Livorno(4), Via Orvieto(4)	8
2	Corso Giulio Cesare, Corso Novara	12
3	Piazza Rivoli	18
4	Piazza Lorenzo Bernini / Corso Francia, Corso Alessandro Tassoni	15
5	Piazza XVIII Dicembre	10
6	Corso Vittorio Emanuele II, Corso Castelfidardo	9
7	Corso Vittorio Emanuele II / Corso Duca Degli Abruzzi(3), Corso Vinzaglio(7)	10
8	Corso Castelfidardo, Corso Peschiera, Corso Einaudi Luigi, Corso Mediterraneo	11
9	Via Monginevro, Via de Francesco Sanctis	7
10	Corso Moncalieri, Corso Fiume	7
11	Piazzale San Gabriele di Gorizia / Corso Unione Sovietica, Via Filadelfia	10

Fig 4.29 : Critical points for VRU, for the period 2015-2016 (red dots represents the traffic collisions)

The following figure shows the critical points for all VRU in the period 2017-2019. Generally, the critical points were detected in the squares of the city for this period. “Piazza Rivoli”, “Piazza Lorenzo Bernini” and “Piazza Statuto” are in the same corridor and, a total of 45 accidents occurred in these squares for the given study period. Piazza Rivoli is in the same corridor with accident no 6 (intersection in corso Vittorio Emanuele II and corso Castelfidardo). There was a total of 30 traffic collisions in this corridor. The number of accidents is relatively high since this period includes three years of crash records.

2017-2019		
No	Location of the accident	The number of accidents
1	Piazza Generale Antonio Baldissera	17
2	Piazza Statuto	13
3	Piazza Lorenzo Bernini	14
4	Piazza Rivoli	18
5	Corso Peschiera, Corso Trapani	10
6	Corso Vittorio Emanuele II / Corso Castelfidardo(8), Corso Inghilterra(4)	12
7	Via Nizza / 1(2),2(1), 3(1), 4(3), 5(2), Via San Pio V(3)	12
8	Corso D' Azeglio Massimo, Via Francesco Petrarca	9
9	Corso Orbassano, Via Gorizia	6

Fig 4.30 : Critical points for VRU, for the period 2017-2019 (red dots represents the traffic collisions)

After the identification of critical points for all VRU, the critical points in the road network which presented 3 out of 6 positive study periods were identified as hazardous road locations (HRL) as shown in Figure 4.31. According to the results, seven hazardous road locations (HRL) are obtained for all VRU in the years from 2006 to 2019. It can be seen from the table that Piazza Rivoli with a total of 94 traffic collisions from 2006 to 2019 is the most dangerous location for all VRU. It can be highlighted that the locations of all hazardous roads are interconnected. Piazza Rivoli relates to three different corridors but, the most critical corridor is in the line of accident no 1, 2 and, 3 with a total of 231 traffic collisions from 2006 to 2019 for all VRU.

No	Hazardous Road Locations
1	Piazza Statuto
2	Piazza Lorenzo Bernini
3	Piazza Rivoli
4	Intersection : corso Vittorio Emanuele II - corso Castelfidardo
5	Intersection : corso Peschiera - corso Trapani
6	Intersection: corso Moncalieri - corso Fiume
7	Intersection: corso Regina Margherita - Corso Potenza

No	Hazardous Road Locations	2006-2007	2008-2009	2010-2011	2012-2014	2015-2016	2017-2019	TOT
1	Piazza Statuto	13	9	12	14	10	13	71
2	Piazza Lorenzo Bernini	11	4	4	18	15	14	66
3	Piazza Rivoli	9	15	14	20	18	18	94
4	Intersection : corso Vittorio Emanuele II - corso Castelfidardo	3	3	2	8	9	12	37
5	Intersection : corso Peschiera - corso Trapani	10	11	4	10	2	10	47
6	Intersection: corso Moncalieri - corso Fiume	8	6	2	5	7	5	33
7	Intersection: corso Regina Margherita - corso Potenza, corso Lecce	10	12	12	12	8	9	63

Figure 4.31 : Hazardous Road locations (HRL) for all VRU (red dots represents the traffic collisions)

By comparing the results for six study periods, false positive and false negative locations are identified. The false-positive problem arises when a safe site is being wrongly identified as hazardous. Conversely, the false-negative problem arises when a high-risk site is not being identified as an HRL. So, those locations are determined in the view of such information with a help of the heat maps:

<u>False Positive Locations for all VRU</u>

- Intersection in strada Settimo, lungo Stura Lazio,
- Intersection in corso Orbassano, via Gorizia,
- Corso Siracusa, Corso Sebastopoli.

<u>False Negative Locations for all VRU</u>

- Piazza Vittorio Veneto,
- Piazza Derna,
- Corso Giulio Cesare, Corso Novara,
- Intersection in corso Vittorio Emanuele II / corso Duca Degli Abruzzi, Corso Vinzaglio.

4.3.2. Pedestrian Analysis

By using the maps including traffic collisions relating to pedestrians for six study periods, the KDE method was applied for six study periods. As a result of the KDE method, heat maps were created. Heat maps of six study periods are shown in Annex 7. Then, the density band of each map was rearranged based on the rule given in the beginning of the Chapter 4.3 with the help of each heatmap statistic. After this step, the location of traffic collisions where the density values are higher than M + 6*SD is identified as the critical point in the road network.

All critical points relating to pedestrians are extracted as given below.

The critical points for pedestrians were analyzed related to each study period and, the number of accidents was determined for each identified point. Firstly, the results were obtained for the period related to years from 2006 to 2007 as shown in Fig 4.33. The intersection in corso Palermo and corso Novara (accident no 1) was the most critical location for pedestrians in the 2006-2007 period. There has been a total of 7 collision events in this location. Another point that should be mentioned is the intersection in via Bologna and corso Novara which is in the same corridor with accident no 1.

Fig 4.32 : All critical points for pedestrians, from 2006 to 2019 (red dots represents the traffic collisions)

Fig. 4.34 shows the critical points for pedestrians in the period 2008-2009. “Piazza Rivoli” (accident no:6) and “Piazza Sabotino” (accident no:7) were the most critical locations for pedestrians in the 2008-2009 although they are not in the same corridor.

Fig 4.35 shows the critical points for pedestrians in the period 2010-2011. It is realized that critical points were far from each other in this study period. As in the previous period, “Piazza Rivoli” (accident no:4) was the most critical location for pedestrians in 2010-2011. There has been a total of 13 collision events in this location. Moreover, accidents no 1 and 2 related to “corso Giulio Cesare” are in the same corridor with a total of 13 traffic collisions.

Fig 4.36 shows the critical points for pedestrians in the period 2012-2014. Generally, the critical points were detected in the squares of the city for this period. “Piazza Baldissera Antonio Generale”, “Piazza Della Republica” and “Piazza Vittorio Veneto” were the critical locations for the pedestrians based on the number of accidents in this study period. The number of accidents is relatively high since this period includes three years of crash records.

Figure 4.37 shows the critical points for pedestrians in the period 2015-2016. “Piazza XVIII Dicembre” was the most critical point with a total of 10 collision events in this period. It can be seen from the figure that the critical points for pedestrians in this period are distributed evenly spaced.

The Fig 4.38 shows the critical points for pedestrians in the period 2017-2019. Generally, the critical points were detected in the squares of the city for this period. It can be seen that “Piazza Vittorio Veneto” was the most critical location with a total of 15 traffic collisions. Generally, it is not possible to make inferences since the critical points were distributed so far from each other. The number of accidents is relatively high since this period includes three years of crash records.

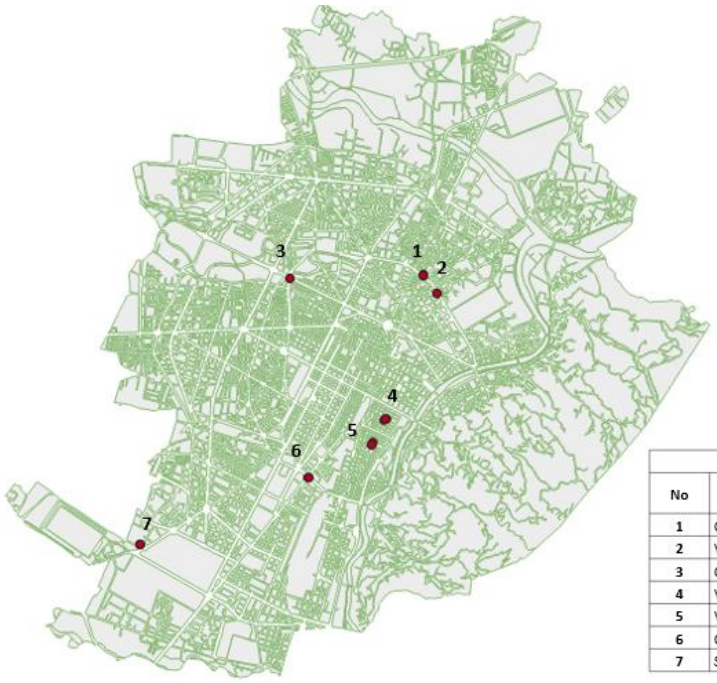

2006 -2007		
No	**Location of the accidents**	**The number of accidents**
1	Corso Palermo, Corso Novara	7
2	Via Bologna, Corso Novara	6
3	Corso Regina Margherita, Corso Tassoni	3
4	Via Madama Cristina, Via Claudio Luigi Berthollet	5
5	Via Madama Cristina, Via Valperga	4
6	Corso Turati, Corso Bramante, Corso Unione Sovietica	4
7	Strada Portone, 10	7

Fig 4.33 : Critical points for pedestrians in the period 2006-2007 (red dots represents the traffic collisions)

2008-2009		
No	**Location of the accident**	**The number of accidents**
1	Corso Giulio Cesare - / Via Luigi Salvatore Cherubini(3),116(2)	5
2	Via Bologna, Via Padova	6
3	Corso Giulio Cesare, 17, 20,**21**,23	7
4	Corso Belgio, Corso Tortona	6
5	Corso Francia, 161(2),163(1)	3
6	Piazza Rivoli : Corso Francia(3), Corso Lecce(2), Vittorio Emanuele II (2)	7
7	Piazza Sabotino : Corso Peschiera(4), Via Monginevro(4), Via dante di Nanni(1)	9

Fig 4.34 : Critical points for pedestrians in the period 2008-2009 (red dots represents the traffic collisions)

2010-2011 / Pedestrians
Critical Points

2010-2011		
No	Location of the accident	The number of accidents
1	Corso Giulio Cesare, Via Baltea(2) / Corso Palermo, Via Baltea(1)/ Corso Giulio Cesare 92,97,98/Corso Palermo,124	7
2	Corso Giulio Cesare, Corso Novara	6
3	Via Francesco Cigna, Strada Fortino(2), Via Urbino(2),50(1), Agrigento(1)	6
4	Piazza Rivoli - / Corso Vittorio Emanuele II(4), Corso Lecce(3), Corso Francia(3), Via Domodossola(1), 14(1), Via Francia(4)	13
5	Corso Vittorio Emanuele II - / Piazza Carlo Felice(3), Via Paolo Sacchi(2), Via Venti Settembre(1), Via Alessandro Volta(1), 57(1)	8
6	Corso Peschiera, Corso Racconigi	7
7	Corso Bramante 85(1),90(3),91(1), 92(1), 94(1)	7

Fig 4.35 : Critical points for pedestrians in the period 2010-2011 (red dots represents the traffic collisions)

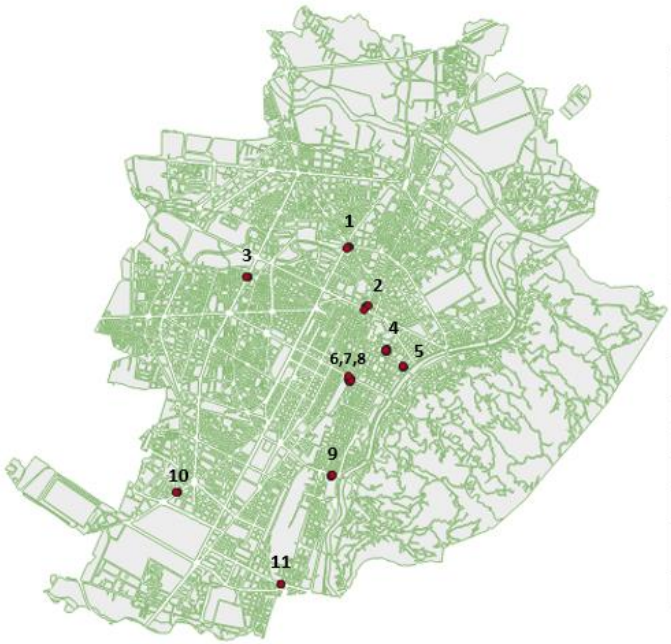

2012-2014 / Pedestrians
Critical Points

2012-2014		
No	Location of the accident	The number of accidents
1	Piazza Baldissera Antonio Generale - /Via Cecchi Antonio(3), Corso Principe Oddone(4), Corso Vigevano(1), Via Enrico Giachino(2)	10
2	Piazza Della Republica - / 18(3), Via Milano(1), Corso Giulio Cesare(1), S. Giuseppe Benedetto Cottolengo(1), Via Clemente Damiano Priocca(1), Corso Regina Margherita(3), others(5)	15
3	Corso Lecce, Via Michele Lessona	6
4	Via Po- / Via Dell' Accademia Albertina(5), Via Gioachino Rossini(3)	8
5	Piazza Vittorio Veneto- / Via Vanchiglia(2),Via Alfonso Bonafous(2), others(10)	14
6	Via Nizza- / 2,3,4,5(2), Via San Pio V(2)	7
7	Via Nizza- Corso Vittorio Emanuele II	2
8	Corso Vittorio Emanuele II, Piazza Carlo Felice	4
9	Corso Lazzari Francesco Detto II Bramante 90(3),94(1), 96(2),88(1), Null(1)	8
10	Corso Orbassano , / Via Reni Guido(2), Carlo Alfonso Nallino(3), Piazza Omero(3) + (Via Guido Reni, Via Paolo Gaidano), others(2)	11
11	Corso Maroncelli Pietro, Via Canelli	7

Fig 4.36 : Critical points for pedestrians in the period 2012-2014 (red dots represents the traffic collisions)

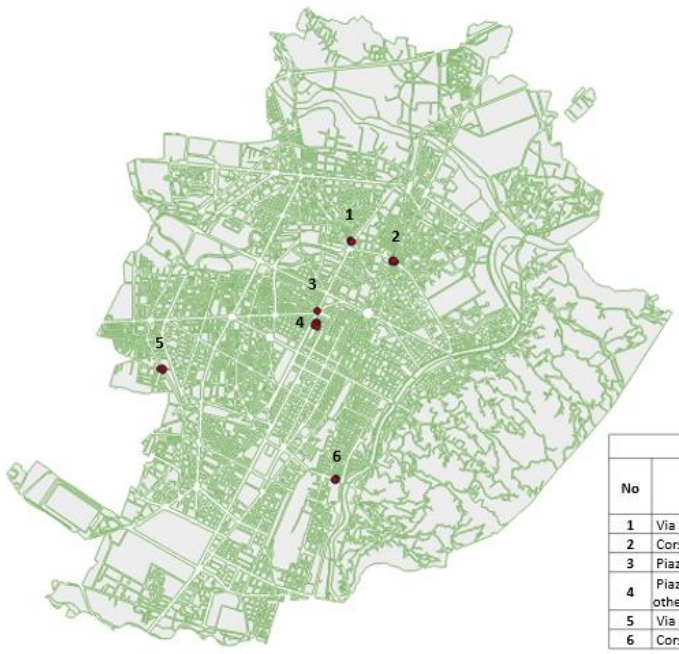

2015-2016		
No	**Location of the accident**	**The number of accidents**
1	Via Stradella- / 22(2),24(1),Corso Venezia(2)	5
2	Corso Novara, Corso Giulio Cesare	8
3	Piazza Statuto - / Via Luigi Cibrario(3), Corso Principe Oddone(1), others(3)	7
4	Piazza XVIII Dicembre- / Corso San Martino(4),Via Santarosa Pietro(1), others(5)	10
5	Via Monginevro, Via de Sanctis Francesco	5
6	Corso Lazzari Francesco Detto Il Bramante 89(2), 92(3), Via Carl Ormea(1)	6

Fig 4.37 : Critical points for pedestrians in the period 2015-2016 (red dots represents the traffic collisions)

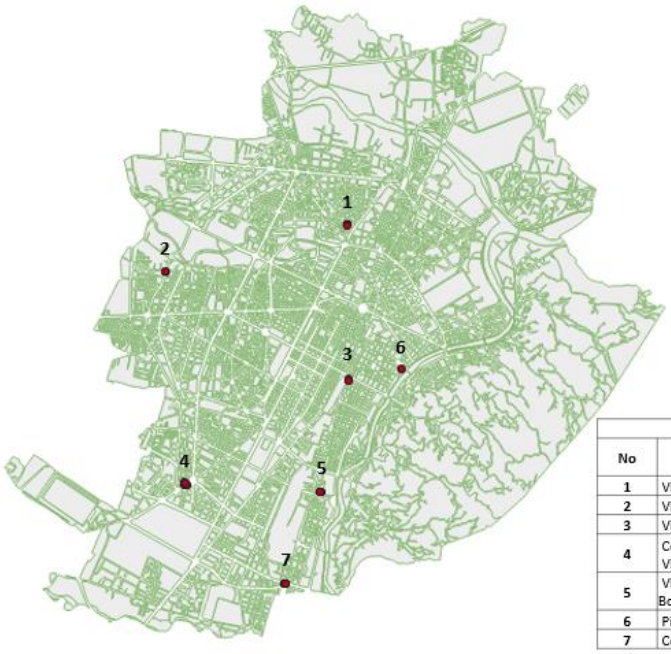

2017-2019		
No	**Location of the accident**	**The number of accidents**
1	Via Chiesa Della Salute, Via Vibo'	7
2	Via Pietro Cossa, Via Giovanni Servais	8
3	Via Nizza - / 1,3, 4(2), 5, Via San Pio V	6
4	Corso Orbassano- / 260(2), 277(3), Via Guido Reni, Via Castelgomberto, Via Don Grazioli Bartolomeo	8
5	Via Genova, Via Varazze -/ Via Genova(4), Via Cherasco(2), Piazza Camillo Bozzolo	7
6	Piazza Vittorio Veneto	15
7	Corso Pietro Maroncelli, Via Nizza	7

Fig 4.38 : Critical points for pedestrians in the period 2017-2019 (red dots represents the traffic collisions)

After the identification of critical points for pedestrians, the critical points in the road network which presented 3 out of 6 positive study periods were identified as hazardous road locations (HRL) as shown in Figure 4.39. According to the results, one hazardous road location (HRL) is obtained for pedestrians in the years from 2006 to 2019. It can be seen from the table that Corso Bramante, 20 with a total of 23 traffic collisions from 2006 to 2019 is the most dangerous location for pedestrians. Although this location is not the most critical location for six study periods, it has been chosen as a hazardous road location since it is presented 3 out of 6 positive study periods.

No	Hazardous Road Locations
1	Corso Bramante,92

No	Hazardous Road Locations	2006-2007	2008-2009	2010-2011	2012-2014	2015-2016	2017-2019	TOT
1	Corso Bramante, 92	3	3	5	7	3	2	23

Figure 4.39: Hazardous Road locations (HRL) for only pedestrians (red dots represents the traffic collisions)

By comparing the results for six study periods, false positive and false negative locations are identified for pedestrians. So, those locations are determined in the view of such information with a help of the heat maps:

<u>False Positive Locations for pedestrians:</u>

- Strada Portone,10 ,
- Via Madama Cristina, Via Claudio Luigi Berthollet.

False Negative Locations for pedestrians:

- Piazza Vittorio Veneto,
- Piazza Rivoli.

4.3.3. Motorcyclists Analysis

By using the maps including traffic collisions relating to motorcycle users for six study periods, the KDE method was applied for six study periods. As a result of the KDE method, heat maps were created. Heat maps of six study periods are shown in Annex 8. Then, the density band of each map was rearranged based on the rule given in the beginning of the Chapter 4.3 with the help of each heatmap statistic. After this step, the location of traffic collisions where the density values are higher than M + 6*SD is identified as the critical point in the road network.

All critical points relating to pedestrians are extracted as given below.

Fig 4.40 : All critical points for motorcycle users, from 2006 to 2019 (red dots represents the traffic collisions)

The critical points for motorcycle users were analyzed related to each study period and, the number of accidents was determined for each identified point. Firstly, the results were obtained for the period related to years from 2006 to 2007 as shown in Fig 4.41. The intersection in corso Regina Margherita & corso Lecce / corso Potenza and Piazza Adriano were the most critical locations for motorcycle users in the 2006-2007 period. It can be seen from the figure that accident no 3 (intersection in corso Regina Margherita and corso Lecce) is in the same corridor with accident no 6 (intersection in corso Trapani and corso Peschiera) with a total of 17 collision events.

The following figure shows the critical points for motorcycle users in the period 2008-2009. While the most critical location was the intersection in corso Regina Margherita & Piazza Maria Ausiliatrice, accident no 5 (intersection in corso Vittorio Emanuele II - / corso Duca Degli Abruzzi, corso Vinzaglio), 7 (intersection in corso Vittorio Emanuele II, via S. Secondo), and 8 (intersection in via Fiume & corso Moncalieri) created the long corridor with a total of 23 traffic collisions related to the motorcyclists. It can be seen from the figure that accident no 3 (intersection in corso Regina Margherita and corso Lecce) is in the same corridor with accident no 6 (intersection in corso Trapani and corso Peschiera) with a total of 13 collision events.
Fig 4.43 shows the critical points for motorcycle users in the period 2010-2011. It is realized that critical points were far from each other in this study period. accidents no 1,2 and 6 related to “corso Regina Margherita” are in the same corridor with a total of 16 traffic collisions.

Figure 4.44 shows the critical points for motorcycle users in the period 2012-2014. The number of accidents is relatively high since this period includes three years of crash records. It is important to highlight that many corridors contain of more than two critical locations. The longest corridor includes accident no 2, 10, 11, 12, 4, and 5 with a total 48 of traffic collisions relating motorcyclists. “Piazza Rivoli” is the most critical location based on the number of accidents.

Figure 4.45 shows the critical points for motorcyclists in the period 2015-2016. The intersection in “corso Moncalieri & corso Fiume “ was the most critical point with a total of 11 collision events in this period. It can be seen from the figure that the critical points for motorcyclists in this period were distributed evenly spaced. Whereas accident no 1 and 2 were in the same corridor with a total 19 of traffic collisions in the years 2015-2016.

Fig 4.46 shows the critical points for motorcycle users in the period 2017-2019. It can be seen that “Piazza Riccardo Cattaneo” was the most critical location with a total of 10 traffic collisions. Generally, it is not possible to make inferences since the critical points were distributed so far from each other.

2006 -2007		
No	Location of the accident	The number of accidents
1	Strada Settimo, Lungo Sturo Lazio	9
2	Via Cigna, Corso Vigevano	5
3	Corso Regina Margherita- / Corso Lecce(6), Corso Potenza(2), others(2)	10
4	Corso Regina Margherita- / Corso S. Maurizio(2), Corso Regio Parco(4), 102(1)	7
5	Piazza Adriano - / Corso Vittorio Emanuele II(3), Corso Francesco Ferrucci(6), Via Frejus(1)	10
6	Corso Trapani, Corso Peschiera	7
7	Corso Agnelli, Corso Traiano	6

Fig 4.41 : Critical points for motorcycle users in the period 2006-2007 (red dots represents the traffic collisions)

2008-2009		
No	Location of the accident	The number of accidents
1	Corso Regina Margherita - / Corso Principe Eugenio(4), others(9)	13
2	Corso Regina Margherita, Piazza Maria Ausiliatrice	3
3	Corso Regina Margherita - / Corso Potenza(8), Corso Lecce(1)	8
4	Via Cernaia,9,11,14(2), Via S. Dalmazzo	5
5	Vittorio Emanuele II - / Corso Duca Degli Abruzzi(4), Corso Vinzaglio(3)	7
6	Corso Trapani, Corso Peschiera	5
7	Vittorio Emanuele II - / Via S. Secondo(4),62, 63, 65, Via Arsenale	8
8	Via Fiume, Corso Moncalieri	4
9	Corso Massimo D' Azeglio - / Via Federico Campana(3), Via Morgari Oddino(2), Via Giuseppe Giacosa(2), 30, 34, 38	10
10	Corso Bramante,20	2

Fig 4.42 : Critical points for motorcycle users in the period 2008-2009 (red dots represents the traffic collisions)

2010-2011 / Motorcycles
Critical Points

2010-2011		
No	Location of the accident	The number of accidents
1	Corso Regina Margherita, Corso Potenza	8
2	Corso Regina Margherita, Corso Lecce	3
3	Corso Vittorio Emanuele II, Corso Duca degli Abruzzi	5
4	Corso Vittorio Emanuele II, Corso Vinzaglio	3
5	Via Borgaro, Via Bernardino Luini	5
6	Corso Umbria - / Corso Margherita Regina, Corso Principe Oddone, Via Caserta,Via S. Giovanni Bosco, 5	5
7	Corso Sebastopoli, Corso Siracusa	7
8	Corso Bramante - / Corso Unione Sovietica(3), Corso Lepanto(2), 5, 6	7
9	Corso Unione Sovietica, Corso Lepanto / Corso Flippo Turati, Corso Lepanto	2

Fig 4.43 : Critical points for motorcycle users in the period 2010-2011 (red dots represents the traffic collisions)

2012-2014 / Motorcycles
Critical Points

2012-2014		
No	Location of the accident	The number of accidents
1	Corso Regina Margherita - / Corso Lecce(6), Corso Potenza(3)	9
2	Piazza Rivoli - / Corso Trapani(3), Corso Vittorio Emanuele II(3), Corso Francia(5),Corso Lecce(1)	12
3	Corso Racconigi, Corso Peschiera	8
4	Corso Vittorio Emanuele II- / Corso Massimo D'Azeglio(4), Via Calandra Fratelli(2), 2(2)	8
5	Corso Vittorio Emanuele II- / Viale Marone Publio Virgilio(4), Corso Cairoli(2), 4, 6(2)	9
6	Corso Mediterraneo - / Corso Francesco Ferrucci(5), Via Cristoforo Colombo(2), Via Paolo Braccini(1), (Via Braccini Paolo, Corso Lione)	9
7	Corso Unione Sovietica, Piazzale San Gabriele di Gorizia	11
8	Corso Giovanni Angelli, Via Filadelfia	5
9	Piazza Massaua- / Via Pietro Cossa(4), Corso Francia((4)	8
10	Corso Vittorio Emanuele II- / Via Paolo Borsellino(2), Via Giovanni Falcone(3), 130(1)	6
11	Corso Vittorio Emanuele II- / Corso Inghilterra(3), Corso Castelfidardo(2), 127(1)	6
12	Corso Vittorio Emanuele II, Corso Re Umberto I	7
13	Corso Trapani, Corso Peschiera	7
14	Corso Galileo Ferraris, Corso Einaudi Liuigi	7

Fig 4.44 : Critical points for motorcycle users in the period in the period 2012-2014 (red dots represents the traffic collisions)

2015-2016		
No	Location of the accident	The number of accidents
1	Corso Vittorio Emanuele II- / Corso Vinzaglio(6), Corso Duca Degli Abruzzi(2)	8
2	Corso Moncalieri- / Corso Fiume(6), Ponte Umberto I(2),Via Volturno(2), Via Curtatone	11
3	Corso Unione Sovietica, Piazzale San Gabriele di Gorizia(6), others (3)	9
4	Corso Re Umberto I, Via Tirreno	4
5	Corso Umbria, Via Macerata	5
6	Corso Novara, Corso Regio Parco	5

Fig 4.45 : Critical points for motorcycle users in the period in the period 2015 -2016 (red dots represents the traffic collisions)

2017-2019		
No	Location of the accident	The number of accidents
1	Corso Regina Margherita - / Corso Lecce(5), Corso Potenza(2)	7
2	Corso Tortona, Corso Belgio	8
3	Via Dell' Accademia Albertina, Via Cavour Camillo Benso	8
4	Corso D'Azeglio Massimo, Via Francesco Petrarca	6
5	Corso Bramante, Corso Unione Sovietica : 2, Corso Bramante, Corso Filippo Turati : 3, Corso Unione Sovietica, Corso Lepanto : 1	6
6	Corso Bramante,20	4
7	Corso Orbassano, Via Gorizia	6
8	Piazza Riccardo Cattaneo, Corso Enrico Tazzoli, Corso Orbassano	10

Fig 4.46 : Critical points for motorcycle users in the period in the period 2017 -2019 (red dots represents the traffic collisions)

After the identification of critical points for motorcyclists, the critical points in the road network which presented 3 out of 6 positive study periods were identified as hazardous road locations(HRL) as shown in Figure 4.47. According to the results, six hazardous road locations

(HRL) are obtained for motorcycle users in the years from 2006 to 2019. It can be seen from the table that the intersection in corso Trapani & corso Peschiera with a total of 27 traffic collisions from 2006 to 2019 is the most dangerous location for motorcyclists. Moreover, the first three hazardous road locations (HRL) were located in the same corridor.

By comparing the results for six study periods, false positive and false negative locations are identified for pedestrians. So, those locations are determined in the view of such information with a help of the heat maps:

<u>False Positive Locations for motorcycle users:</u>

- Via Cigna, Corso Vigevano,
- Piazza Riccardo Cattaneo.

<u>False Negative Locations for motorcycle users:</u>

- The intersection in corso Moncalieri & corso Fiume.

No	Hazardous Road Locations
1	Intersection : corso Regina Margherita - corso Potenza
2	Intersection : corso Regina Margherita - corso Lecce
3	Intersection : corso Trapani - corso Peschiera
4	Intersection : corso Vittorio Emanuele II - corso Vinzaglio
5	Intersection : corso Vittorio Emanuele II - corso Duca degli Abruzzi
6	Intersection : corso Bramante - corso Unione Sovietica

No	Hazardous Road Locations	2006-2007	2008-2009	2010-2011	2012-2014	2015-2016	2017-2019	TOT
1	Intersection : corso Regina Margherita - corso Potenza	2	8	8	3	1	2	24
2	Intersection : corso Regina Margherita - corso Lecce	6	1	3	6	3	5	24
3	Intersection : corso Trapani - corso Peschiera	7	5	2	7	1	5	27
4	Intersection : corso Vittorio Emanuele II - corso Vinzaglio	-	3	3	2	6	1	15
5	Intersection : corso Vittorio Emanuele II - corso Duca degli Abruzzi	1	4	5	1	2	2	15
6	Intersection : corso Bramante - corso Unione Sovietica	1	1	3	3	3	1	12

Figure 4.47: Hazardous Road locations (HRL) for only motorcycle users (red dots represents the traffic collisions)

4.3.4. Velocipede users Analysis

By using the maps including traffic collisions relating to velocipede users for six study periods, the KDE method was applied for six study periods. As a result of the KDE method, heat maps were created. Heat maps of six study periods are shown in Annex 9. Then, the density band of each map was rearranged based on the rule given in the beginning of the Chapter 4.3 with the help of each heatmap statistic. After this step, the location of traffic collisions where the density values are higher than M + 6*SD is identified as the critical point in the road network.

All critical points relating to velocipede users are extracted as given below in Fig 4.48.

Fig 4.48 : All critical points for velocipede users, from 2006 to 2019 (red dots represents the traffic collisions)

The critical points for velocipede users were analyzed related to each study period and, the number of accidents was determined for each identified point. Generally, a limited number of

critical locations are obtained since the number of crash records related to the velocipede users is low. Firstly, the results were obtained for the period related to years from 2006 to 2007 as shown in Fig 4.49. There were two critical locations which are far from each other.

Fig 4.50 shows the critical points for velocipede users in the period 2008-2009. It can be seen from the figure that two intersection points were identified as critical points.
Fig 4.51 shows the critical points for velocipede users in the period 2010-2011. It is realized that critical points were far from each other in this study period. “Piazza Generale Antonio Baldissera” is the most critical location in this study period.

Fig 4.52 shows the critical points for velocipede users in the period 2012-2014. The number of accidents is relatively high since this period includes three years of crash records. It is important to highlight that Piazza Statuto was in the crossing point of the two different corridors. Corridor 1 which includes accidents no 3, 4, and 5 had the same number of accidents as corridor 2 (accident no 3, 2, and 6) with a total 19 of accidents in each. Moreover, the most critical location was the intersection in corso Vittorio Emanuele II & corso Castelfidardo with a total of 8 traffic collisions in this study period. This location was also in the same corridor with the accident no 7 (the intersection in corso Vittorio Emanuele II & Via Nizza).

Figure 4.53 shows the critical points for velocipede users in the period 2015-2016. There were three different corridors obtained as accidents no 1&2, 3&4 and, 4&5 with a total number of 15, 14, and 13 traffic collisions respectively. “Piazza Rivoli” was the most critical point in the road network for this period and it was also in the most critical corridor based on the number of accidents.

Fig 4.54 shows the critical points for velocipede users in the period 2017-2019. “Piazza Statuto” was the most critical location with a total of 12 traffic collisions. Piazza Statuto was crossing with the two different corridors.

2006 -2007		
No	Location of the accident	The number of accidents
1	Corso Filadelfia, Corso Orbassano	5
2	Via Nizza, Corso Piero Maroncelli	5

Fig 4.49 : Critical points for velocipede users in the period 2006 -2007 (red dots represents the traffic collisions)

2008-2009		
No	Location of the accident	The number of accidents
1	Corso Trapani, Piazza Rivoli	4
2	Corso Galileo Ferraris, Corso Stati Uniti(2) / Corso Stati Uniti(2)	4

Fig 4.50 : Critical points for velocipede users in the period 2008 -2009 (red dots represents the traffic collisions)

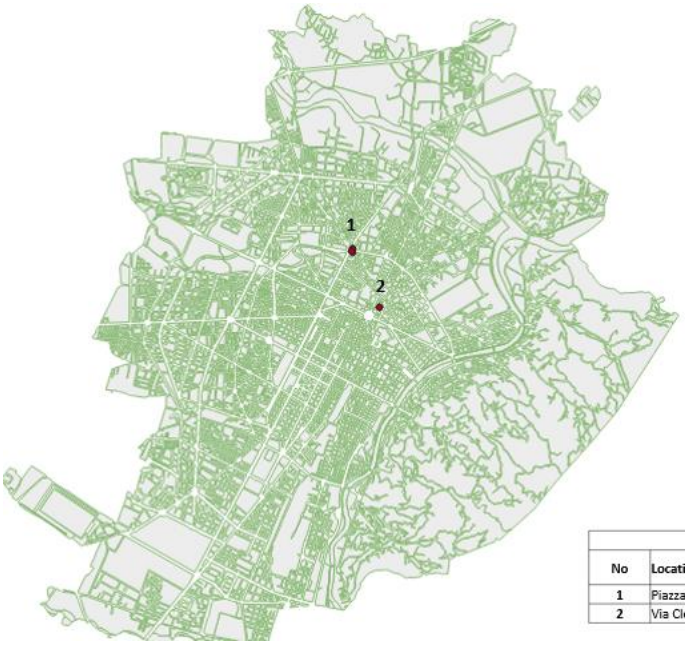

2010-2011 / Velocipede
Critical Points

2010-2011		
No	Location of the accident	The number of accidents
1	Piazza Antonio Generale Baldissera - / Via Stradella(3), Via Antonio Cecchi(2)	5
2	Via Clemente Damiano Priocca, Via Carlo Antonio Porporati	4

Fig 4.51 : Critical points for velocipede users in the period 2010 -2011 (red dots represents the traffic collisions)

2012-2014 / Velocipede
Critical Points

2012-2014		
No	Location of the accident	The number of accidents
1	Corso Mortara- / Via Orvieto(4), Via Livorno(1)	5
2	Corso Principe Oddone, Via Maria Ausiliatrice(3), Via San Giovanni Bosco(1), 32(1)	5
3	Piazza Statuto- / Via Cibrario Luigi(3), 24, Corso Francia, Corso Principe Eugenio	6
4	Piazza Lorenzo Bernini, Corso Alessandro Tassoni(2), Corso Francia(4), Corso Francesco Ferrucci	7
5	Piazza Rivoli, Corso Trapani :3, Corso Trapani, Corso Francia:1, Piazza Rivoli, Corso Vittorio Emanuele II :2	6
6	Corso Vittorio Emanuele II, Corso Castelfidardo	8
7	Corso Vittorio Emanuele II, Via Nizza	5
8	Corso Trapani, Corso Carlo e Nello Rosselli:5 / Corso Rosselli Carlo e Nello, Via San Paolo:2	7
9	Piazza Marmolada - / Corso Carlo e Nello Rosselli(3), Corso Racconigi, Corso Lione	5

Fig 4.52 : Critical points for velocipede users in period 2012-2014 (red dots represents the traffic collisions)

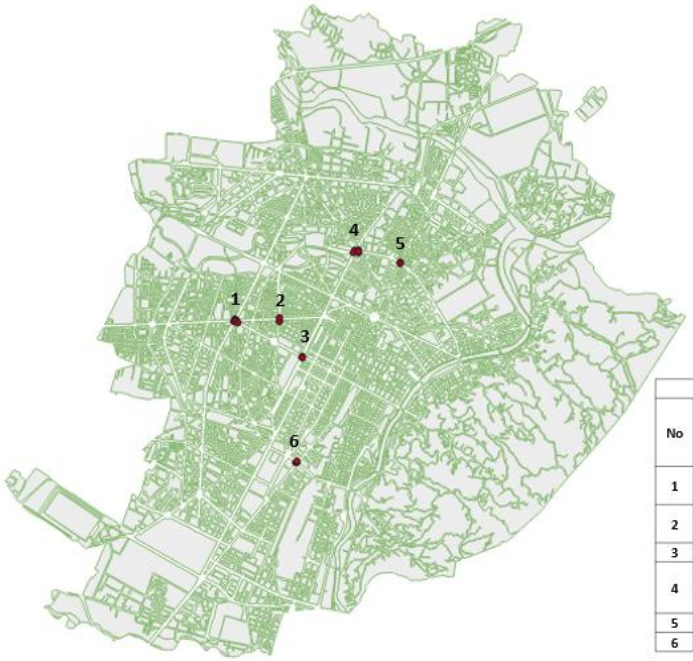

2015-2016		
No	Location of the accident	The number of accidents
1	Piazza Rivoli- / Corso Lecce(3), Corso Trapani(2), Corso Francia(2), Corso Vittorio Emanuele II, 237 (2)	9
2	Piazza Lorenzo Bernini - / Corso Francesco Ferrucci(3), Via Giacomo Medici, Corso Alessandro Tassoni, 9(1)	6
3	Corso Vittorio Emanuele II, Corso Castelfidardo	5
4	Piazza Baldissera Antonio Generale ,Corso Vigevano : 6 / Corso Mortara, Via Udine:2 / Piazza Baldissera Antonio Generale ,Via Giachino Errico : 1	9
5	Corso Novara, Corso Giulio Cesare	4
6	Corso Lepanto - / Corso Unione Sovietica(2), Corso Turati Filippo(1)	3

Fig 4.53 : Critical points for velocipede users in the period 2015-2016 (red dots represents the traffic collisions)

2017-2019		
No	Location of the accident	The number of accidents
1	Piazza Baldissera Antonio Generale - / Corso Mortara(4), Corso Principe Oddone(3), Corso Vigevano(2) / Corso Venezia, Corso Vigevano:1	10
2	Piazza Statuto- / Via San Donato(3), 22(2), Via Luigi Cibrario(3), Corso Principe Eugenio(1), 17, Via San Donato, Corso San Martino	12
3	Corso Pirincipe Oddone , / Via San Giovanni Bosco(2), Via Maria Ausiliatrice, 30	4
4	Piazza Lorenzo Bernini - / Corso Francia(5), Via Duchessa Jolanda, Corso Alessandro Tassoni(2)	8
5	Piazza Rivoli - / Corso Vittorio Emanuele II, Corso Francia(4), Corso Trapani, Corso Lecce	7
6	Corso Vittorio Emanuele II - / Corso Castelfidardo(4), Corso Inghilterra(2)	6

Fig 4.54 : Critical points for velocipede users in the period 2017-2019 (red dots represents the traffic collisions)

After the identification of critical points for velocipede users, the critical points in the road network which presented 3 out of 6 positive study periods were identified as hazardous road locations(HRL) as shown in Figure 4.55. According to the results, four hazardous road locations (HRL) are obtained for velocipede users in the years from 2006 to 2019. It can be seen from the table that “Piazza Rivoli” with a total of 29 traffic collisions from 2006 to 2019 is the most dangerous location for velocipede users. Moreover, “Piazza Rivoli” is in the same corridor with “Piazza Lorenzo Bernini”. This corridor has a high risk for velocipede users based on the evaluation in the number of accidents (a total of 52 traffic collisions).

By comparing the results for six study periods, false positive and false negative locations are identified for velocipede users. So, those locations are determined in the view of such information with a help of the heat maps:

<u>False Positive Locations for velocipede users:</u>

- Intersection corso Galileo Ferraris, corso Stati Uniti.

<u>False Negative Locations for velocipede users:</u>

- Piazza Statuto.

No	Hazardous Road Locations
1	Intersection : corso Vittorio Emanuele II - corso Castelfidardo
2	Piazza Rivoli
3	Piazza Lorenzo Bernini
4	Piazza Generale Antonio Baldissera

No	Hazardous Road Locations	2006-2007	2008-2009	2010-2011	2012-2014	2015-2016	2017-2019	TOT
1	Intersection : corso Vittorio Emanuele II - corso Castelfidardo	-	1	1	6	5	6	19
2	Piazza Rivoli	2	4	1	6	9	7	29
3	Piazza Lorenzo Bernini	2	-	1	6	6	8	23
4	Piazza Generale Antonio Baldissera	2	-	5	3	6	10	26

Figure 4.55 : Hazardous Road locations (HRL) for only velocipede users (red dots represents the traffic collisions)

4.3.5. Moped Analysis

By using the maps including traffic collisions relating to moped users for six study periods, the KDE method was applied for six study periods. As a result of the KDE method, heat maps were created. Heat maps of six study periods are shown in Annex 10. Then, the density band of each map was rearranged based on the rule given in the beginning of the Chapter 4.3 with the help of each heatmap statistic. After this step, the location of traffic collisions where the density values are higher than M + 6*SD is identified as the critical point in the road network.

All critical points relating to moped users are extracted as given below in Fig 4.56.

The critical points for moped users were analyzed related to each study period and, the number of accidents was determined for each identified point. Generally, a limited number of critical locations are obtained since the number of crash records related to the moped users is relatively lower than other vulnerable users. Firstly, the results were obtained for the period related to years from 2006 to 2007 as shown in Fig 4.57. There were two critical locations which are far from each other.

Fig 4.56 : All critical points for moped users, from 2006 to 2019 (red dots represents the traffic collisions)

Fig 4.58 shows the critical points for moped users in the period 2008-2009. It can be seen from the figure that two intersection points were identified as critical points.

Fig 4.59 shows the critical points for moped users in the period 2010-2011. Only one critical location was obtained for this period.

Fig 4.60 shows the critical points for moped users in the period 2012-2014. Only one intersection point was obtained as a critical location for this period in the west side of the city.

Figure 4.61 shows the critical points for moped users in the period 2015-2016. There was only one critical location obtained in this period.

Fig 4.62 shows the critical points for moped users in the period 2017-2019. Two critical locations were identified for this type of road users in this period. It is clear to see that these locations far from each other.

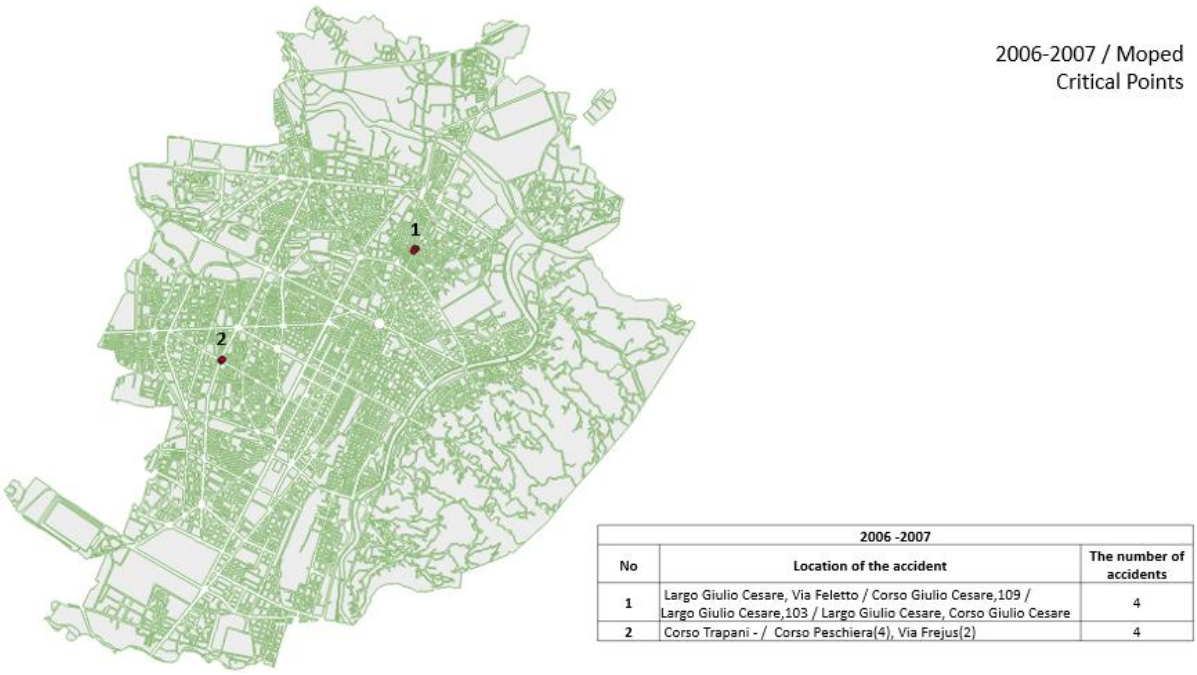

2006 -2007		
No	Location of the accident	The number of accidents
1	Largo Giulio Cesare, Via Feletto / Corso Giulio Cesare,109 / Largo Giulio Cesare,103 / Largo Giulio Cesare, Corso Giulio Cesare	4
2	Corso Trapani - / Corso Peschiera(4), Via Frejus(2)	4

Fig 4.57 : Critical points for moped users in the period 2006-2007 (red dots represents the traffic collisions)

2008-2009 / Moped
Critical Points

2008-2009		
No	Location of the accident	The number of accidents
1	Corso Novara, Corso Giulio Cesare	4
2	Via Passo Buole, Via Pio VII	3

Fig 4.58 : Critical points for moped users in the period 2008-2009 (red dots represents the traffic collisions)

2010-2011 / Moped
Critical Points

2010-2011		
No	Location of the accident	The number of accidents
1	Corso Vittorio Emanuele II, Via Madama Cristina(5), Via Accademia Albertina (1)	6

Fig 4.59 : Critical points for moped users in the period 2010-2011 (red dots represents the traffic collisions)

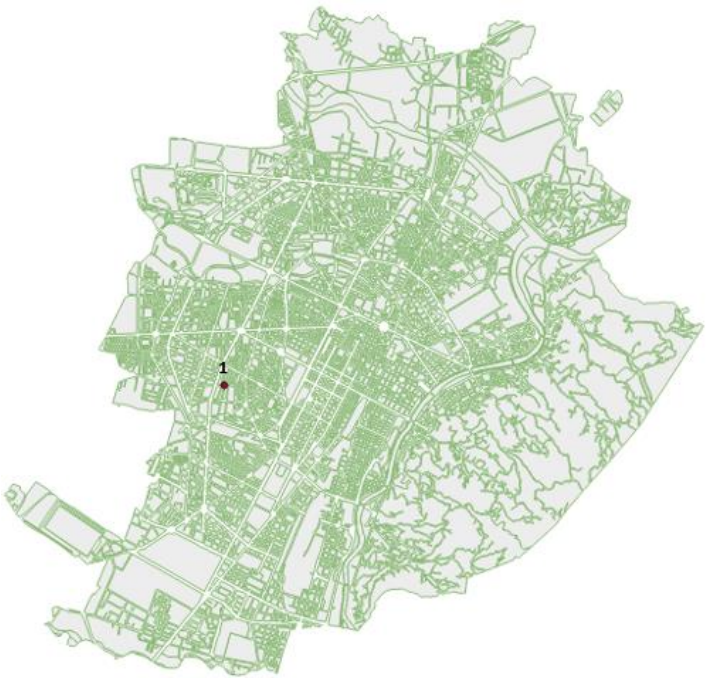

2012-2014 / Moped
Critical Points

2012-2014		
No	Location of the accident	The number of accidents
1	Via Isonzo, Via Monginevro	3

Fig 4.60 : Critical points for moped users in the period 2012-2014 (red dots represents the traffic collisions)

2015-2016 / Moped
Critical Points

2015-2016		
No	Location of the accident	The number of accidents
1	Via di Nanni Dante, 83, 90 / Piazza Sabotini, Corso Peschiera	3

Fig 4.61 : Critical points for moped users in the period 2015-2016 (red dots represents the traffic collisions)

2017-2019		
No	Location of the accident	The number of accidents
1	Via Antonio Giuseppe Bertola, Via San Tommaso	3
2	Corso Bramante - / 40(1), Via Giordano Bruno(3)	4

Fig 4.62 : Critical points for moped users in the period 2017-2019 (red dots represents the traffic collisions)

After the identification of critical points for moped users, hazardous road locations (HRL) were not identified since the critical locations that should be in 3 out of the 6 positive study periods could not be present. Based on this rule , it is not possible to identify hazardous road locations (HRL) for moped users. Moreover, the limited number of critical locations were obtained due to low number of crash records related to the moped users in database.

5. ANALYSIS AND DISCUSSION

Hazardous road locations (HRL) for overall VRU and the sub-categories of VRU were identified for the city of Turin in the period from 2006 to 2019 by using the ISTAT crash database. Within the scope of the case study, analyses were carried out for all sub-categories of VRU respectively. The results of the NN method provided the point patterns of the collision events were closely clustered together regarding six study periods. Moreover, G and F functions were used to verify the NN method. The outputs of the G and F functions also highlighted that a clustered structure was evident for all VRU and related sub-categories. As a result of the clustered structures of the point patters, we expected to identify HRL in some high-density areas that was exactly what we observed in KDE method. The kernel analysis indicates that some corridors in the city are more hazardous than others for specific sub-categories of VRU. However, the lack of geographic coordinates from the years 2006 to 2011 and 2017 to 2019 causes some difficulties in the identification of hazardous roads. For example, the address of one traffic collision is “Corso Vittorio Emanuele II, Via Nizza” while another one is “Via Nizza, 1”. These two addresses are so close to each other as shown in Fig. 5.1, and that could belong to the same location. Therefore, the presence of geographic coordinates of traffic collisions is so crucial to increase the accuracy of the analyses.

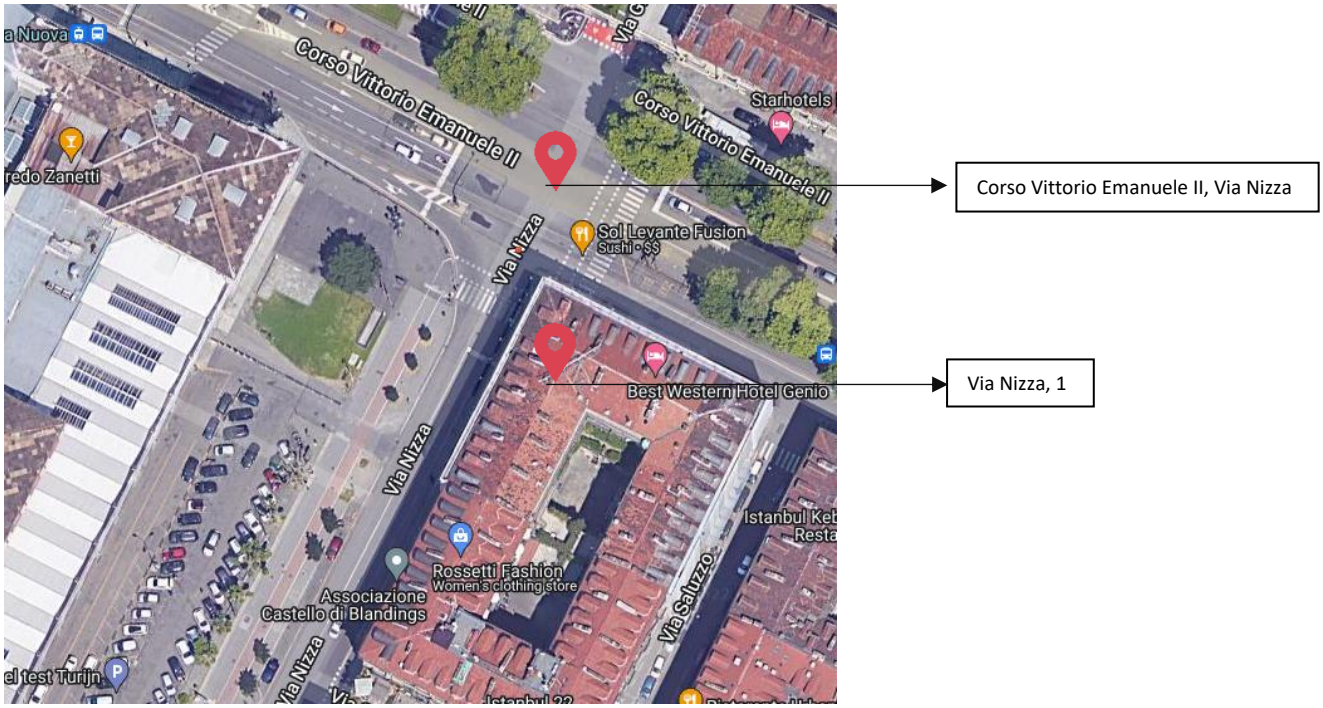

Fig 5.1 : The locations of the “Corso Vittorio Emanuele II, Via Nizza” and “Via Nizza, 1”

The entire study period from 2006 to 2019 was subdivided into 2–3-year periods to limit false-positive and false-negative locations. It is reasonable to identify a high number of HRL in three-year periods since the number of accidents is high for three years. In overall VRU, it is clarified the corridor which includes Piazza Rivoli, Piazza Lorenzo Bernini, and Piazza Statuto is the most critical line with a total of 231 traffic collisions from 2006 to 2019. Hazardous road locations (HRL) were also identified based on the sub-categories of VRU since safety countermeasures should be differentiated based on the specific VRU sub-category. Corso Bramante,92 was identified as HRL for pedestrians. When this location as given in Fig 5.3 is examined, it has been determined that there are many pedestrian roads in front of this address. Traffic accidents may have occurred on one of these pedestrian roads, but it is not so clear to identify which road segment and the location this address refers to. Corso Bramante is one of the main streets in the city of Turin and Corso Bramante,92 is the address where pedestrians interact with vehicles frequently since it is very close to the intersection. The safety of pedestrians can be improved by rearranging the pedestrian roads in this location.

Fig 5.2 : The corridor including Piazza Rivoli, Piazza Lorenzo Bernini, and Piazza Statuto

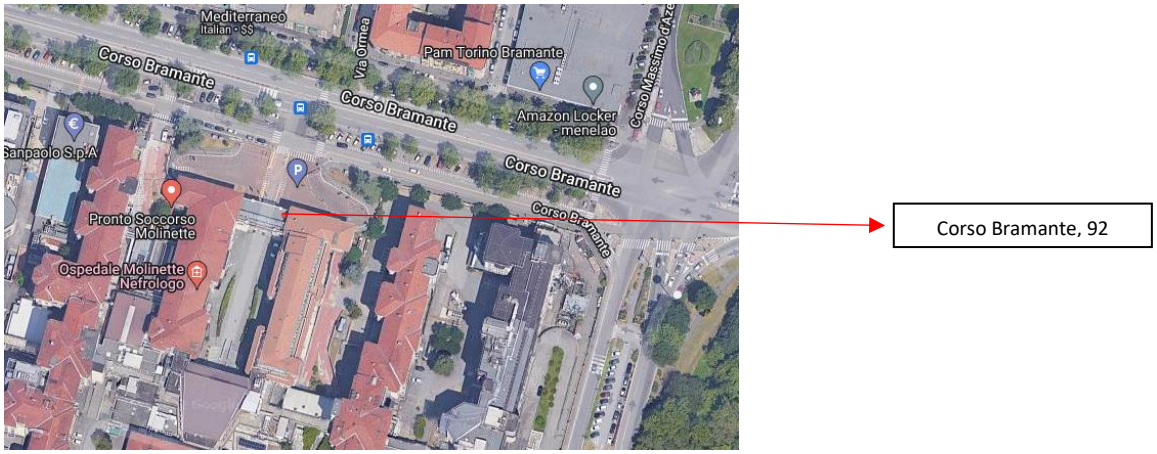

Fig 5.3 : The location of the Corso Bramante, 92

For motorcyle users, six hazardous road locations are identified in the city of Turin. All HRL for motorcylists are in the intersections and, 3 out of 6 HRL are located in the same corridor as given in Figure 5.4. It has been determined that these roads have more than 2 lanes and they are the main roads for public transportation in the city of Turin. Therefore, the traffic density is relatively high in these roads and it is likely to pose a danger to motorcycles since motorcycle users are using the same roads with vehicles.

For velocipede users, four hazardous road locations (HRL) are identified. When these specific points were examined, the presence of cycle paths was observed as shown in Fig 5.5 with red rectangular. These HRLs are the points where the traffic density is high and have many crossing points with other roads in the road network. Therefore, the interaction of the bicycles with the vehicles may be high due to the speed difference. To increase the safety of cyclists, the existence of a sufficient number of traffic lights and the adequacy of cycling paths at these points can be investigated.

Fig 5.4 : The corridor including three intersection points

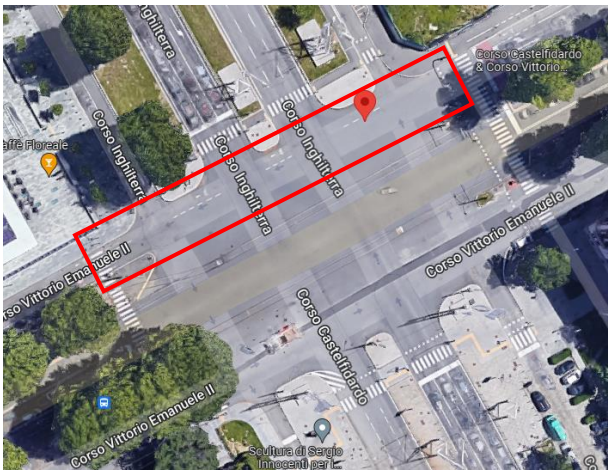

Intersection : corso Vittorio Emanuele II - corso Castelfidardo

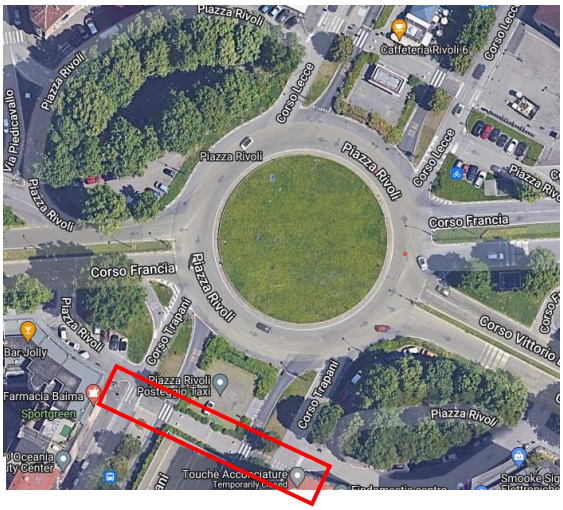

Piazza Rivoli

Piazza Lorenzo Bernini

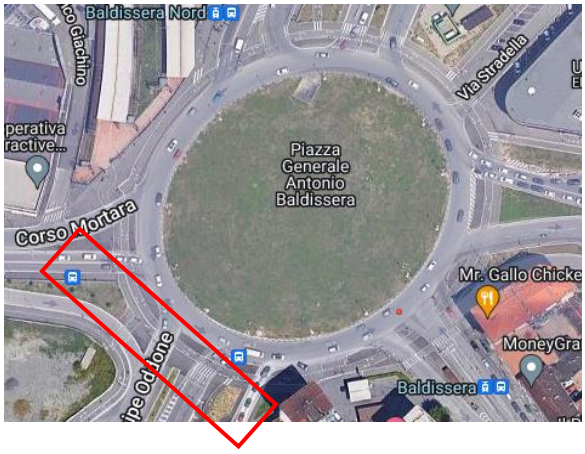

Piazza Generale Antonio Baldissera

Fig 5.5 : HRL's for cyclists

For moped users, critical points related to each study period were obtained but it was not possible to find the hazardous road locations (HRL) since the critical locations that should be in 3 out of the 6 positive study periods could not be captured. Moreover, it was also hard to identify the clustered structure of the point patterns due to the low number of traffic collisions in the crash database. While the number of accidents decreases, the distance between the collision events rises at a certain level. So, it is also more difficult to identify the clustered structure.

6. CONCLUSIONS

The thesis deals with the geospatial analysis of traffic collisions to identify HRL in Turin from 2006 to 2019 by considering all VRU and related sub-categories (pedestrians, cyclists, moped and motorcycle users respectively). The Italian National Institute of Statistics (ISTAT) provided the official database of traffic collisions.

According to the literature, there are two approaches for the spatial analysis of traffic collisions: the link-attribute and the event-based approaches. In the first, spatial events such as traffic crashes are not analyzed directly but assigned to geographic features, such as areas or segments of the road network. In event-based analyzes, traffic collisions are just points in space. In this study, event-based approach is used and this approach consists of distance-based and density-based methods. The distance-based and density-based methods were used for the spatial distribution analyses of the traffic collisions. While distance-based methods (Nearest Neighbor Analysis, G and F Functions) evaluate distances between events to define areas where traffic crashes are clustered, density-based methods (the Kernel Density Estimation) were used to examine the crash density to identify HRL.

All results combined give a general picture that the methods carried out are reliable and robust in a scientific way. The results indicate collisions were concentrated in the main intersections of the city, which deal with heavy traffic flows and conflicts between users during the day. It seems that most hazardous road locations (HRL) are for specific sub-categories rather than others. Some critical road corridors for the motorcyclists and cyclists that include more than two HRL were determined. It was obtained that all HRL for motorcyclists have more than 2 lanes and, this means that these road locations suffer from heavy traffic flows which determine severe conflict points.

Furthermore, it is concluded from the results that cyclists have a high risk in intersections and main squares of the city. It is a clear fact that wide cross-sections in the urban road environment cause some difficulties to cyclists, and pedestrians due to significant speed differences concerning motorized users, the absence of signalized junctions, and protected pedestrian crossings in some points. Conversely, high speed sport cyclists increase risks for the other vulnerable road users. Especially in those countries which typically have combined routes for both pedestrians and cyclists, the speed differences between the groups cause

problems. So, safety countermeasures should be differentiated based on the specific VRU sub-category to be protected.

The results of the analyses promote actions for the safety of the urban road environment and sustainable mobility since road traffic crashes have become one of the world's largest public-health and injury-prevention problems. Today the growing view is that road safety is a system-wide and shared multi-sectoral responsibility. It is extremely important that all road users are properly briefed and provided with necessary training based on the risk factors of the related vehicle. It is also important to highlight that every road user must follow the rules for their own safety.

REFERENCES

INTRODUCTION

Peden, M., Scurfield, R., Sleet, D., Mathers, C., Jarawan, E., Hyder, A. A., ... & Jarawan, E. (2004). World report on road traffic injury prevention. World Health Organization.

World Health Organization, retrieved from :

https://www.who.int/health-topics/road-safety#tab=tab_1, 2021

https://www.who.int/data/gho/data/themes/road-safety

Global Status Report on Road Safety,2018. Retrieved from: https://www.who.int/publications/i/item/9789241565684

European Commission (2018). Communıcatıon from the Commıssıon to the European Parlıament, the Councıl, the European Economıc and Socıal Commıttee and the Commıttee of the Regıons, Europe on the Move, Sustainable Mobility for Europe: Safe, Connected, and Clean. Retrieved from:

https://eurlex.europa.eu/resource.html?uri=cellar%3A0e8b694e-59b5-11e8-ab41-01aa75ed71a1.0003.02/DOC_1&format=PDF

Ritchie, H. and Roser, M. (2018). Urbanization. Published online at OurWorldInData.org. Retrieved from:

https://ourworldindata.org/urbanization.

European Comission Article,April 2021. Retrieved from:

https://transport.ec.europa.eu/news/road-safety-4-000-fewer-people-lost-their-lives-eu-roads-2020-death-rate-falls-all-time-low_en

Horizon Europe, Work Programme 2021-2022, Climate, Energy and Mobilty, HORIZON-CL5-2022-D6-01-06: Predictive safety assessment framework and safer urban environment for vulnerable road users, European Commission Decision C(2021)6096 of 23 August 2021.

Anderson, T. K. (2009). Kernel density estimation and K-means clustering to profile road accident hotspots. Accident Analysis & Prevention, 41(3), 359-364.

Choudhary, J., Ohri, A., & Kumar, B. (2015, December). Spatial and statistical analysis of road accidents hot spots using GIS. In 3rd Conference of Transportation Research Group of India (3rd CTRG).

CHAPTER – II

United Nations, Department of Economic and Social Affairs, Population Division (2018). The World's Cities in 2018—Data Booklet (ST/ESA/ SER.A/417).

Loo, B. P., & Anderson, T. K. (2015). Spatial analysis methods of road traffic collisions. CRC Press, pp. 3-4.

Organisation for Economic Co-operation and Development(OECD), DIRECTORATE FOR SCIENCE, TECHNOLOGY AND INDUSTRY PROGRAMME OF CO-OPERATION IN THE FIELD OF RESEARCH ON ROAD TRANSPORT AND INTERMODAL LINKAGES, Safety of Vulnerable Road Users,1998 - Data Booklet (DSTI/DOT/RTR/RS7(98)1/FINAL).

Bliss, T., & Breen, J. (2009). Country guidelines for the conduct of road safety management capacity reviews and the specification of lead agency reforms, investment strategies and safe system projects.

Bliss and Breen, building on the frameworks of Land Transport Safety Authority, 2000; Wegman, 2001; Koornstra et al, 2002; Bliss, 2004.

Bassani, M., Rossetti, L., & Catani, L. (2020). Spatial analysis of road crashes involving vulnerable road users in support of road safety management strategies. Transportation research procedia, 45, 394-401.

Loo, B. P., & Anderson, T. K. (2015). Spatial analysis methods of road traffic collisions. CRC Press.,p. 24.

Cliff, A. D., & Ord, J. K. (1973). Spatial Autocorrelation, Pion, London. Doreian & Patrick, 1981, Estimating linear models with spatially distributed data. Sociological methodology, San Francisco, CA: The Jossey-Bass Publishers, 359-388.

Goodchild, M. F. (1986). Spatial autocorrelation (Vol. 47). Geo Books.

Daniel A. Griffith (1987) Teaching spatial autocorrelation by simulation,Journal of Geography in Higher Education, 11:2, 143-153.

Odland, J. (1988). Spatial Autocorrelation.

Black, W. R., (1991). Highway Accidents: A Spatial and Temporal Analysis. Transportation Research Record 1318, 75–82.

Loo, B. P., & Yao, S. (2013). The identification of traffic crash hot zones under the link-attribute and event-based approaches in a network-constrained environment. Computers, Environment and Urban Systems, 41, 249-261.

Loo, B. P., & Anderson, T. K. (2015). Spatial analysis methods of road traffic collisions. CRC Press.,p. 16.

O'Sullivan, D. and D. J. Unwin. (2003). Geographic Information Analysis. Hoboken, NJ: John Wiley & Sons.

CHAPTER - III

The population data of Turin, retrieved from ISTAT :

https://demo.istat.it/bilmens/query.php?anno=2021&lingua=ita&Rip=S1&Reg=R01&Pro=P001&Com=272&submit=Tavola

Yamada, I., & Thill, J.-C. (2007). Local indicators of network-constrained clusters in spatial point patterns. Geographical Analysis, 39(3), 268–292.

Loo, B. P., Yao, S., 2013. The Identification of Traffic Crash Hot Zones Under the Link-attribute and Event-based Approaches in a Network-constrained Environment. *Computers, Environment and Urban Systems* 41, 249–261.

Clark, P. J., Evans, F. C., 1954. Distance to nearest neighbor as a measure of spatial relationships in populations. *Ecology* 35.4, 445–453.

Loo, B. P., & Anderson, T. K. (2015). Spatial analysis methods of road traffic collisions. CRC Press., p.13.

Shi, H., You, Z., Feng, Z., & Yang, Y. (2019). Numerical simulation and spatial distribution of transportation accessibility in the regions involved in the belt and road initiative. *Sustainability*, 11(22), 6187.

O'Sullivan, D., & Unwin, D. J. (2010). Geographic information analysis and spatial data. *Geographic information analysis*, 1-32.

O'sullivan, D., & Unwin, D. (2003). *Geographic information analysis*. John Wiley & Sons.

Silverman, B. W. 1986. Density Estimation for Statistics and Data Analysis, 1st edn. London, U.K.: Chapman & Hall.

Bailey, T. C. and A. C. Gatrell. 1995. Interactive Spatial Data Analysis. Essex, U.K.: Longman Scientific & Technical.

Loo, B. P., & Anderson, T. K. (2015). Spatial analysis methods of road traffic collisions. CRC Press.,pp. 27-30.

Fotheringham, A. S., M. E. Charlton, and C. Brunsdon. 2000. Quantitative Geography: Perspectives on Spatial Data Analysis. Thousand Oaks, CA: Sage.

Mohaymany, A. S., Shahri, M., & Mirbagheri, B. (2013). GIS-based method for detecting high-crash-risk road segments using network kernel density estimation. Geo-spatial Information Science, 16(2), 113-119.

Ratcliffe, J. H. 1999. Spatial pattern analysis machine version 1.2 users guide. http://web.archive.org/web/20071029014716/http://www.jratcliffe.net/ware/spam1.htm(accessed October 29, 2007).

Gutierrez-Osuna, R. (2004). Kernel density estimation. URL research. cs. tamu. edu/prism/lectures/pr/pr_l7. pdf.[Online.

Okabe, A., Satoh, T., Sugihara, K., 2009. A kernel density estimation method for networks, its computational method and a GIS-based tool. International Journal of Geographical Information Science 23.1, 7–32.

Porta, S., Strano, E., Iacoviello, V., Messora, R., Latora, V., Cardillo, A., Wang, F., Scellato, S., 2009. Street Centrality and Densities of Retail and Services in Bologna, Italy. Environment and Planning B: Planning and design 36.3, 450–465.

ANNEX 1 : THE RESULTS OF NEAREST NEIGHBOR ANALYIS FOR VRU

Average Nearest Neighbor Summary

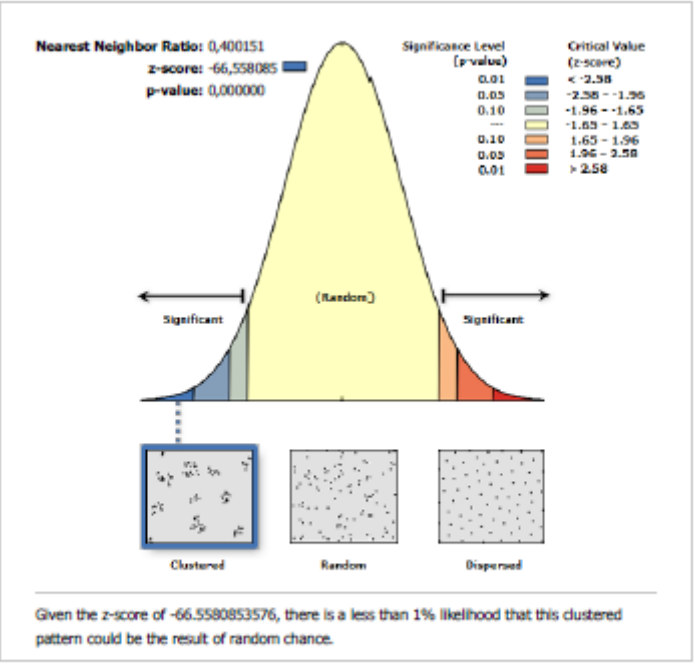

Average Nearest Neighbor Summary

Observed Mean Distance:	45,5944 Meters
Nearest Neighbor Ratio:	0,400151
z-score:	-66,558085
p-value:	0,000000

Dataset Information

Input Feature Class:	06_07_VRU_PC
Distance Method:	EUCLIDEAN
Study Area:	174699278,767174
Selection Set:	False

The results of NNA for 2006-2007 / VRU

Average Nearest Neighbor Summary

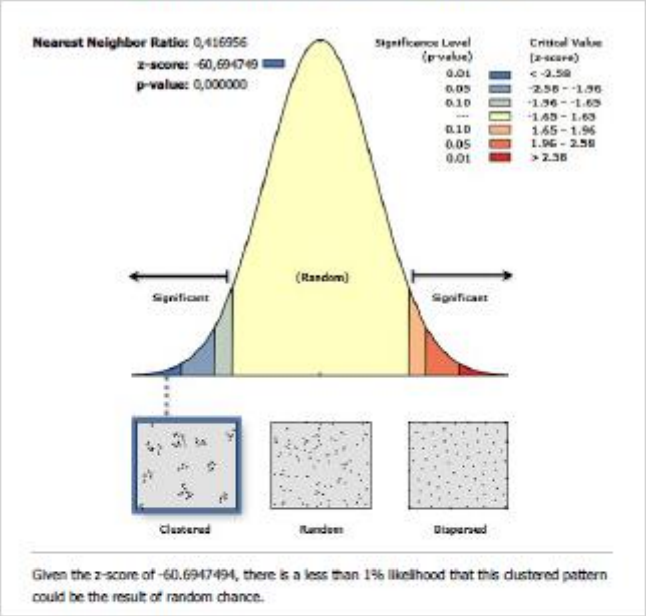

Average Nearest Neighbor Summary

Observed Mean Distance:	49,3453 Meters
Expected Mean Distance:	118,3465 Meters
Nearest Neighbor Ratio:	0,416956
z-score:	-60,694749
p-value:	0,000000

Dataset Information

Input Feature Class:	08_09_VRU_PC
Distance Method:	EUCLIDEAN
Study Area:	165885701,886112
Selection Set:	False

The results of NNA for 2008-2009 / VRU

Average Nearest Neighbor Summary

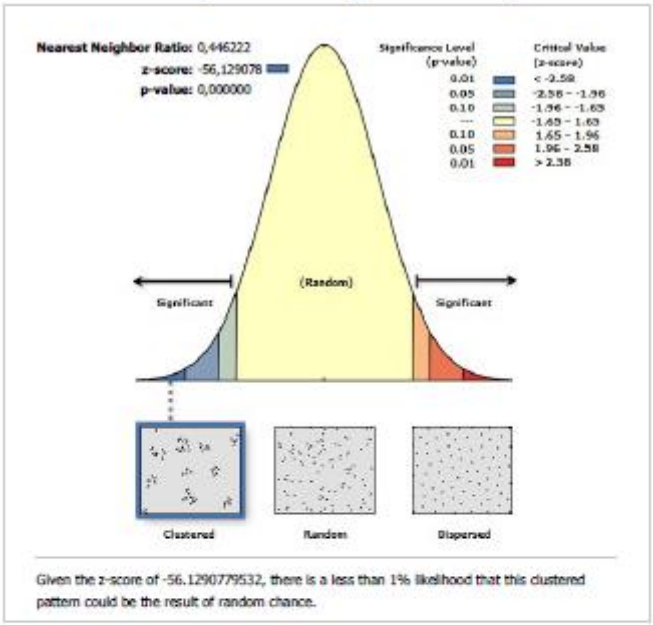

Average Nearest Neighbor Summary

Observed Mean Distance:	55,2137 Meters
Expected Mean Distance:	123,7359 Meters
Nearest Neighbor Ratio:	0,446222
z-score:	-56,129078
p-value:	0,000000

Dataset Information

Input Feature Class:	10_11_VRU_PC
Distance Method:	EUCLIDEAN
Study Area:	171907045,056864
Selection Set:	False

The results of NNA for 2010-2011 / VRU

Average Nearest Neighbor Summary

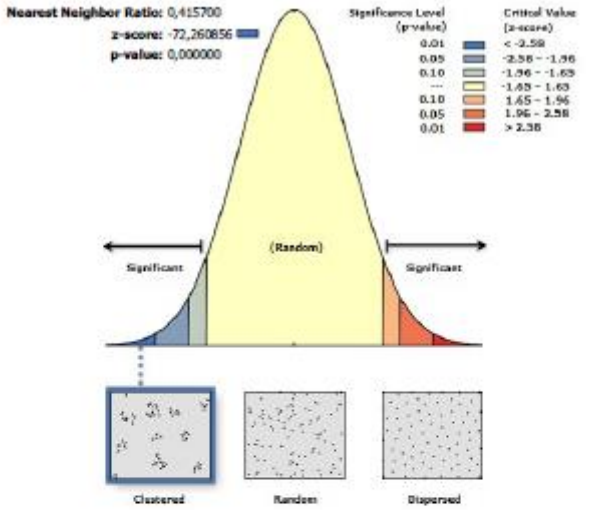

Given the z-score of -72.2608558129, there is a less than 1% likelihood that this clustered pattern could be the result of random chance.

Average Nearest Neighbor Summary

Observed Mean Distance:	42,4379 Meters
Expected Mean Distance:	102,0879 Meters
Nearest Neighbor Ratio:	0,415700
z-score:	-72,260856
p-value:	0,000000

Dataset Information

Input Feature Class:	12_14_VRU_PC
Distance Method:	EUCLIDEAN
Study Area:	174212979,096522
Selection Set:	False

The results of NNA for 2012-2014 / VRU

Average Nearest Neighbor Summary

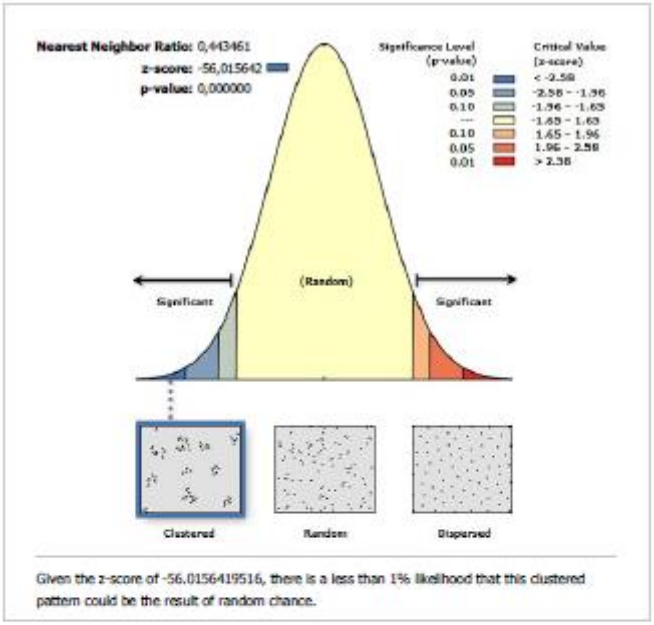

Average Nearest Neighbor Summary

Observed Mean Distance:	55,7111 Meters
Expected Mean Distance:	125,6279 Meters
Nearest Neighbor Ratio:	0,443461
z-score:	-56,015642
p-value:	0,000000

Dataset Information

Input Feature Class:	15_16_VRU_PC
Distance Method:	EUCLIDEAN
Study Area:	174742273,179829
Selection Set:	False

The results of NNA for 2015-2016 / VRU

Average Nearest Neighbor Summary

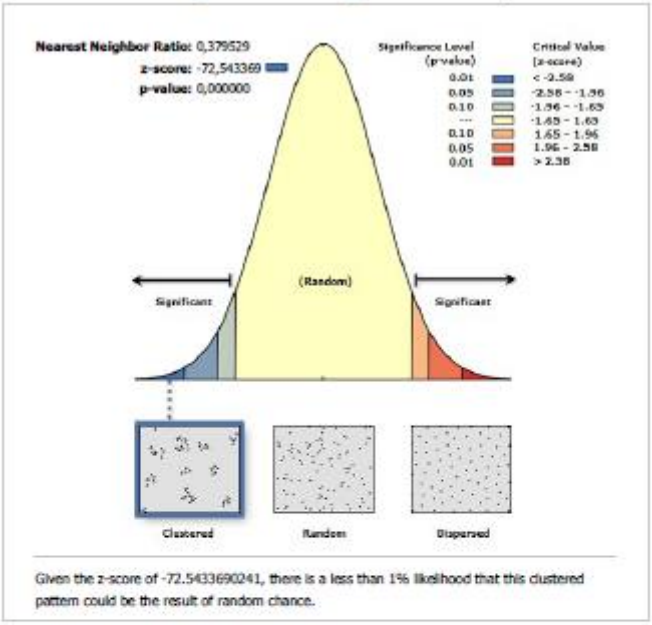

Average Nearest Neighbor Summary

Observed Mean Distance:	41,8116 Meters
Expected Mean Distance:	110,1670 Meters
Nearest Neighbor Ratio:	0,379529
z-score:	-72,543369
p-value:	0,000000

Dataset Information

Input Feature Class:	17_19_VRU_PC
Distance Method:	EUCLIDEAN
Study Area:	181323407,806746
Selection Set:	False

The results of NNA for 2017-2019 / VRU

ANNEX 2 : THE RESULTS OF NEAREST NEIGHBOR ANALYIS FOR PEDESTRIANS

Average Nearest Neighbor Summary

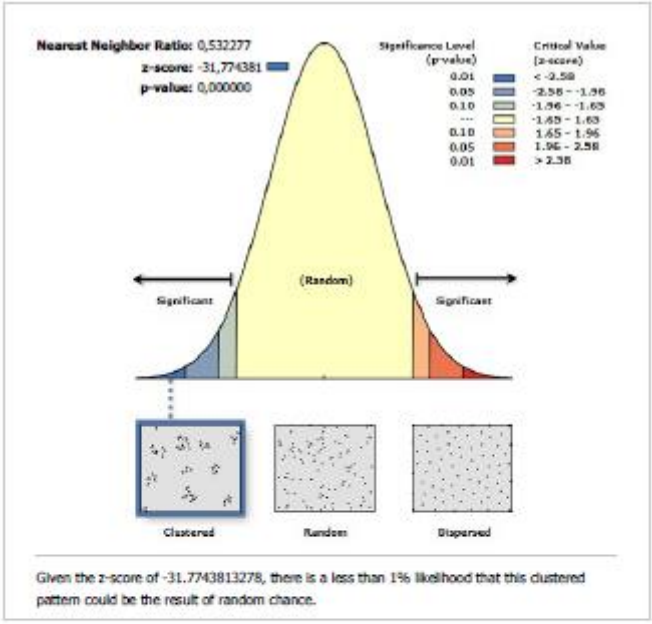

Average Nearest Neighbor Summary

Observed Mean Distance:	87,5651 Meters
Expected Mean Distance:	164,5103 Meters
Nearest Neighbor Ratio:	0,532277
z-score:	-31,774381
p-value:	0,000000

Dataset Information

Input Feature Class:	06_07_PEDESTRIAN_PC
Distance Method:	EUCLIDEAN
Study Area:	136509014,891855
Selection Set:	False

The results of NNA for 2006-2007 / PEDESTRIANS

Average Nearest Neighbor Summary

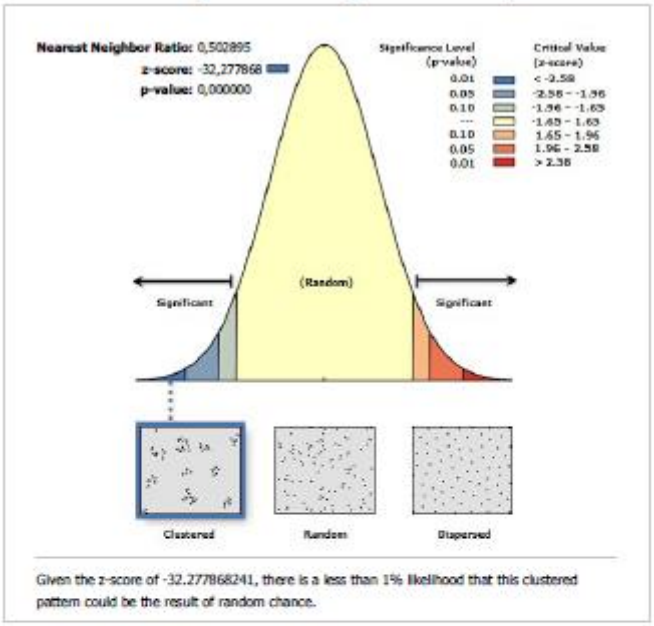

Average Nearest Neighbor Summary

Observed Mean Distance:	86,8027 Meters
Expected Mean Distance:	172,6058 Meters
Nearest Neighbor Ratio:	0,502895
z-score:	-32,277868
p-value:	0,000000

Dataset Information

Input Feature Class:	08_09_PEDESTRIAN_PC
Distance Method:	EUCLIDEAN
Study Area:	137284990,556613
Selection Set:	False

The results of NNA for 2008-2009 / PEDESTRIANS

Average Nearest Neighbor Summary

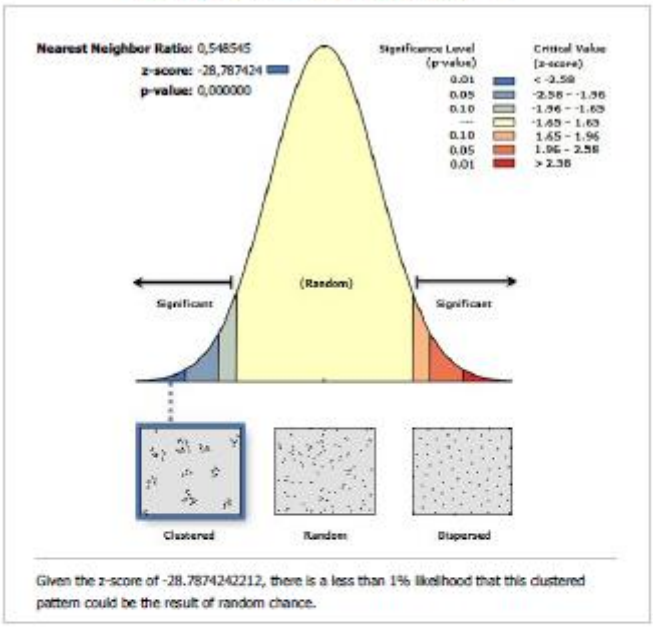

Average Nearest Neighbor Summary

Observed Mean Distance:	97,1551 Meters
Expected Mean Distance:	177,1143 Meters
Nearest Neighbor Ratio:	0,548545
z-score:	-28,787424
p-value:	0,000000

Dataset Information

Input Feature Class:	10_11_PEDESTRIAN_PC
Distance Method:	EUCLIDEAN
Study Area:	139405924,533036
Selection Set:	False

The results of NNA for 2010-2011 / PEDESTRIANS

Average Nearest Neighbor Summary

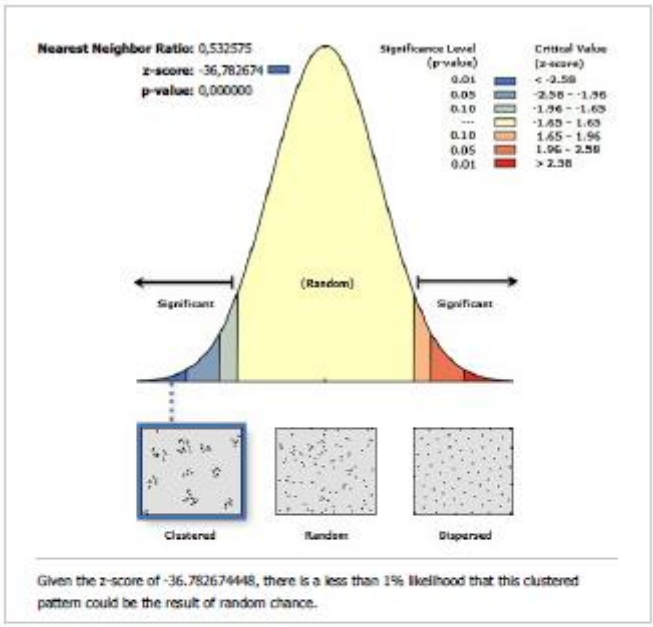

Average Nearest Neighbor Summary

Observed Mean Distance:	75,8949 Meters
Expected Mean Distance:	142,5057 Meters
Nearest Neighbor Ratio:	0,532575
z-score:	-36,782674
p-value:	0,000000

Dataset Information

Input Feature Class:	12_14_PEDESTRIAN_PC
Distance Method:	EUCLIDEAN
Study Area:	137443611,353600
Selection Set:	False

The results of NNA for 2012-2014 / PEDESTRIANS

Average Nearest Neighbor Summary

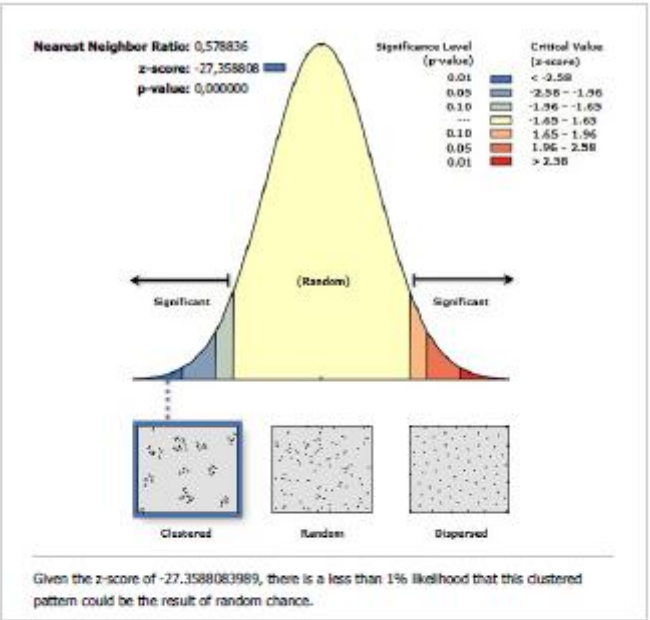

Average Nearest Neighbor Summary

Observed Mean Distance:	95,4507 Meters
Expected Mean Distance:	164,9012 Meters
Nearest Neighbor Ratio:	0,578836
z-score:	-27,358808
p-value:	0,000000

Dataset Information

Input Feature Class:	15_16_PEDESTRIAN_PC
Distance Method:	EUCLIDEAN
Study Area:	125411306,294782
Selection Set:	False

The results of NNA for 2015-2016 / PEDESTRIANS

Average Nearest Neighbor Summary

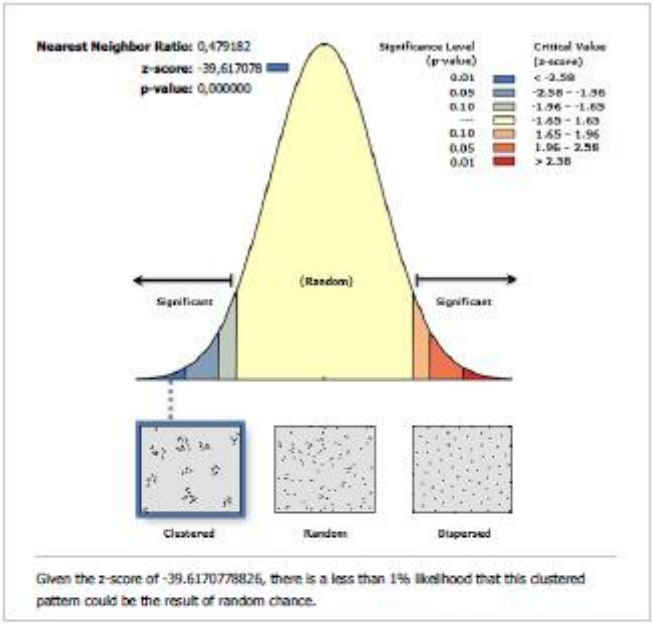

Average Nearest Neighbor Summary

Observed Mean Distance:	72,0928 Meters
Expected Mean Distance:	150,4495 Meters
Nearest Neighbor Ratio:	0,479182
z-score:	-39,617078
p-value:	0,000000

Dataset Information

Input Feature Class:	17_19_PEDESTRIAN_PC
Distance Method:	EUCLIDEAN
Study Area:	143144065,776994
Selection Set:	False

The results of NNA for 2017-2019 / PEDESTRIANS

ANNEX 3 : THE RESULTS OF NEAREST NEIGHBOR ANALYIS FOR MOTORCYCLE USERS

Average Nearest Neighbor Summary

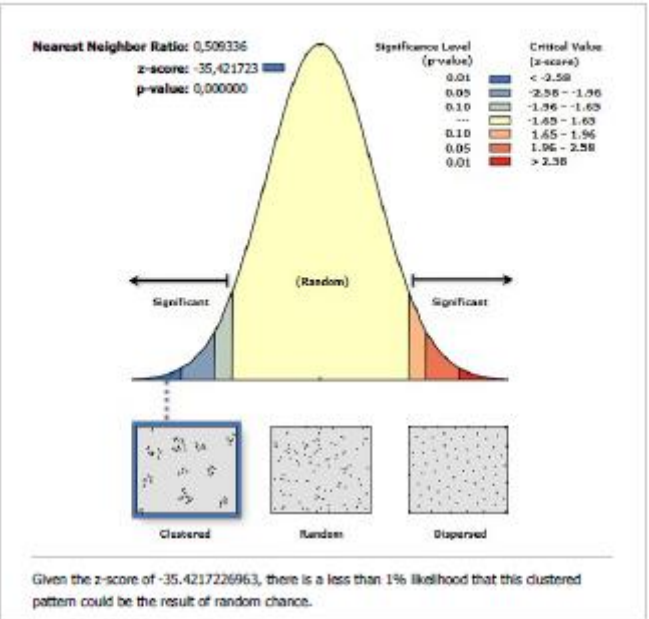

Average Nearest Neighbor Summary

Observed Mean Distance:	87,1002 Meters
Expected Mean Distance:	171,0072 Meters
Nearest Neighbor Ratio:	0,509336
z-score:	-35,421723
p-value:	0,000000

Dataset Information

Input Feature Class:	06_07_MOTORCYCLE_PC
Distance Method:	EUCLIDEAN
Study Area:	166570821,294781
Selection Set:	False

The results of NNA for 2006-2007 / MOTORCYCLE USERS

Average Nearest Neighbor Summary

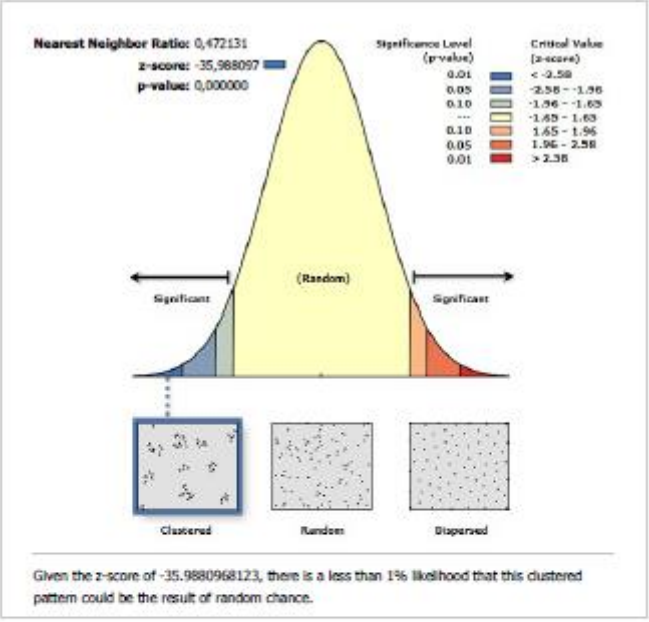

Average Nearest Neighbor Summary

Observed Mean Distance:	84,3605 Meters
Expected Mean Distance:	178,6803 Meters
Nearest Neighbor Ratio:	0,472131
z-score:	-35,988097
p-value:	0,000000

Dataset Information

Input Feature Class:	08_09_MOTORCYCLE_PC
Distance Method:	EUCLIDEAN
Study Area:	162187436,373515
Selection Set:	False

The results of NNA for 2008-2009 / MOTORCYCLE USERS

Average Nearest Neighbor Summary

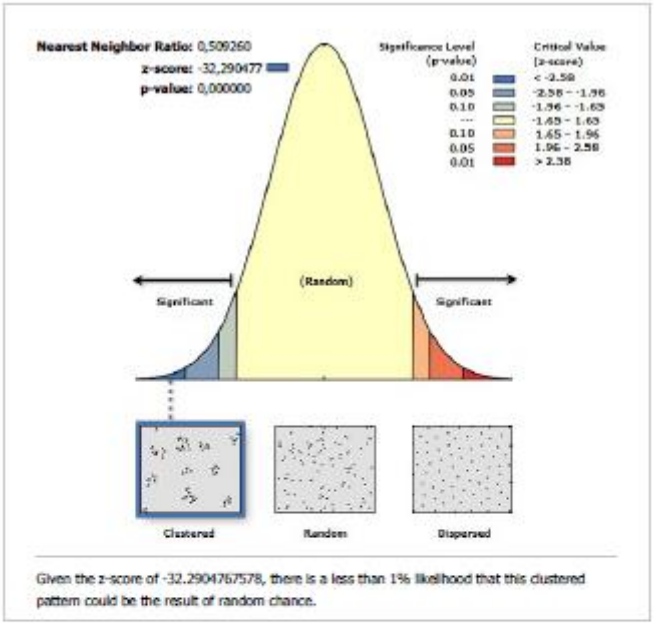

Average Nearest Neighbor Summary

Observed Mean Distance:	95,5224 Meters
Expected Mean Distance:	187,5708 Meters
Nearest Neighbor Ratio:	0,509260
z-score:	-32,290477
p-value:	0,000000

Dataset Information

Input Feature Class:	10_11_MOTORCYCLE_PC
Distance Method:	EUCLIDEAN
Study Area:	166485027,563765
Selection Set:	False

The results of NNA for 2010-2011 / MOTORCYCLE USERS

Average Nearest Neighbor Summary

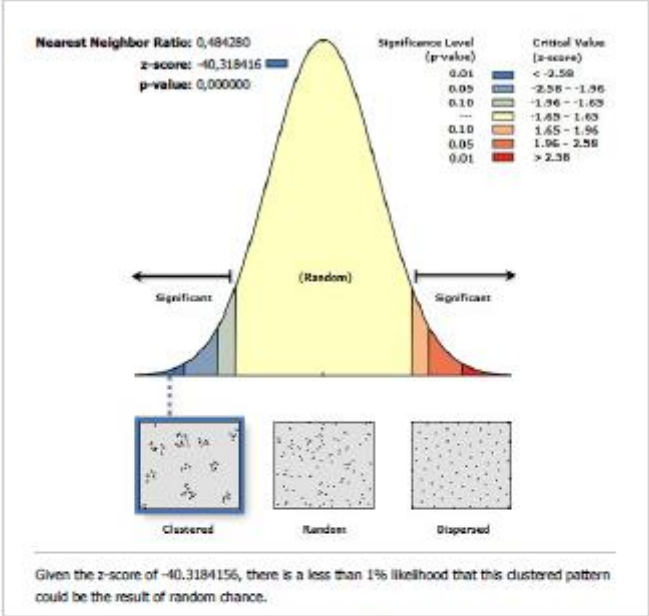

Average Nearest Neighbor Summary

Observed Mean Distance:	77,4817 Meters
Expected Mean Distance:	159,9937 Meters
Nearest Neighbor Ratio:	0,484280
z-score:	-40,318416
p-value:	0,000000

Dataset Information

Input Feature Class:	12_14_MOTORCYCLE_PC
Distance Method:	EUCLIDEAN
Study Area:	170994460,174088
Selection Set:	False

The results of NNA for 2012-2014 / MOTORCYCLE USERS

Average Nearest Neighbor Summary

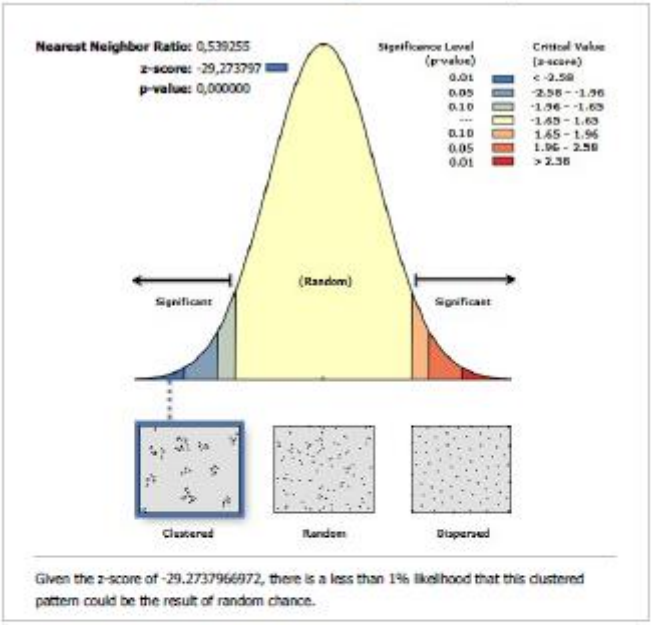

Average Nearest Neighbor Summary

Observed Mean Distance:	103,2803 Meters
Expected Mean Distance:	191,5240 Meters
Nearest Neighbor Ratio:	0,539255
z-score:	-29,273797
p-value:	0,000000

Dataset Information

Input Feature Class:	15_16_MOTORCYCLE_PC
Distance Method:	EUCLIDEAN
Study Area:	161838571,409609
Selection Set:	False

The results of NNA for 2015-2016 / MOTORCYCLE USERS

Average Nearest Neighbor Summary

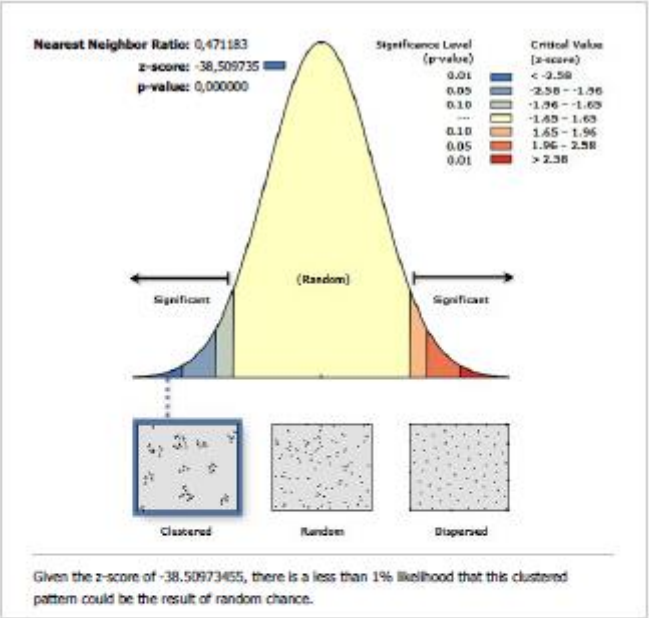

Average Nearest Neighbor Summary

Observed Mean Distance:	79,7109 Meters
Expected Mean Distance:	169,1718 Meters
Nearest Neighbor Ratio:	0,471183
z-score:	-38,509735
p-value:	0,000000

Dataset Information

Input Feature Class:	17_19_MOTORCYCLE_PC
Distance Method:	EUCLIDEAN
Study Area:	165876229,797911
Selection Set:	False

The results of NNA for 2017-2019 / MOTORCYCLE USERS

ANNEX 4 : THE RESULTS OF NEAREST NEIGHBOR ANALYIS FOR VELOCIPEDE USERS

Average Nearest Neighbor Summary

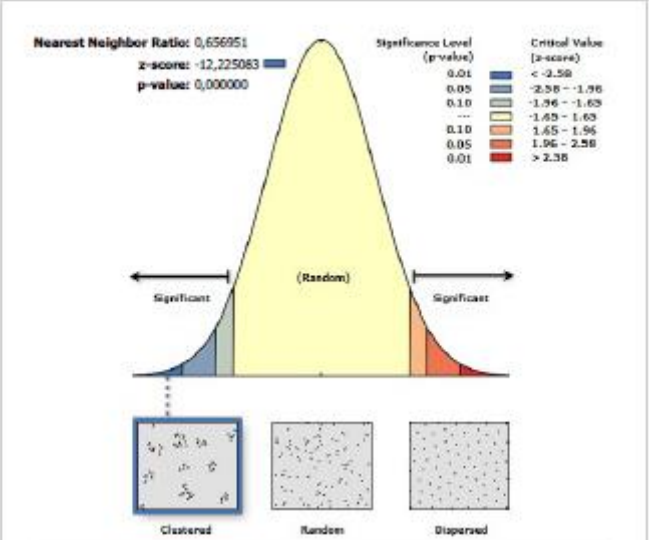

Average Nearest Neighbor Summary

Observed Mean Distance:	227,1802 Meters
Expected Mean Distance:	345,8100 Meters
Nearest Neighbor Ratio:	0,656951
z-score:	-12,225083
p-value:	0,000000

Dataset Information

Input Feature Class:	06_07_VELOCIPEDE_PC
Distance Method:	EUCLIDEAN
Study Area:	165983395,572213
Selection Set:	False

The results of NNA for 2006-2007 / VELOCIPEDE USERS

Average Nearest Neighbor Summary

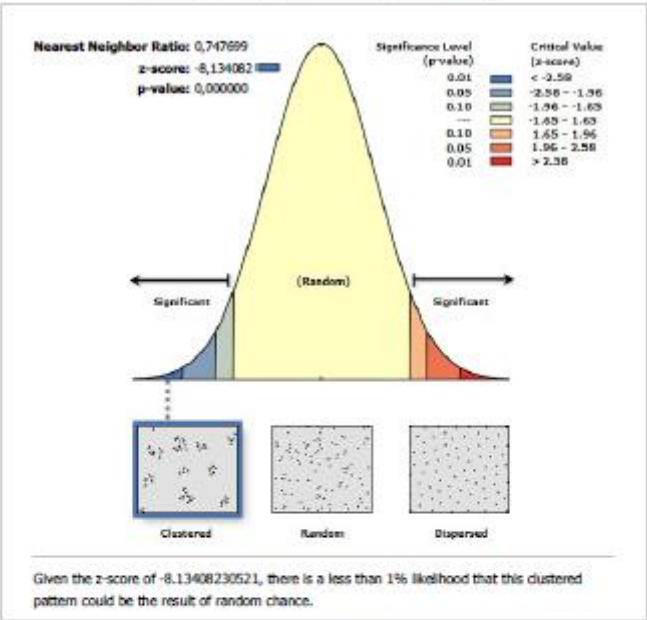

Average Nearest Neighbor Summary

Observed Mean Distance:	259,5789 Meters
Expected Mean Distance:	347,1702 Meters
Nearest Neighbor Ratio:	0,747699
z-score:	-8,134082
p-value:	0,000000

Dataset Information

Input Feature Class:	08_09_VELOCIPEDE_PC
Distance Method:	EUCLIDEAN
Study Area:	136918877,618330
Selection Set:	False

The results of NNA for 2008-2009 / VELOCIPEDE USERS

Average Nearest Neighbor Summary

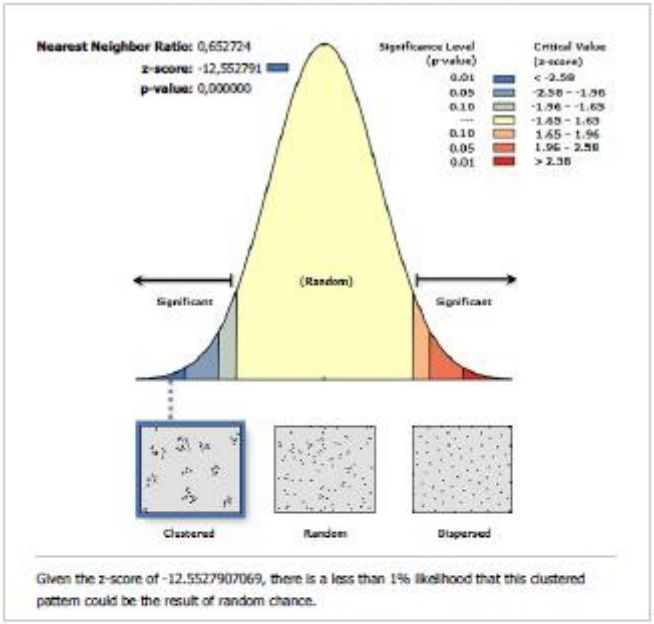

Average Nearest Neighbor Summary

Observed Mean Distance:	199,4745 Meters
Expected Mean Distance:	305,6033 Meters
Nearest Neighbor Ratio:	0,652724
z-score:	-12,552791
p-value:	0,000000

Dataset Information

Input Feature Class:	10_11_VELOCIPEDE_PC
Distance Method:	EUCLIDEAN
Study Area:	133365760,015980
Selection Set:	False

The results of NNA for 2010-2011 / VELOCIPEDE USERS

Average Nearest Neighbor Summary

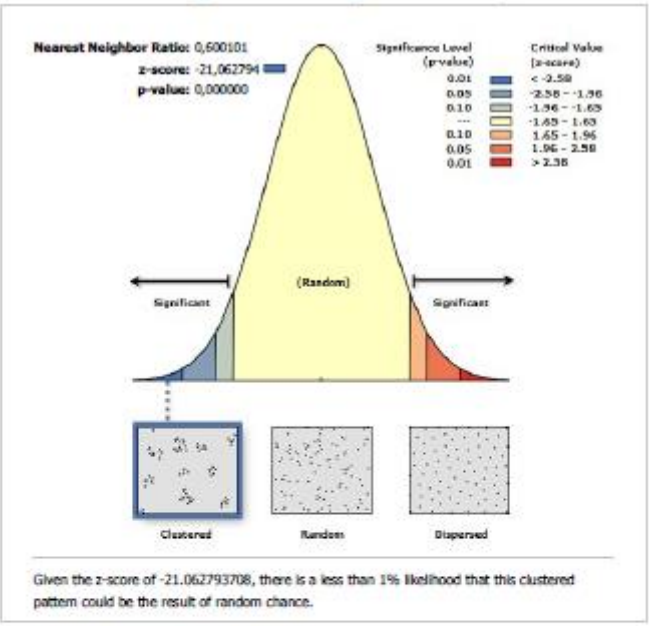

Average Nearest Neighbor Summary

Observed Mean Distance:	134,5243 Meters
Expected Mean Distance:	224,1695 Meters
Nearest Neighbor Ratio:	0,600101
z-score:	-21,062794
p-value:	0,000000

Dataset Information

Input Feature Class:	12_14_VELOCIPEDE_PC
Distance Method:	EUCLIDEAN
Study Area:	152363931,394971
Selection Set:	False

The results of NNA for 2012-2014 / VELOCIPEDE USERS

Average Nearest Neighbor Summary

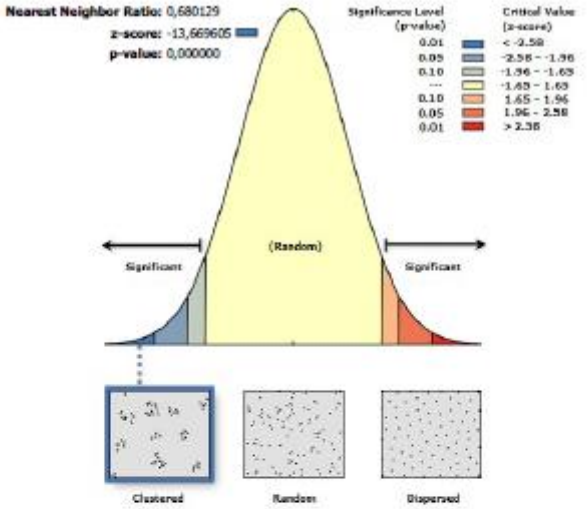

Average Nearest Neighbor Summary

Observed Mean Distance:	189,1724 Meters
Expected Mean Distance:	278,1419 Meters
Nearest Neighbor Ratio:	0,680129
z-score:	-13,669605
p-value:	0,000000

Dataset Information

Input Feature Class:	15_16_VELOCIPEDE_PC
Distance Method:	EUCLIDEAN
Study Area:	154416357,566258
Selection Set:	False

The results of NNA for 2015-2016 / VELOCIPEDE USERS

Average Nearest Neighbor Summary

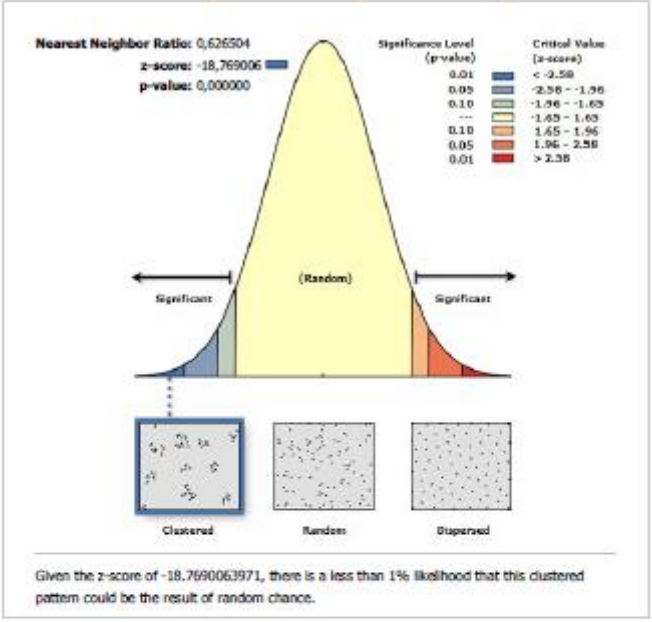

Average Nearest Neighbor Summary

Observed Mean Distance:	147,2773 Meters
Expected Mean Distance:	235,0779 Meters
Nearest Neighbor Ratio:	0,626504
z-score:	-18,769006
p-value:	0,000000

Dataset Information

Input Feature Class:	17_19_VELOCIPEDE_PC
Distance Method:	EUCLIDEAN
Study Area:	152522040,102661
Selection Set:	False

The results of NNA for 2017-2019 / VELOCIPEDE USERS

ANNEX 5 : THE RESULTS OF NEAREST NEIGHBOR ANALYIS FOR MOPED USERS

Average Nearest Neighbor Summary

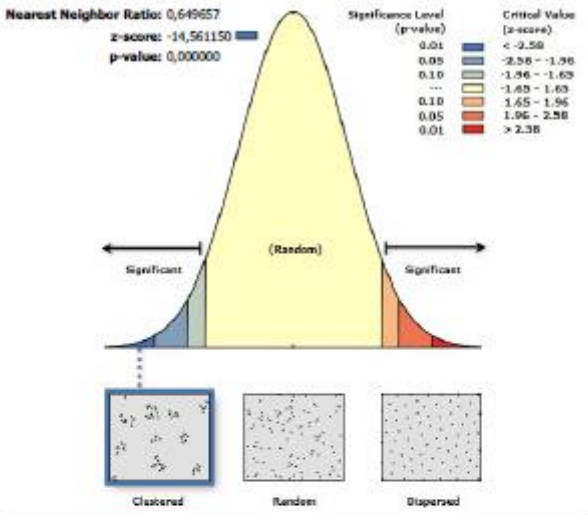

Average Nearest Neighbor Summary

Observed Mean Distance:	181,1091 Meters
Expected Mean Distance:	278,7766 Meters
Nearest Neighbor Ratio:	0,649657
z-score:	-14,561150
p-value:	0,000000

Dataset Information

Input Feature Class:	06_07_MOPED_PC
Distance Method:	EUCLIDEAN
Study Area:	146728508,735042
Selection Set:	False

The results of NNA for 2006-2007 / MOPED USERS

Average Nearest Neighbor Summary

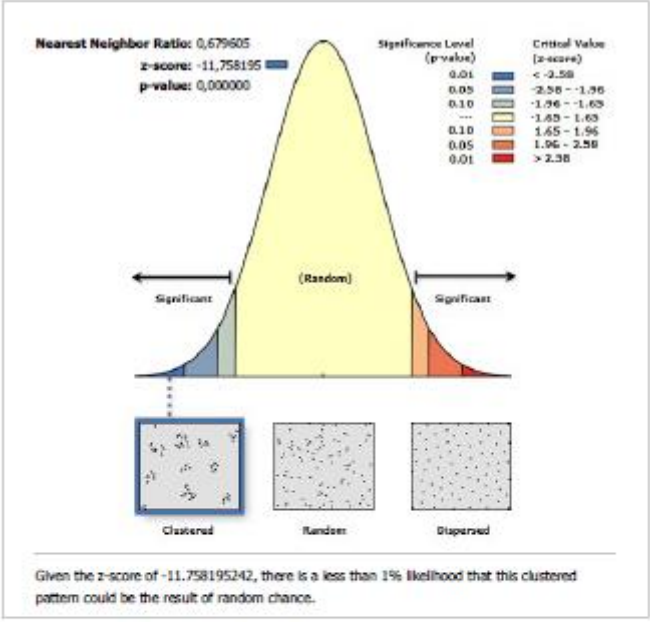

Average Nearest Neighbor Summary

Observed Mean Distance:	187,7207 Meters
Expected Mean Distance:	276,2203 Meters
Nearest Neighbor Ratio:	0,679605
z-score:	-11,758195
p-value:	0,000000

Dataset Information

Input Feature Class:	08_09_MOPED_PC
Distance Method:	EUCLIDEAN
Study Area:	112310155,559102
Selection Set:	False

The results of NNA for 2008-2009 / MOPED USERS

Average Nearest Neighbor Summary

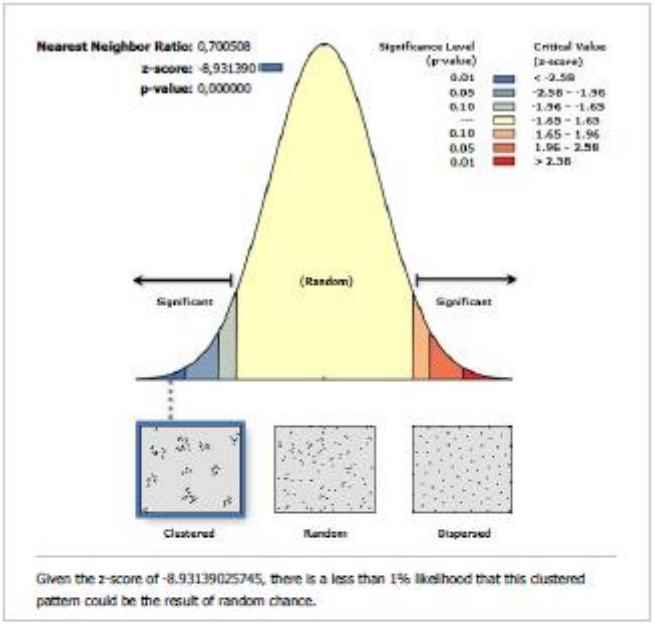

Average Nearest Neighbor Summary

Observed Mean Distance:	266,0516 Meters
Expected Mean Distance:	379,7981 Meters
Nearest Neighbor Ratio:	0,700508
z-score:	-8,931390
p-value:	0,000000

Dataset Information

Input Feature Class:	10_11_MOPED_PC
Distance Method:	EUCLIDEAN
Study Area:	140207667,358191
Selection Set:	False

The results of NNA for 2010-2011 / MOPED USERS

Average Nearest Neighbor Summary

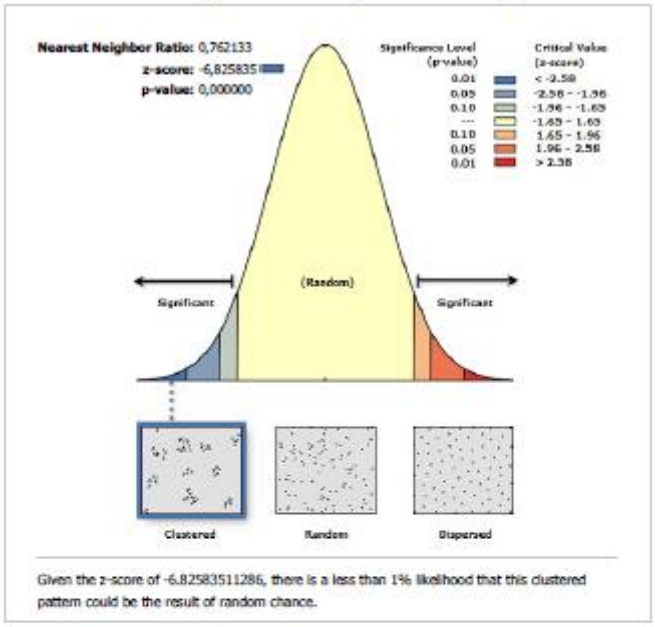

Average Nearest Neighbor Summary

Observed Mean Distance:	263,4574 Meters
Expected Mean Distance:	345,6841 Meters
Nearest Neighbor Ratio:	0,762133
z-score:	-6,825835
p-value:	0,000000

Dataset Information

Input Feature Class:	12_14_MOPED_PC
Distance Method:	EUCLIDEAN
Study Area:	107547757,439158
Selection Set:	False

The results of NNA for 2012-2014 / MOPED USERS

Average Nearest Neighbor Summary

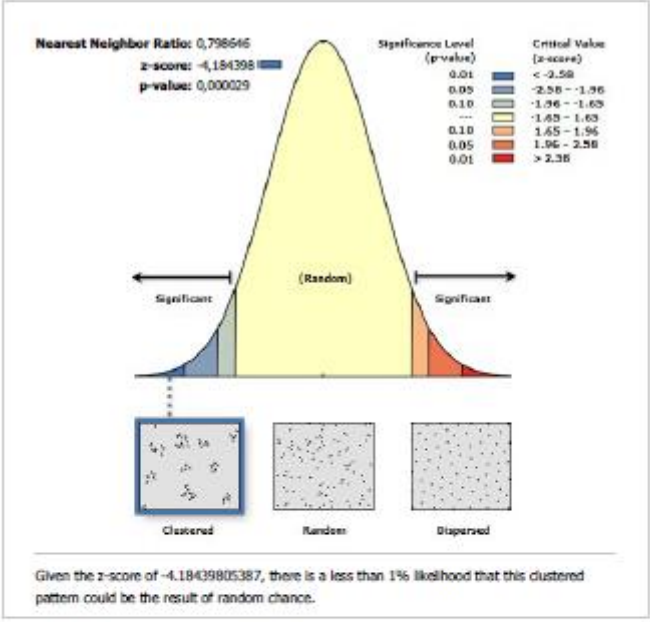

Average Nearest Neighbor Summary

Observed Mean Distance:	416,2926 Meters
Expected Mean Distance:	521,2482 Meters
Nearest Neighbor Ratio:	0,798646
z-score:	-4,184398
p-value:	0,000029

Dataset Information

Input Feature Class:	15_16_MOPED_PC
Distance Method:	EUCLIDEAN
Study Area:	128242242,649623
Selection Set:	False

The results of NNA for 2015-2016 / MOPED USERS

Average Nearest Neighbor Summary

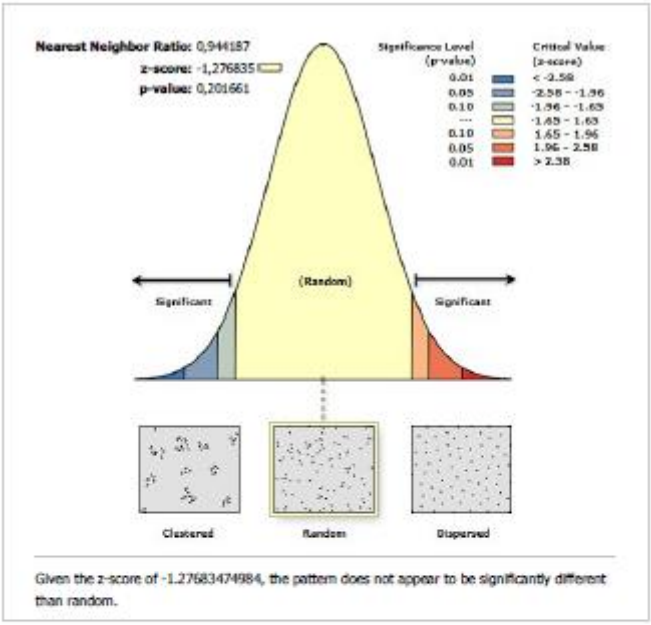

Average Nearest Neighbor Summary

Observed Mean Distance:	406,5256 Meters
Expected Mean Distance:	430,5562 Meters
Nearest Neighbor Ratio:	0,944187
z-score:	-1,276835
p-value:	0,201661

Dataset Information

Input Feature Class:	17_19_MOPED_PC
Distance Method:	EUCLIDEAN
Study Area:	106036588,813228
Selection Set:	False

The results of NNA for 2017-2019 / MOPED USERS

ANNEX 6 : THE RESULTS OF KDE ANALYIS FOR VRU

Heat map of traffic collisions including all VRU for the period 2006-2007

Heat map of traffic collisions including all VRU for the period 2008-2009

Heat map of traffic collisions including all VRU for the period 2010-2011

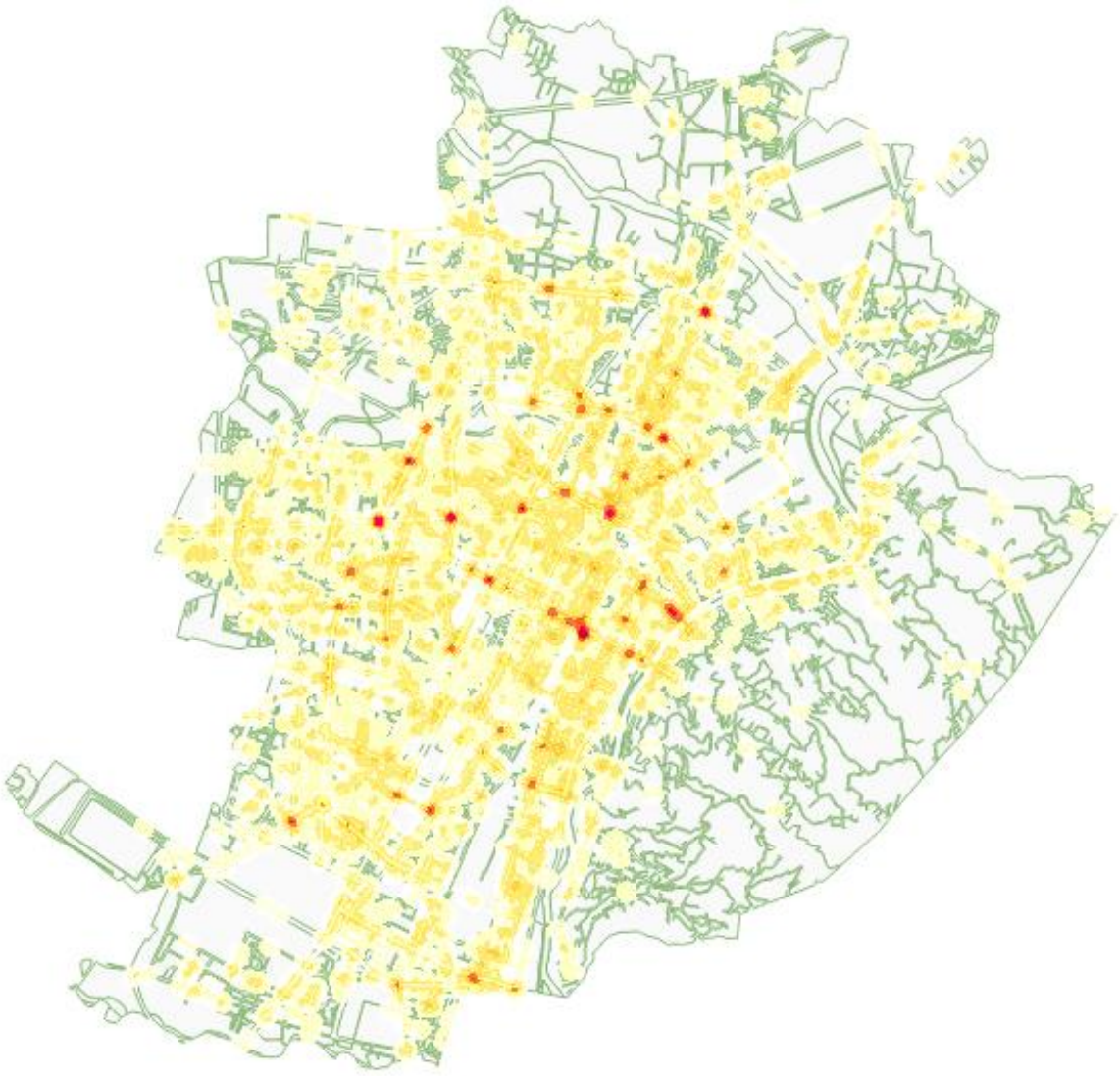

Heat map of traffic collisions including all VRU for the period 2012-2014

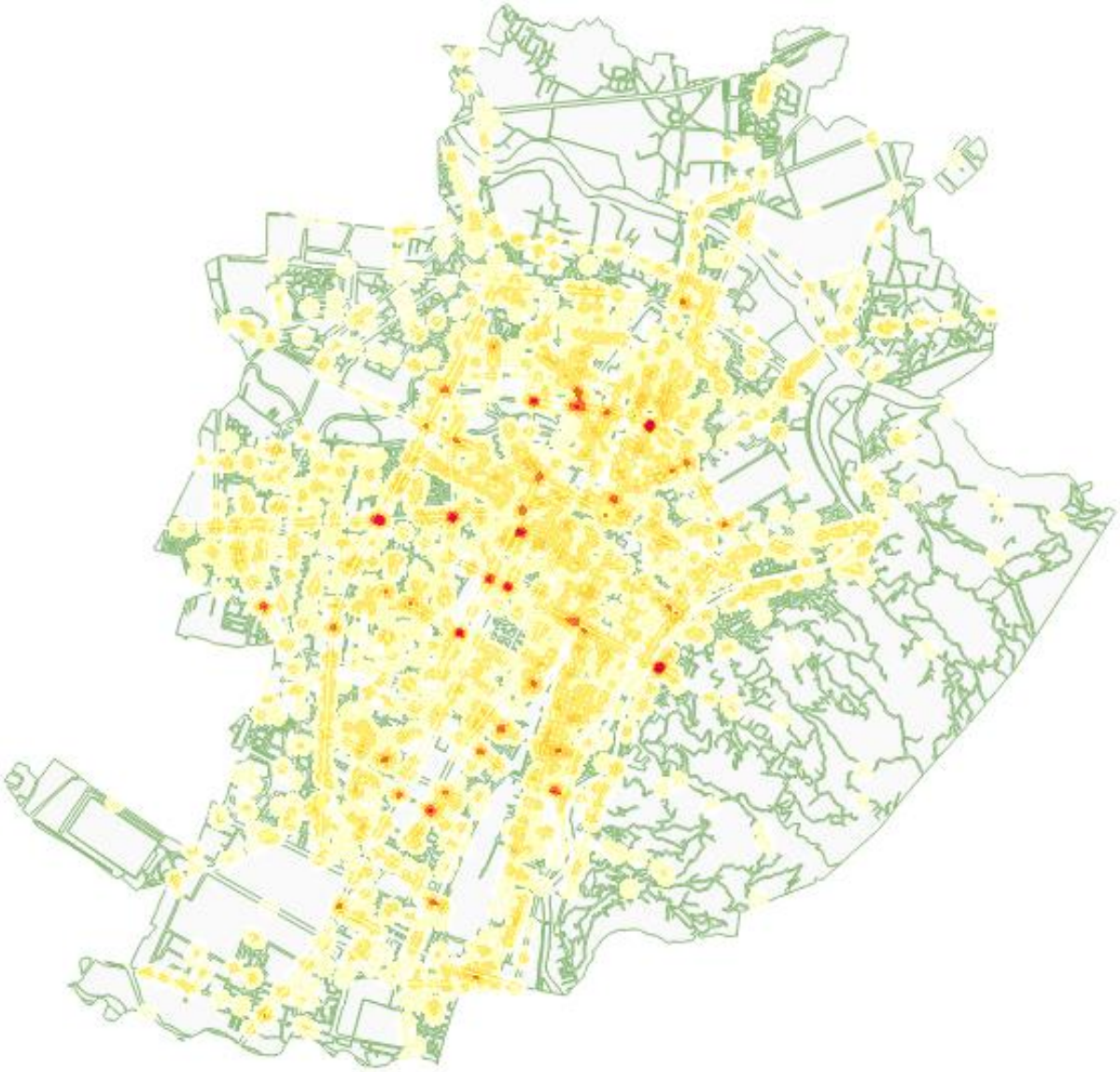

Heat map of traffic collisions including all VRU for the period 2015-2016

Heat map of traffic collisions including all VRU for the period 2017-2019

ANNEX 7 : THE RESULTS OF KDE ANALYIS FOR PEDESTRIANS

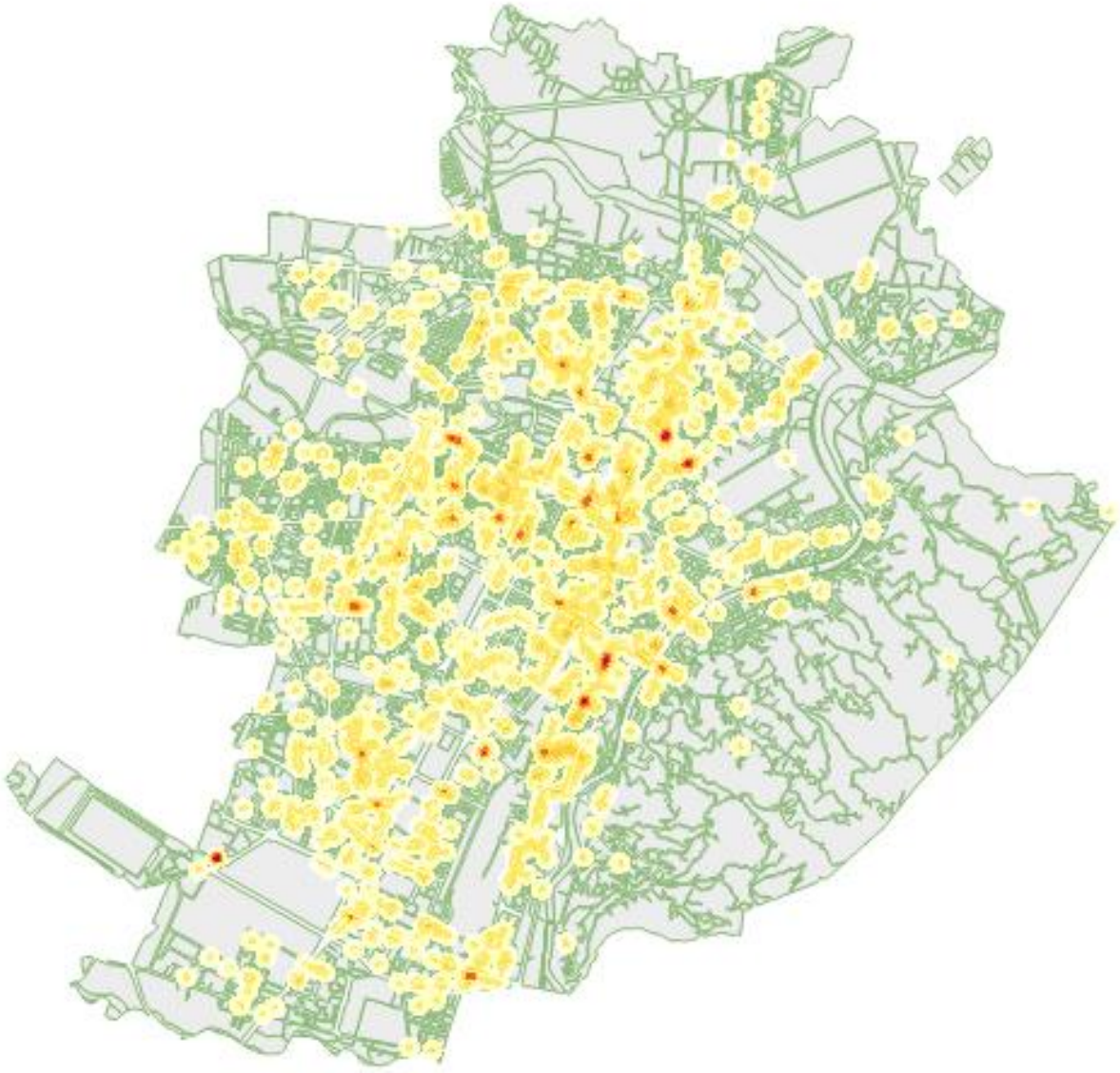

Heat map of traffic collisions including only pedestrians for the period 2006-2007

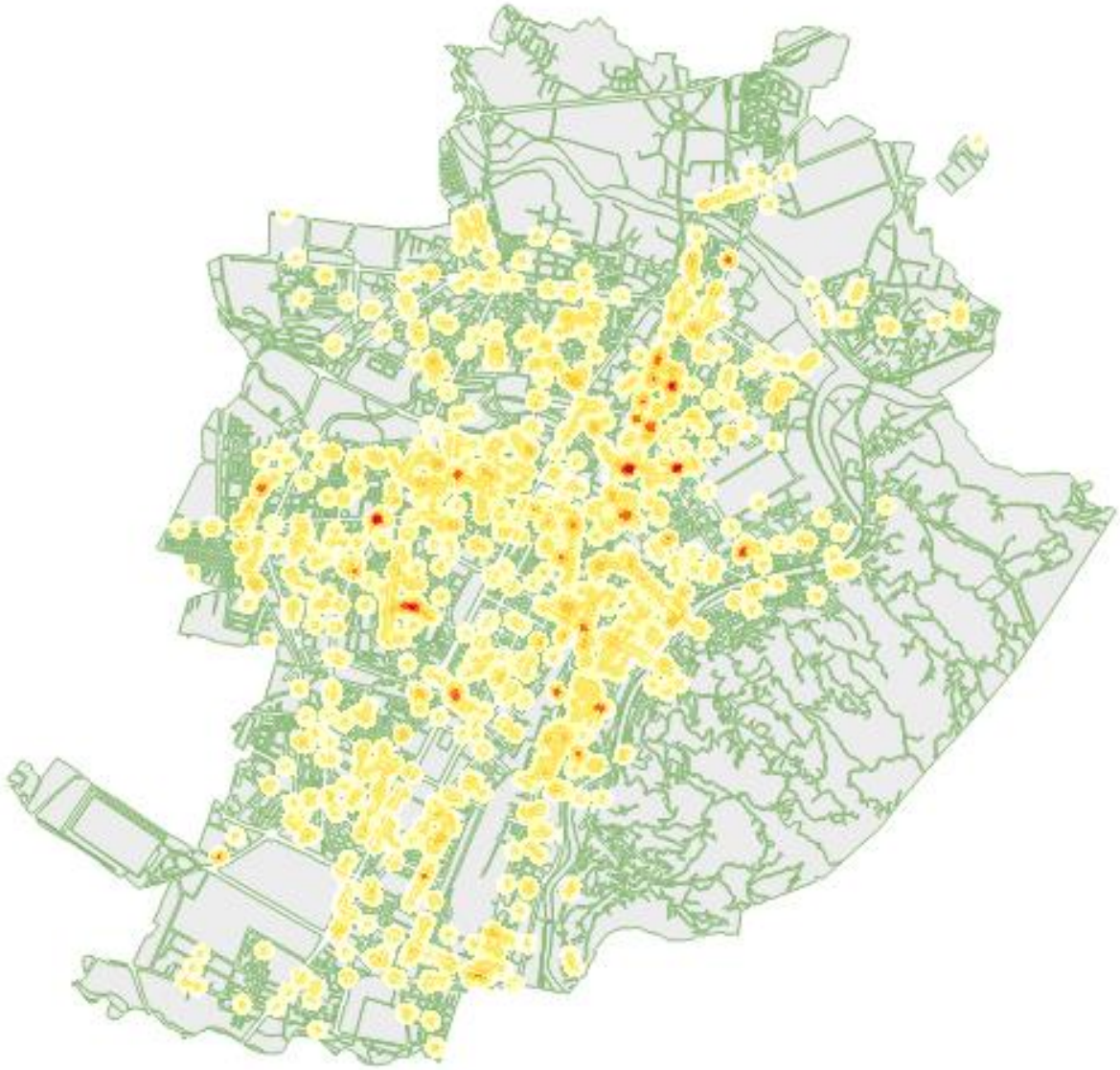

Heat map of traffic collisions including only pedestrians for the period 2008-2009

Heat map of traffic collisions including only pedestrians for the period 2010-2011

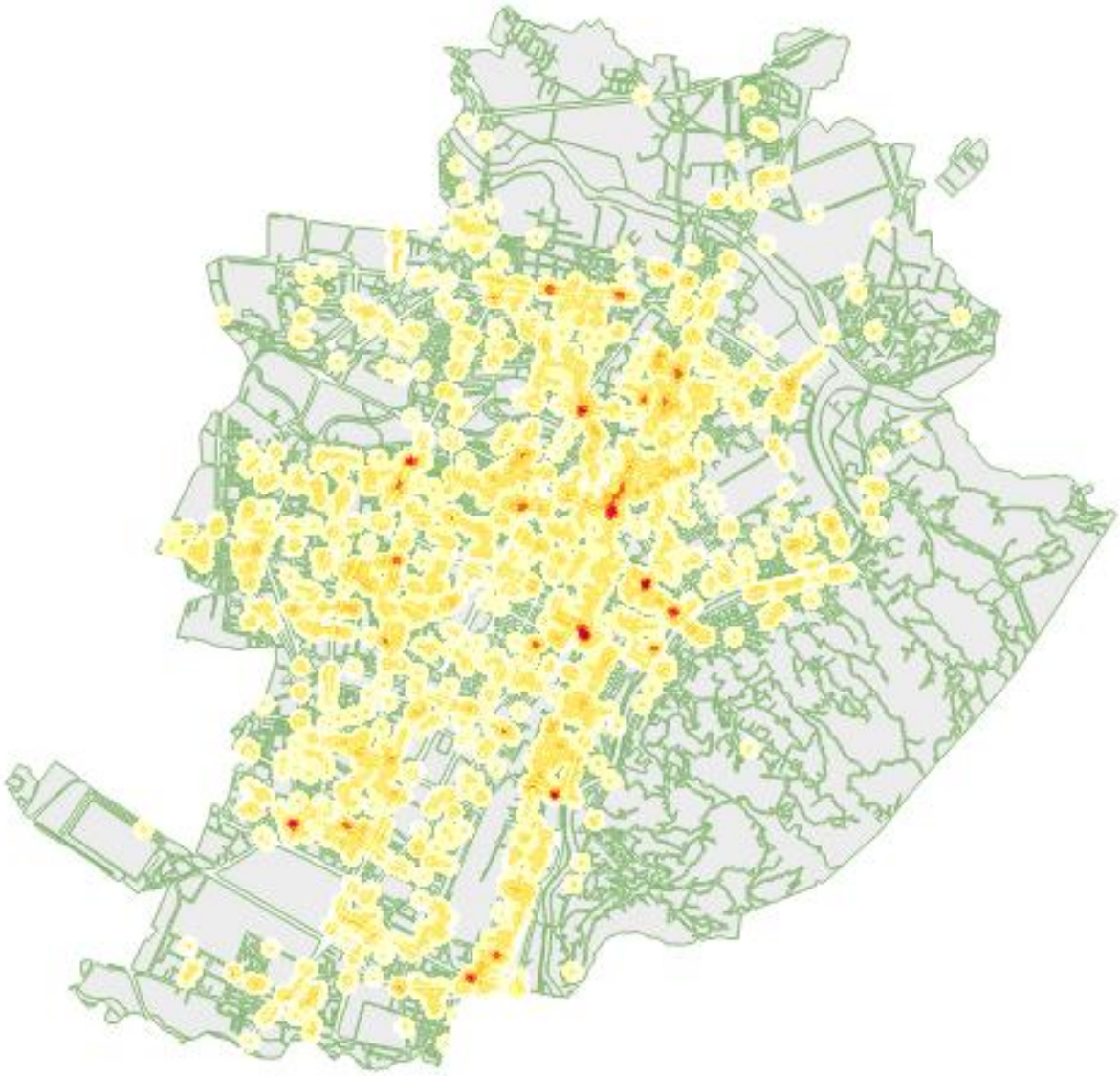

Heat map of traffic collisions including only pedestrians for the period 2012-2014

Heat map of traffic collisions including only pedestrians for the period 2015-2016

Heat map of traffic collisions including only pedestrians for the period 2017-2019

ANNEX 8 : THE RESULTS OF KDE ANALYIS FOR MOTORCYCLE USERS

Heat map of traffic collisions including only motorcycle users for the period 2006-2007

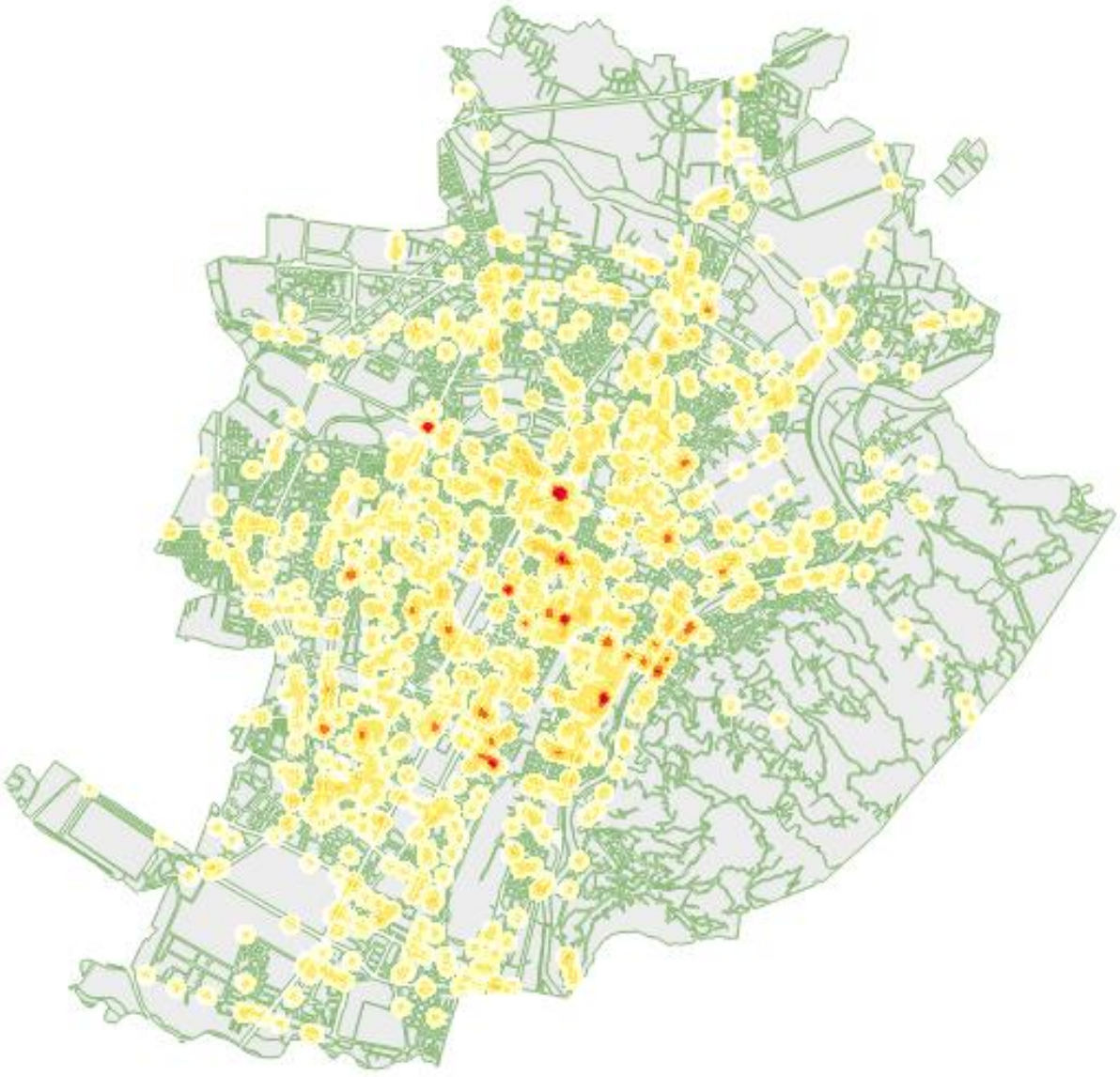

Heat map of traffic collisions including only motorcycle users for the period 2008-2009

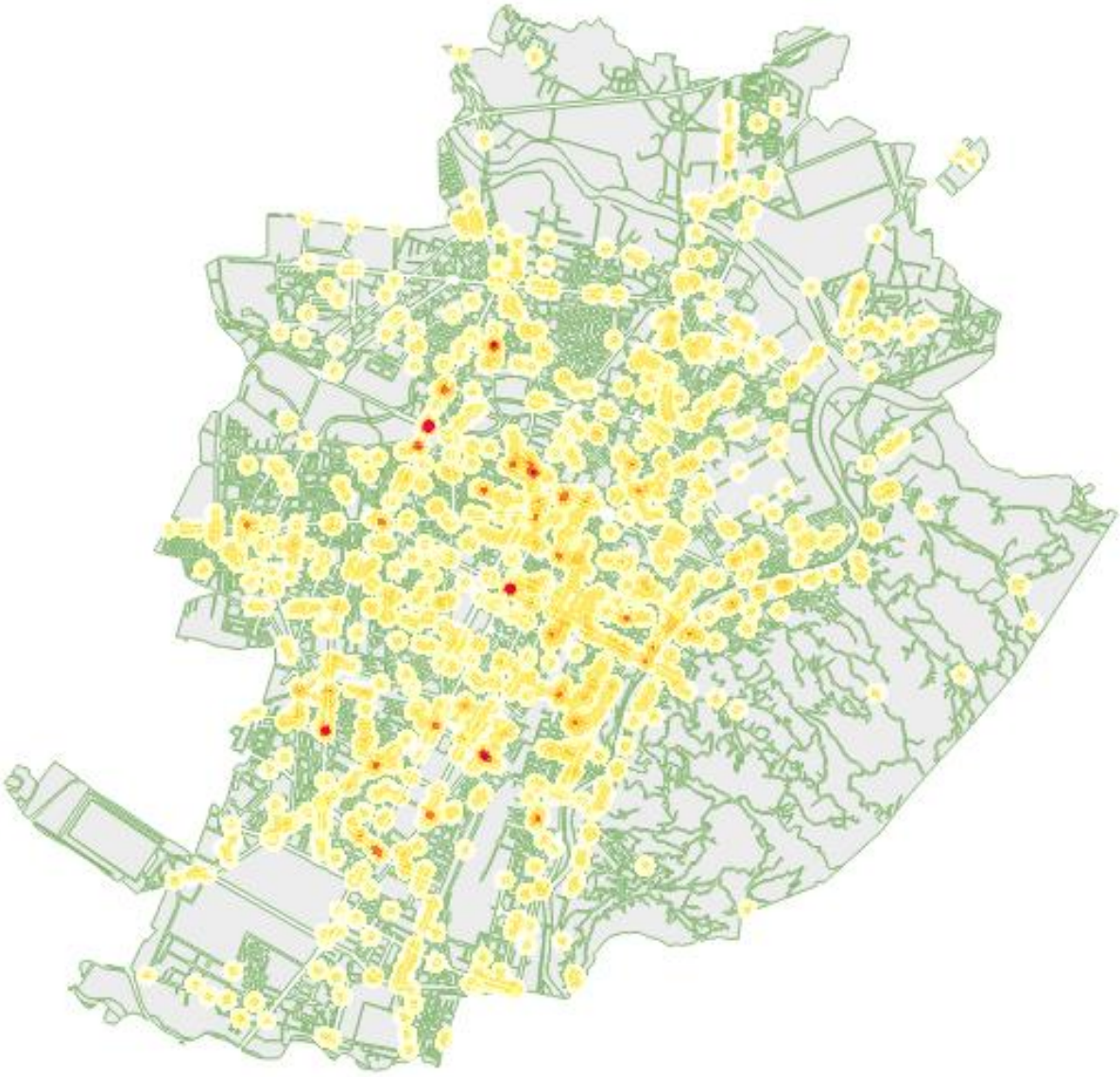

Heat map of traffic collisions including only motorcycle users for the period 2010-2011

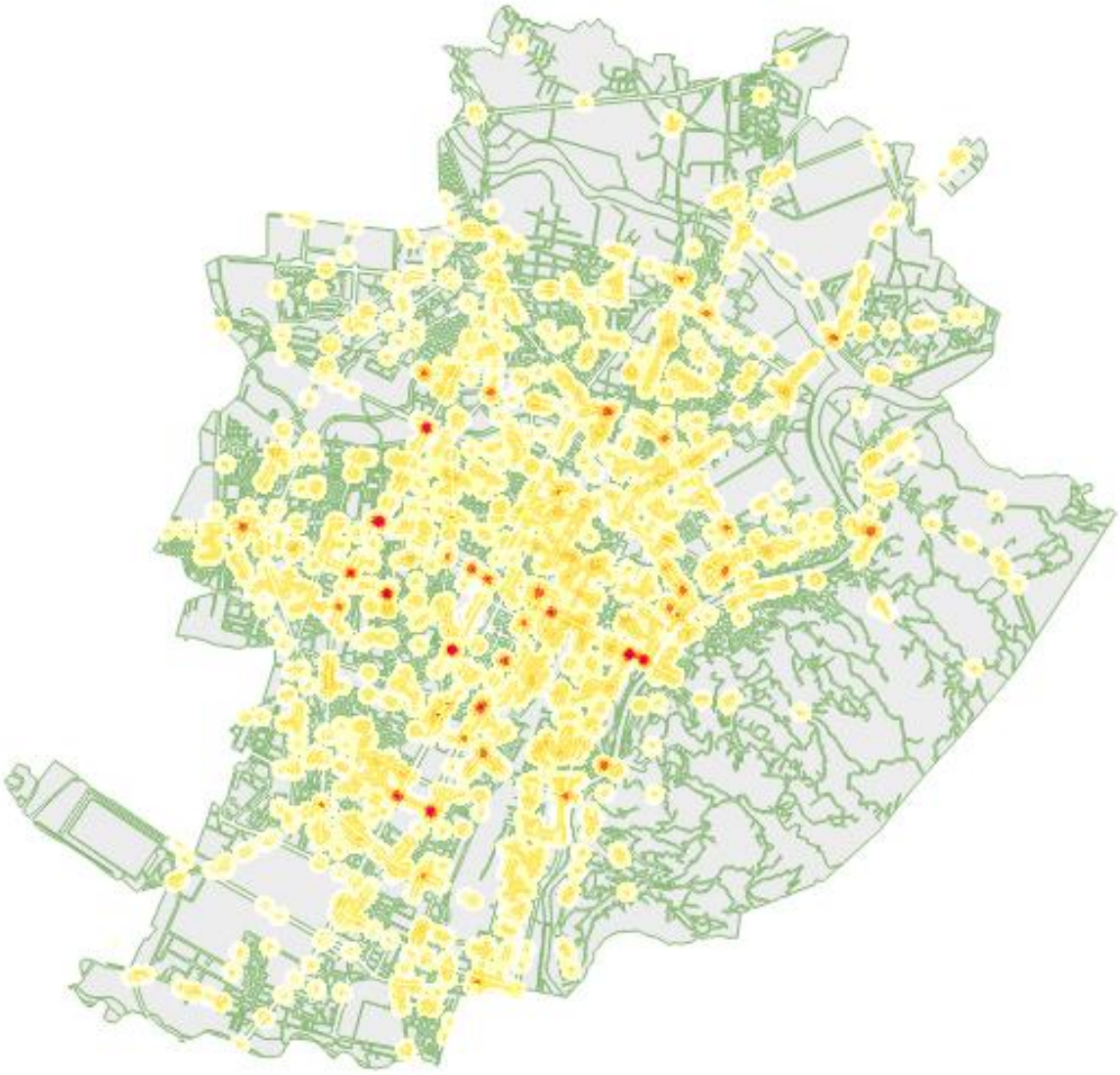

Heat map of traffic collisions including only motorcycle users for the period 2012-2014

Heat map of traffic collisions including only motorcycle users for the period 2015-2016

Heat map of traffic collisions including only motorcycle users for the period 2017-2019

ANNEX 9 : THE RESULTS OF KDE ANALYIS FOR VELOCIPEDE USERS

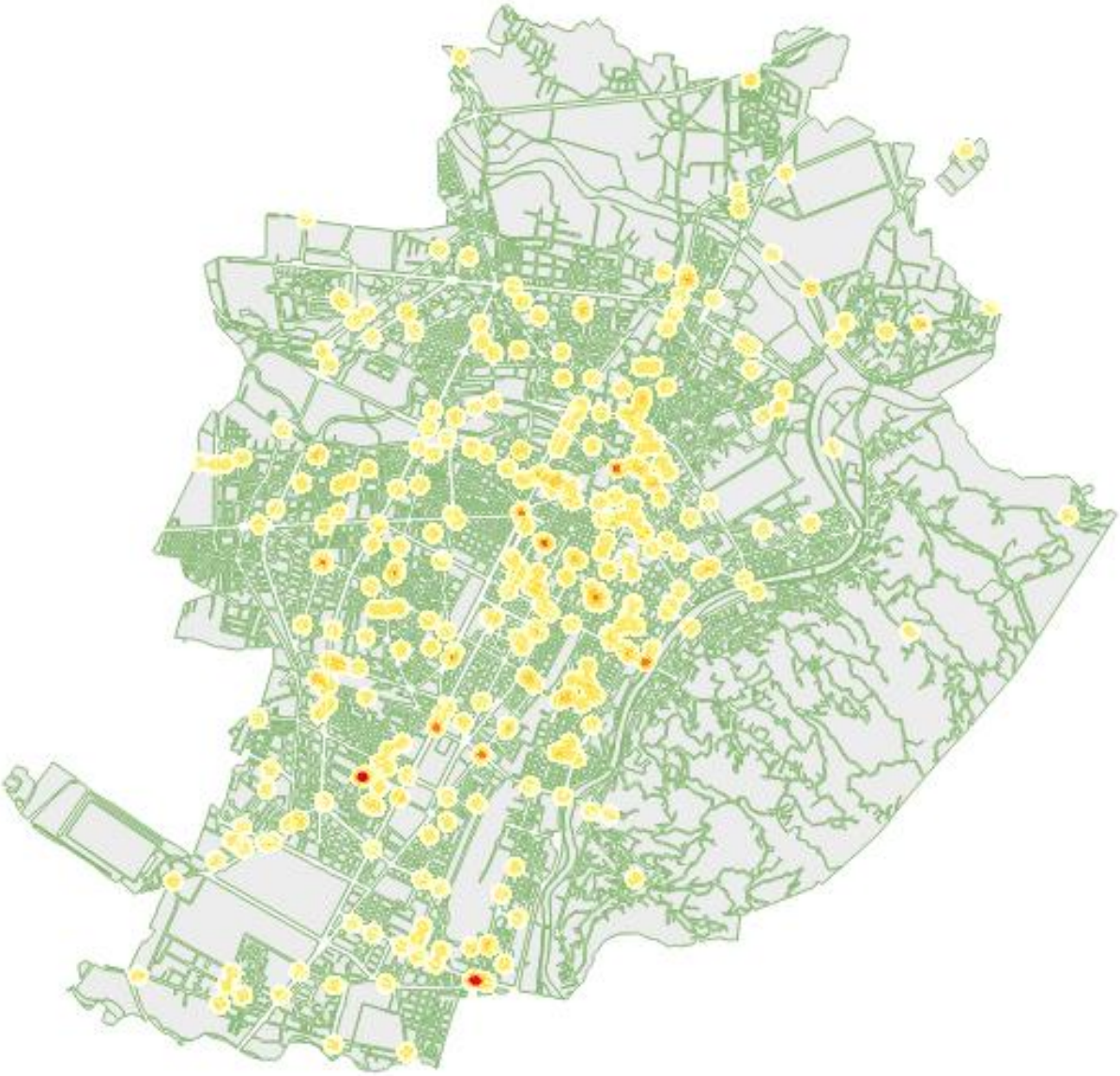

Heat map of traffic collisions including only velocipede users for the period 2006-2007

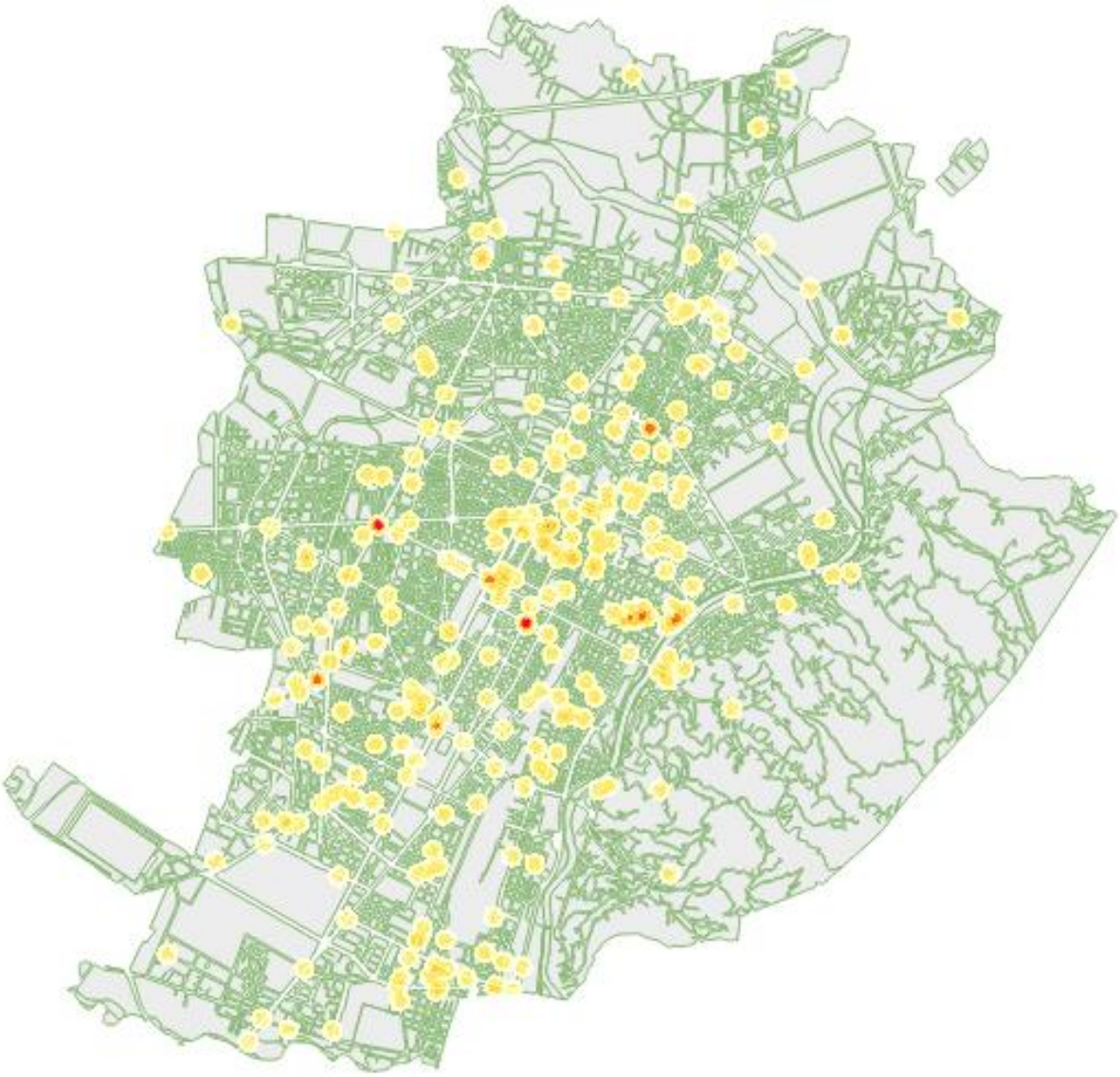

Heat map of traffic collisions including only velocipede users for the period 2008-2009

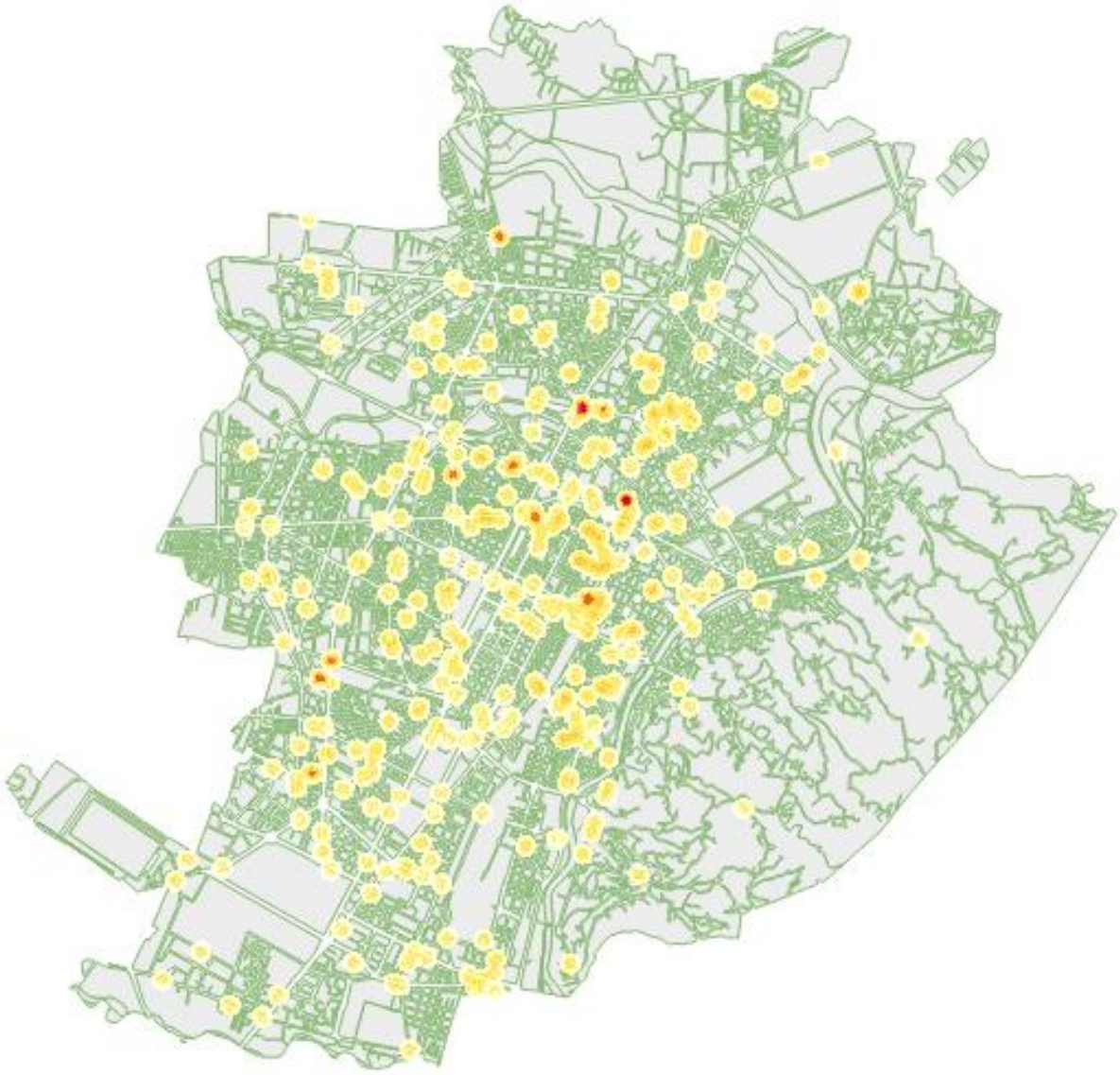

Heat map of traffic collisions including only velocipede users for the period 2010-2011

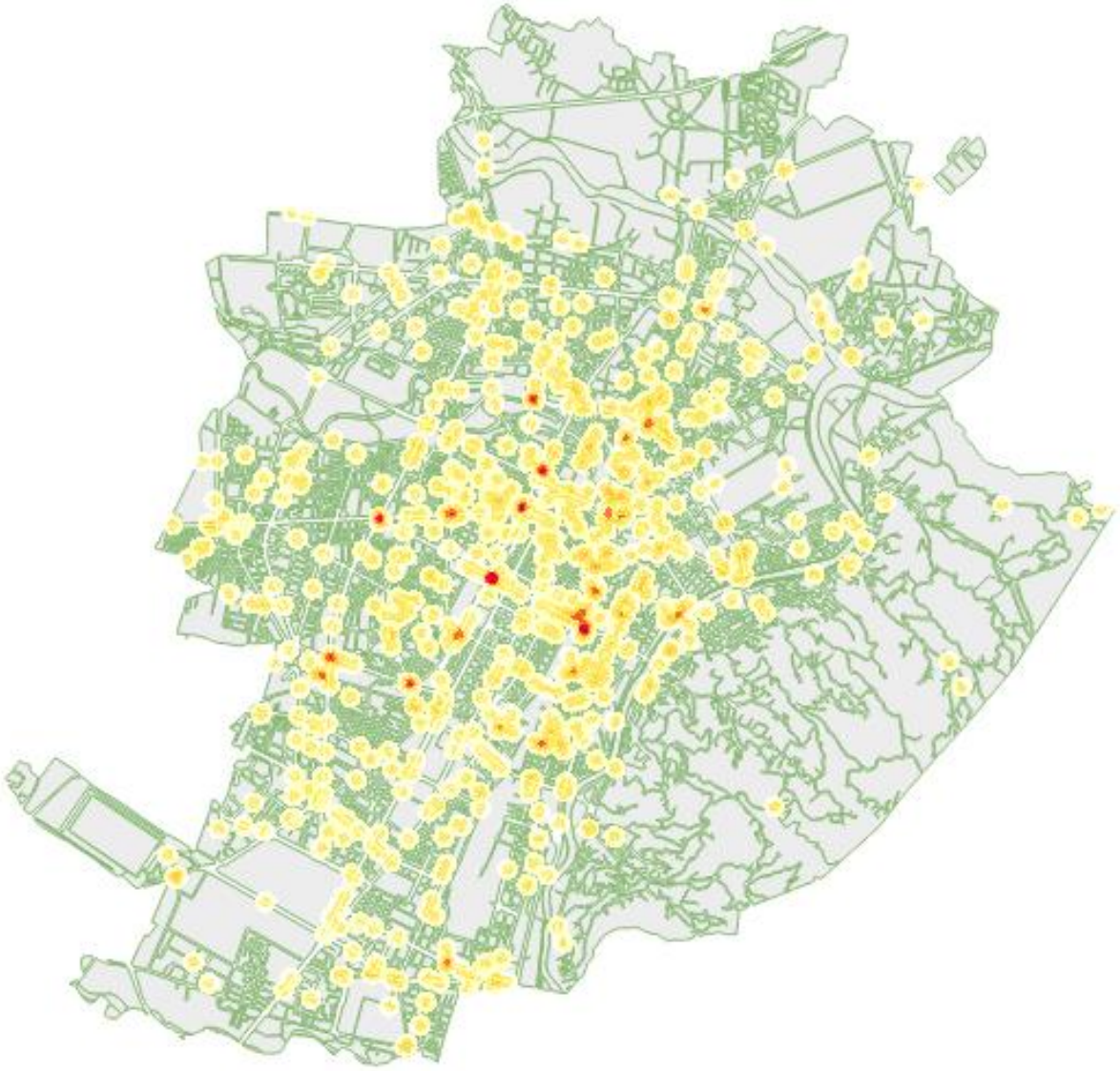

Heat map of traffic collisions including only velocipede users for the period 2012-2014

Heat map of traffic collisions including only velocipede users for the period 2015-2016

Heat map of traffic collisions including only velocipede users for the period 2017-2019

ANNEX 10 : THE RESULTS OF KDE ANALYIS FOR MOPED USERS

Heat map of traffic collisions including only moped users for the period 2006-2007

Heat map of traffic collisions including only moped users for the period 2008-2009

Heat map of traffic collisions including only moped users for the period 2010-2011

Heat map of traffic collisions including only moped users for the period 2012-2014

Heat map of traffic collisions including only moped users for the period 2015-2016

Heat map of traffic collisions including only moped users for the period 2017-2019